2004

The Mission diamicton and associated geohazards Santa Barbara, California

Robert James Urban
San Jose State University

THE MISSION DIAMICTON AND ASSOCIATED GEOHAZARDS SANTA BARBARA, CALIFORNIA

A Thesis

Presented to

The Faculty of the Geology Department

San Jose State University

In Partial Fulfillment

of the Requirements for the Degree

Master of Sciences

by

Robert James Urban

May 2004

ProQuest Information and Learning Company
300 North Zeeb Road
P.O. Box 1346
Ann Arbor, MI 48106-1346

APPROVED FOR THE GEOLOGY DEPARTMENT

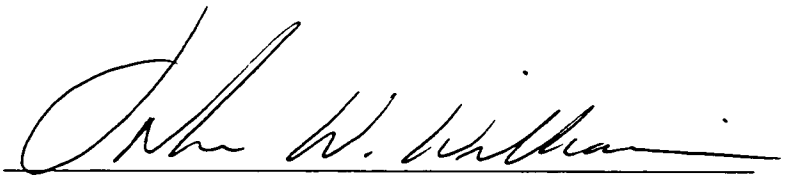

Dr. John W. Williams

Dr. Donald Reed

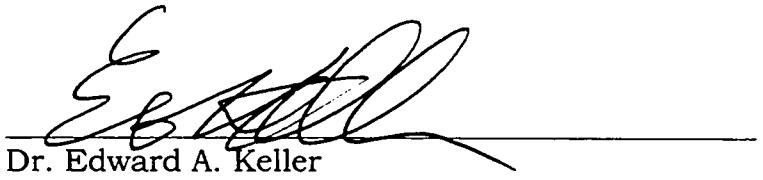

Dr. Edward A. Keller
University of California at Santa Barbara

APPROVED FOR THE UNIVERSITY

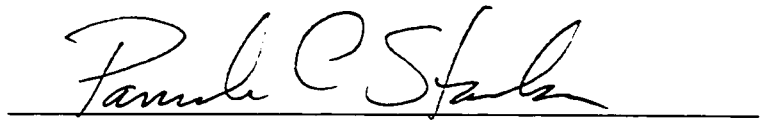

ABSTRACT

THE MISSION DIAMICTON AND ASSOCIATED GEOHAZARDS
SANTA BARBARA, CALIFORNIA

by Robert James Urban

A large debris flow fan, comprised of deposits of the Mission diamicton, associated with the failure of a landslide dam, is recognized in the residential development of the foothills of the City of Santa Barbara, California. The Skofield landslide dam and associated slope failures contributed to the genesis of the Mission diamicton. The Mission diamicton represents multiple episodes of debris flow history. Geophysical investigations identified the 8.7-meter average thickness of Mission diamicton deposits and More Ranch – Mission Ridge fault locations. The Skofield landslide failure occurred in bedrock of the Sespe Formation and mobilized overlying fanglomerate. Radiocarbon dating of Mission diamicton deposits indicates the deposits are younger than 1000 ± 40 ka in age. Quantitative geohazard evaluation and spatial analysis of Rattlesnake Canyon were used to identify critical slope orientations for present day slope instability, which allows for the recognition that slope failure, landslide dam formation, and associated debris flows from landslide dam failure pose threats to the City of Santa Barbara and perhaps the Santa Barbara coastal region.

ACKNOWLEDGEMENTS

How does one acknowledge and give proper thanks to all of the influences, inspiration, and aid that have culminated in this resulting work? It is not accomplished in the forthcoming words but only the preface of bestowments for the following individuals. The following is an inception of thanks and gratitude:

To my wife, Mae, and my daughters, Jadin, Zoi, and Noelle, for not only innumerable ways of support but also for inspiration. With your love and support you have eased the challenges of accomplishing this work.

To my advisor and thesis committee member, Dr. John W. Williams, for not only aiding me to obtain and develop the skills to shape me into the geologist I desire to be but, also for inspiration and being a model of aspiration.

To my thesis committee member, Dr. Donald Reed, for equipping me with skills for this thesis work and my future. For insightful suggestions, stimulating discussion, and bringing light to the subject of geophysics.

To my thesis committee member, Dr. Edward Keller, for introducing me to this project. You were an inspiration while I was an undergraduate at UCSB and are an influence in my career today.

To all of the professors from whom I have had the benefit of being instructed. Thank you for teaching me of this remarkable planet!

To the technical support at San Jose State University: Alphonse Odisho and Ginny Smith who had countless incidences came to my aid with support such as assisting with technical logistics.

Thank you Geometrics, Inc.! The geophysical investigations of this thesis work would not have been possible, and hence many of the findings of this work, would it not have been for Geometrics, Inc. not graciously loaning the geophysical equipment to perform the seismic refraction and resistivity surveys and software to interpret the collected data. A special thanks is necessary to Robert Huggins, Craig Lippus, and Douglas Groom for arranging the generous loan of equipment. I would encourage those with geophysical equipment needs to inquire with

Geometrics, Inc. for they generously give back to the geological community.

Thank you to Scott Minor at the United States Geological Survey for arranging and funding the radiocarbon dating of charcoal collected during this investigation.

Thank you to Harold Van Aller for generously donating the WinSTED slope stability analysis software used in the geohazard evaluation portion of this study. Your generosity aids in recognition of the geohazards in the Santa Barbara region.

To my sister, Amy Berberi, for housing me and providing a steady supply of electricity for recharging batteries during the geophysical field investigation of this research.

And finally, thank you to my field assistants during the geophysical investigations of this study. To my daughters, Jadin and Zoi, for their help during the GPR surveys! To Mark Swank and Chanie Abuye Wossen from San Jose State University and Kevin Ingham from my alma mater at the University of California at Santa Barbara, thank you for the labor intensive help with the seismic refraction investigation.

TABLE OF CONTENTS

LIST OF FIGURES

LIST OF TABLES

INTRODUCTION

Research Problem

An alluvial fan with an unusual morphology is located on the piedmont of the southern flank of the Santa Ynez coastal mountain range, within the City of Santa Barbara, California and the Transverse Range geomorphic provenance (Figures 1 and 2). Though many alluvial fans are present on the coastal piedmont of the Santa Ynez Range in the Santa Barbara region, the lobate and digitate morphology of the fan indicate that debris flow processes were a dominant mechanism for the formation of this fan. The debris flow fan is evident on the Santa Barbara 3m grid DEM (digital elevation model) due to its distinct morphology (Fig. 2).

The pristine morphology of the approximately 1 square kilometer lobate and digitate fan suggests a young age. The sediments, termed the *Mission diamicton*, that comprise the debris flow fan include a catastrophic debris flow event resulting from the failure of a landslide dam, formed by the Skofield landslide (Figs. 2 and 3). The debris flows resulting from the failure of the Skofield landslide dam include an event of unknown duration, hereafter called the *Mission debris flow*. Additional

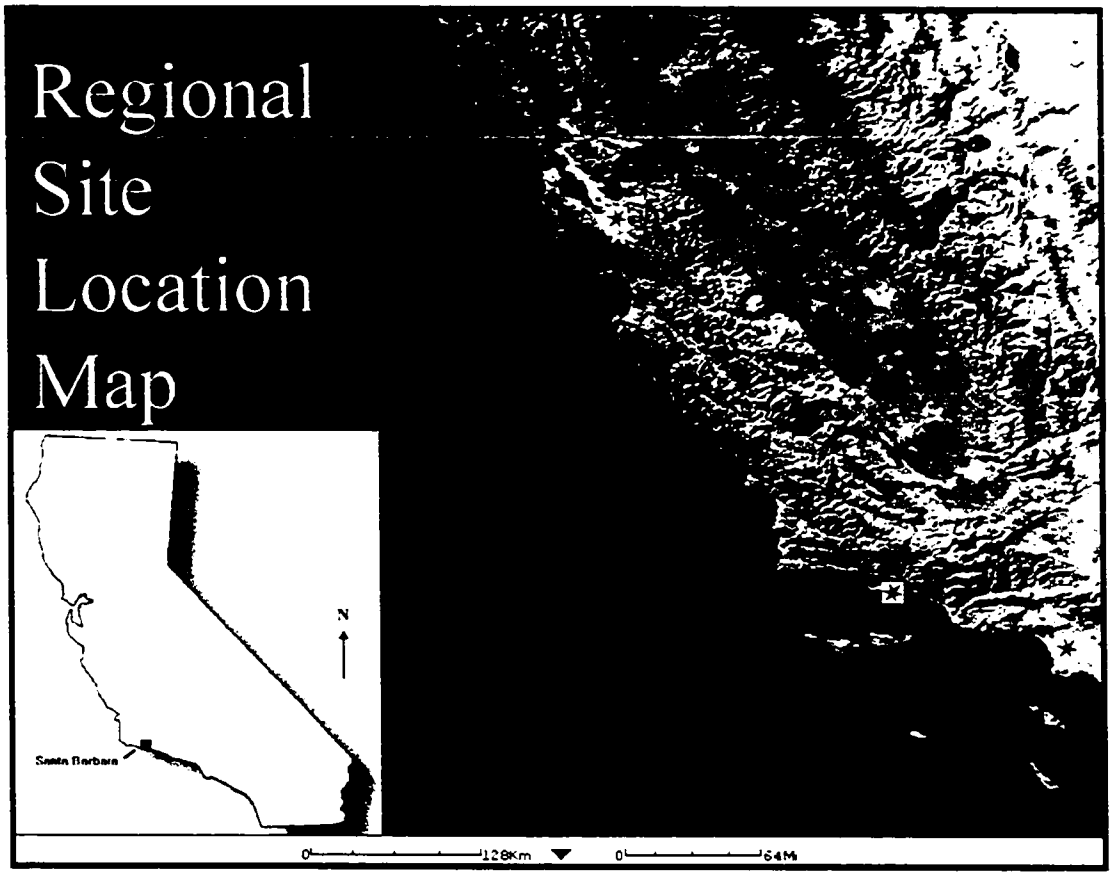

Figure 1. Regional site location map depicting the location of the City of Santa Barbara, where the study is located, in relation to major cities in the state of California.

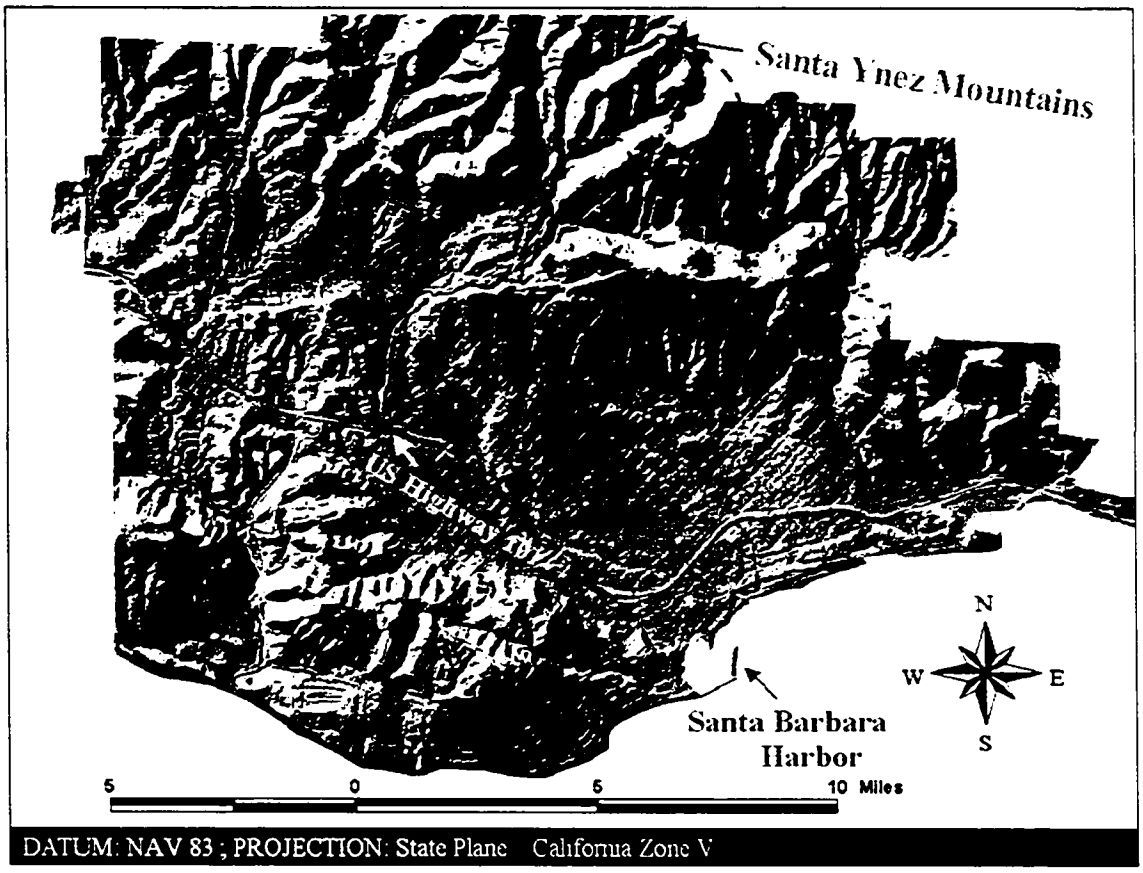

Figure 2. The 3-meter grid digital elevation model (DEM) of the City of Santa Barbara, California depicting the regional topography. The red dashed ellipse indicates the region of the Mission diamicton piedmont deposits. The red dashed circle indicates the location of the Skofield landslide.

Figure 3. Geologic map of the Mission diamicton and associated features, Santa Barbara, California.

Please refer to back cover sleeve

large volume slope failures in Rattlesnake Canyon also may provide debris flow materials in the Mission diamicton.

The close proximity of urban development to the steep topography of the rising Santa Ynez Range poses geologic hazards to the habitants of the City of Santa Barbara in the forms of mass movements and associated processes such as the formation of landslide dams and their subsequent failure. Landslides, debris slides, and debris flows have historically affected residents of the Santa Barbara region (Keller, 1999). The presence of the approximately 1 square kilometer debris flow fan indicates geologic hazards that have been unevaluated, until this thesis work, for the Santa Barbara region.

Research Objectives

Though prior work has speculated on the origins of this debris flow fan (Urban, 2000 and Selting 2002), conclusive evidence has been lacking on its origins. The poor understanding of the origin has resulted in speculation by previous workers as to the geohazards that the debris flow fan poses to the City of Santa Barbara (Selting, 2002).

This thesis presents evidence for the origins of the debris flow fan and, in the context of available and field-collected data, quantitatively

evaluates the geohazards posed by the debris flow fan to the City of Santa Barbara.

PREVIOUS WORK

Previous works have used differing terminology for the deposits that are found within the region of the debris flow fan that is the subject of this study (Keller, 1999; Urban 1999 and 2000; Selting and Urban, 2001; Selting 2002). These deposits, which include the fan described in this study, have been referred to as the Santa Barbara debris flow (Urban, 1999 and 2000), Mission debris flow (Selting and Urban, 2001; Selting, 2002), and the Mission diamicton (Urban, 2002). The name "Mission" refers to the geographic proximity of the sediments to the Santa Barbara Mission.

The name "Mission debris flow" used by previous authors implies that the deposits of the fan have origins related to a single debris flow or single debris flow event. A single debris flow consists of one debris flow whereas a single debris flow event may consist of multiple debris flows related to one specific geologic event in time. The name, Mission debris flow, is presumptuous and a misleading concept for understanding the origin of the sediments investigated by this study. No conclusive evidence has been presented that indicates that the Mission diamicton is the result of a single debris flow.

Because of the limitations the name "Mission debris flow", this author adapts the term Mission diamicton. The name, Mission diamicton, does not preclude a history of multiple debris flows, either due to a single or multiple debris flow event. In order to separate the depositional interpretation from physical characteristics of the deposits, it is adopted for this study and suggested that future work refer to the sediments related to the debris flow fan as the Mission diamicton. The term, *diamicton*, is a non-genetic term and refers unconsolidated and poorly sorted sediments with a bimodal sedimentologic signature. The term, *diamicton*, appropriately describes the physical characteristics of the sediments that comprise the debris flow fan.

However, the name *Mission debris flow* should be retained to refer to a specific geologic event, identified by this study and described herein, consisting of the failure of the Skofield landslide dam and the resulting massive debris flows that came to rest on the Santa Barbara piedmont. The evidence collected during this investigation and description of the interpreted geologic history of the Mission debris flow will be presented and discussed in further sections of this thesis.

The debris flow fan was first recognized by Keller (1999) and described in a field guide for the Santa Barbara Natural History museum grounds. Keller (1999) briefly described the sedimentary characteristics of the fan, suggested a debris flow origin and believed that the fan

developed from the many debris flows originating in the Mission and Rattlesnake Canyons.

As part of an undergraduate research project, Urban (1999 and 2000) investigated the origins of the Mission diamicton. Urban (1999) performed the first mapping of the sedimentary deposits comprising the fan. Urban (1999) mapped a laterally continuous, with the exception of modern stream channel dissection, debris flow fill terrace deposit through Rattlesnake Canyon to Skofield Park. The termination of the Mission diamicton is coincident with the location of a mega-landslide identified and named by Urban (1999) as the Skofield landslide. Urban (1999 and 2000) mapped and described this large geologic feature and suggested that the Skofield landslide was a compound and composite translational and rotational landslide. Urban (1999) hypothesized that the Skofield landslide formed a landslide dam that had blocked drainage of Rattlesnake Canyon, which subsequently failed and resulted in catastrophic debris flows that contributed to the bulk of Mission diamicton sediments. As part of the undergraduate research, Urban (2000) presented preliminary volumetric calculations for the Mission diamicton (9.1×10^6 m^3) and the exhumed material of the Skofield landslide (7.8×10^6 m^3) to correlate the two geologic features.

Based largely on Urban's undergraduate investigation (1999 and 2000), Selting and Urban (2001) described the state of research on the

Mission diamicton in a field guide for the 2001 Geologic Society of America Cordilleran Section meeting.

The Mission diamicton was also the subject of a previous master's thesis (Selting, 2002). Selting (2002) performed volumetric estimations, geologic mapping, sedimentologic descriptions, and interpreted a geologic history similar to the study presented by Urban (2000). Selting (2002) interpreted the deposition sequence of the debris flow lobes, based on the morphology evident in the 3-meter grid digital elevation model (DEM) of the City of Santa Barbara. Selting (2002) also provided boulder size and distribution data supporting the Skofield landslide dam hypothesis proposed by Urban (1999).

Selting's (2002) mapping of deposits is based largely on digital image analysis and lacked verification by field studies. The morphology of the study area was interpreted with a digital elevation model dataset that contains subtle flaws and does not accurately depict terrain conditions of the study area.

Urban (2002) presented 3-dimensional volumetric calculations for the fan deposits of the Mission diamicton and evacuated slopes of the Skofield landslide. Urban (2002) also demonstrated that without defining the 3-dimensional contact on which the Mission diamicton rests, any volumetric calculations are limited at best in hypothesizing the origin of these deposits using volumetric methods. Urban (2003) presented, to

the Association of Engineering Geologists, a summary of the findings and a quantitative geohazard identification evaluation of slope failures in Rattlesnake Canyon that are described in this thesis.

INVESTIGATION

Introduction

This study is comprised of a geomorphic analysis, traditional geologic mapping and field description of the geologic units, aerial photography review and analysis, digital image creation and analysis, geophysical investigation of the Mission diamicton piedmont deposits and Skofield landslide dam region, identification of slope failures and kinematics, and collection of geotechnical data to evaluate slope instability geohazards.

In addition to the field investigation, modeling of acquired data was accomplished. Geophysical data were analyzed and models were developed. A three-dimensional geologic map was generated and computer modeling of the study area was accomplished to make a volumetric comparison of source and depositional areas. Slope stability analysis in Rattlesnake Canyon used Limit Equilibrium methods with discontinuity data collected during the field investigation and geotechnical data collected from publicly available geotechnical reports. Geographic information system (GIS) modeling and analysis of the study area were accomplished to determine locations of slopes that are at or

exceeding their critical orientation for slope failure under present day conditions.

Digital Data and Modeling

The creation of digital shaded relief images, or photo-realistic renders, directly from the vector based TIN minimizes misrepresentation of topographic surfaces. Unlike images generated from a TIN, digital images created from a DEM are more susceptible to terrain misrepresentations. During the generation of a DEM from a vector TIN, additional computer manipulation and numerical interpretations transform vector spatial information, representing topographic surfaces, into a raster grid representation of the surface. Transferring topographic surfaces represented as TINs into raster grids, which are DEMs, can lead to numerical and geometric misinterpretations of the surface being transformed.

A 3-meter grid DEM of the study area was previously generated utilizing the Santa Barbara Flood Control topographic maps with some topographic data removed to minimize file size (De LaGarza, 2001 personal commun.). The removal of topographic data during genesis of the 3-meter grid DEM makes the DEM inherently inferior to the topographic representation of the landscape when compared to the

digital terrain model generated during this study. The digital terrain model is a vector based TIN that lacks the extra numerical modeling interpolations experienced in the genesis of the 3-meter DEM of the study area.

Another inherent limitation of the 3-meter grid DEM is the depiction of topography that is beyond the resolution of data from which the DEM was constructed. For instance, in the region of the Skofield landslide, the only available contour interval data are 7.6 meters. During construction of the 3-meter grid DEM, numerical interpolation of the topography in this region was necessary to generate 3-meter grid cells that are smaller than the 7.6-meter contour interval of the original dataset.

Though the 3-meter grid Santa Barbara DEM was useful for the initial recognition of the gross morphology of the Mission diamicton fan, the lack of topographic accuracy does not allow for the detailed analysis the geomorphic relationships accomplished during this investigation. The digital flaws inherent in the 3-meter DEM warrant reconstruction of a digital model to depict terrain if detailed geomorphic analysis of terrain is to be used as part of this scientific study. Therefore, the geomorphic and volumetric analysis of this study is based on a digital terrain model (DTM) and TIN generated during the course of this investigation.

The digital modeling produced during this study does not exceed the resolution of the available topographic data of the study area. The vertical resolution of available digital topographic data from which the DTM was constructed ranges from 0.61 to 7.62 meters. The digital topographic maps from which the DTM of this study and the 3-meter grid DEM was constructed, are the Santa Barbara Flood Hazard Control maps for the County of Santa Barbara, California. With respect to these maps, topographic resolution decreases in regions with steeper topography and increases in less steep regions.

Mission Diamicton

Morphology

The pristine morphology of the Mission diamicton fan deposits are best seen on the topographic map and photo-realistic rendering of the digital terrain model (DTM) generated during this study (Figs. 3 and 4). The DTM of the study area was created by generating a triangulated-irregular-network from all digital topographic data available on the Santa Barbara County Flood Control topographic maps. The use of all available and unaltered topographic data minimizes misrepresenting topographic conditions.

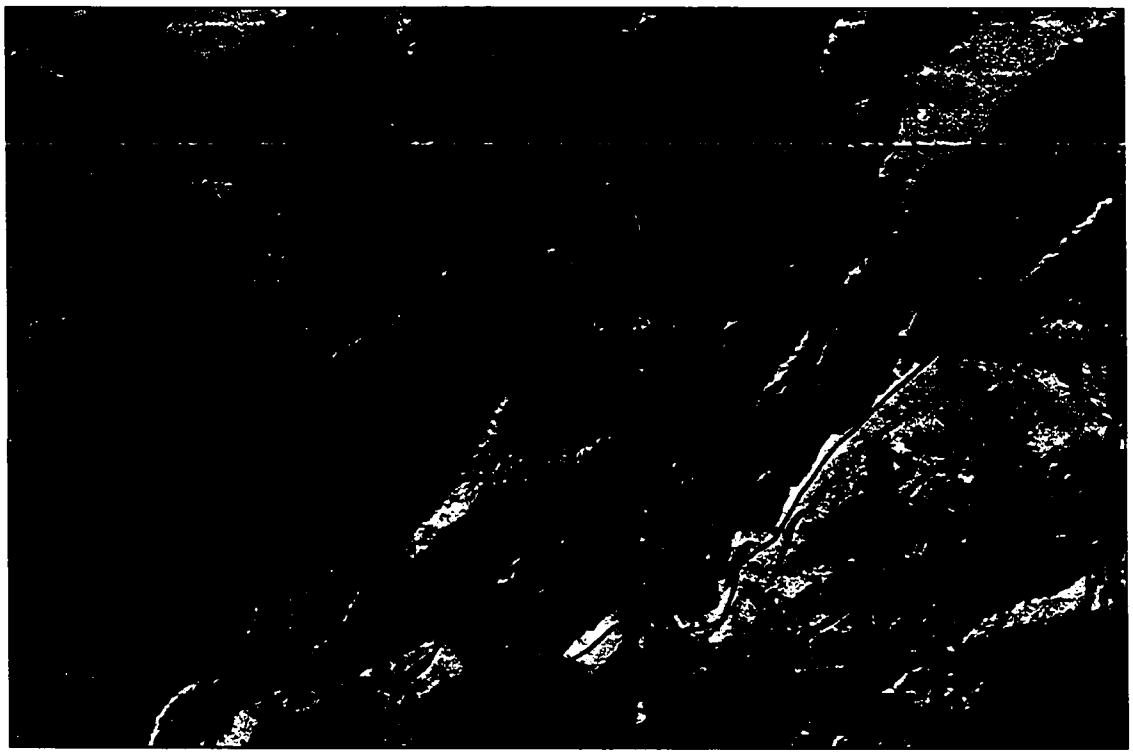

Figure 4. Photo-realistic render of the digital terrain model triangulated-irregular-network (TIN) for the Mission diamicton piedmont deposits. The red line indicates approximate boundary of the Mission diamicton piedmont deposits. Piedmont deposits have characteristic digitate and lobate morphology indicative of debris flow depositional processes. The high-resolution image indicates that the large morphologic lobes evident on the 3-meter DEM are actually compound morphologic lobes (compare to Figure 5). The complex morphology and lack of paired levees within the fan deposits makes interpretation of debris flow sequence history impractical. Linear features trending north-south and east-west, respectively, are streets.

The Mission diamicton is characterized by lobate and digitate morphology with steep and blunt margins at the terminus of morphologic lobes (Fig. 4). Initial geomorphic analysis and field mapping by Urban (1999) indicated the presence of three massive morphologic terminal lobes evident on the 3-meter DEM (Fig. 2). The photo-realistic render image of the digital terrain model TIN generated during this study shows that the morphology of the piedmont deposits is more complex than the 3-meter grid DEM depicts (Fig. 4). After Urban (1999), Selting (2001) also indicated the presence of three massive lobes within the Mission diamicton and refers to each of the lobes as a debris flow pulse (Fig. 5). Selting (2002) interprets these morphologic lobes as actual depositional debris flow lobes without supporting evidence such as paired levees (Fig. 5).

Using the high-resolution image generated from the DTM, created with 2 feet contour data in this region, the large morphologic lobes are interpreted as compound lobate and digitate lobes (Fig. 4). Because paired boulder levees are not observed along the margins of these lobes, it is unclear whether these lobes represent actual debris flow lobes or larger lobes that were dissected into smaller lobes. It is possible that flood and outwash waters could have channelized an individual lobe to give the morphologic expression of two or more debris flow lobes. Costa

Figure 5. 3-meter DEM depiction of Mission diamicton piedmont morphology and debris flow lobe depositional history interpreted by Selting (from Selting, 2002). The morphology of the 3-meter DEM does not depict the complex morphology of the Mission diamicton piedmont deposits as indicated in Figure 4. Comparison of Figures 4 and 5 indicates it is erroneous to interpret depositional history from the 3-meter DEM based on morphology. Paired levees along the morphologic lobes are lacking. Selting's (2002) mapping of debris flow materials at the apex of the fan agrees with this author's recognition of super elevated debris flow deposits. Super-elevation of Mission diamicton deposits is evident on Selting's (2002) map of piedmont deposits. Though Selting (2002) reports not observing super-elevation of debris flow deposits observed by Urban (1999), deposits are super-elevated by over 12 meters near the apex of fan deposits.

(1986) documents such morphologic dissection of singular debris flow lobes into multiple morphologic lobes.

Geologic Mapping

Initial geologic mapping of the Mission diamicton deposits was accomplished by the author as part of an undergraduate research project (Urban, 1999 and 2000). As part of this thesis work, the Mission diamicton deposits were remapped and additional descriptions of the Mission diamicton deposit were accomplished.

The Mission diamicton was mapped onto a compiled Santa Barbara Flood Control topographic map (contour interval 0.61 to 7.62 meters), and digitized in the AutoDesk Land Development R2 geographic information system (GIS) environment (Fig. 3). The diamond-shaped debris flow fan is approximately 1830 meters long along a northeast to southwest trend and approximately 790 meters across. The areal extent of the piedmont deposits is 1.01×10^6 m^2 (Urban, 2000), as computed utilizing the Land Development R2 program.

Field observation of surficial characteristics of the Mission diamicton on the piedmont is best at Rocky Nook Park where residential development has not disturbed or observation of features, such as levees, terminal lobes, and open-framework boulder berms. A continuous

geomorphic lobe up to 100 meters in length is present in Rocky Nook Park. Selting and Urban (2001) report that lobe is accompanied with a 100 m long continuous paired levee, traceable through the park. Other depositional features indicating debris flow deposition include boulder berms such as the clast-supported boulder berm that is located at the entrance of the park (Fig. 6).

Costa (1986) distinguishes the formation of levees and terminal lobes from open-framework boulder-berms. He further describes how the mass of debris and water of a debris flow moves and stops in place when internal friction is exceeded by the shear strength of a debris flow. A fine-grained matrix is retained at the base of the flow during deposition and may not be present at the top of levees or terminal lobes where large boulders are pushed to the top of the flow or where rain waters are able to remove the fine-grain matrix (Costa, 1986). Open-framework boulder berms are distinctly different in that the clast supported framework of the boulder berms lack a fine-grained matrix and are localized along stream channels whereas levees can be continuous for long distances and are matrix-supported (Costa, 1986).

The Mission diamicton displays sedimentary characteristics common to documented debris flows. The entire Mission diamicton has a very crude reverse grading with large diameter boulders concentrated near or at the top of the deposit. Outcrops of the Mission diamicton have

Figure 6. Boulder berm located at the entrance to Rocky Nook Park. For scale, the author is sitting on one of the Coldwater formation clasts that are both of typical size and type for clasts on the surface of the Mission diamicton piedmont deposits. Boulder berms are associated with debris flow deposition.

a similar youthful and sedimentologic appearance throughout the deposit. Type locality outcrops preserve clues to the Mission diamicton origin. At a stream-cut of the Mission diamicton, just south of where Mission Creek comes in contact with the Santa Barbara piedmont, there is an outcrop of classic debris flow sedimentary sequences (Fig. 7). Distinct internal reverse grading is present with multiple debris flow depositional sequences. Though stream-cuts through the Mission diamicton expose massive deposition and gross inverse grading, this exposure indicates at least two pulses or separate events deposited debris flow sediments. Figure 7 depicts the multiple debris flow sequences within the Mission diamicton piedmont deposits at this location.

Massive boulders (0.5 m - 7 m) largely supported in a matrix ranging from clay to cobble-sized sediments characterize this massive and poorly sorted diamicton. Fine-grained sands dominate the matrix of the Mission diamicton in outcrop (Fig. 7). Sediment size distribution data of Mission diamicton matrix were collected from geotechnical reports available at the City of Santa Barbara Public Works offices. Table 1 depicts a tabulated list of Mission diamicton geotechnical data that are included in this report. A presentation of the matrix grain size distribution is presented in Table 2. The sediment size distribution of the Mission diamicton matrix is correlative with matrix grain

Figure 7. Multiple debris flow sequences exposed in the Mission Creek stream-cut near the confluence with Rattlesnake Creek. Rock hammer, separating two debris flows in the Mission diamicton, is for scale. Here is a classic debris flow sedimentary sequence of fine grain materials followed by inversely graded clasts in fine-grain matrix. At the top of this sequence and out of the photograph range are the large clasts such as those depicted in Figure 6.

Table 1. Tabulation of geotechnical data used in investigation. Geotechnical data on geologic materials in the study area is available at the City of Santa Barbara Public Works Department.

	Depth (feet)	Wet Density (pcf)	Dry Density (pcf)	Moisture (percent)	Phi Value (degrees)	Cohesion (psf)
Mission diamicton	3	116.4	106.9	8.9	26.9	222
	3	113.1	102.8	10.0	25.9	179
	5	108.4	98.2	10.4	29.8	152
	6	116.5	107.8	8.1	n/a	n/a
	7	113.8	102.3	11.2	n/a	n/a
fanglomerate	10	130.0	110.0	18.0	22.8	147
	15	129.3	112.1	15.3	28.9	245

Table 2. Mission diamicton matrix grain size distribution data.

	Sediment	Percent by Weight		
Mission diamicton	Gravel	17.6	51.8	6.3
	Sand	56.0	33.5	62.8
	Silt	19.8	11.4	23.0
	Clay	6.6	3.3	7.9

distributions for other documented debris flows by Costa (1986). Costa (1986) documented that debris flows become mudflows when clay content is greater than 10 percent. Because the matrix of the Mission diamicton contains no more than 10 percent clay content, this supports the interpretation that the Mission diamicton was deposited as debris flows and not mudflows.

Massive sub-rounded to rounded boulders are present at the surface of the Mission diamicton. Arkosic sandstone boulders, characteristic of the Coldwater Formation origin, are present in the Mission diamicton. Other boulder clasts originating from the Juncal, Matilija, and Sespe formations are present in the Mission diamicton but are not as ubiquitous as Coldwater Formation clasts. The Mission diamicton has a remarkable lithologic similarity to sediments present in the nearby mid- to late-Pleistocene fanglomerate deposits.

A lichen growth is present on many of the boulders exposed at the surface and lichenometry dating has been suggested by Keller (1999, personal commun.) to constrain the age of the Mission diamicton. One of the distinguishing characteristics that identifies the boulders of the Mission diamicton from nearby fanglomerate deposit boulders, is that the majority of the Mission diamicton boulders lack oxidation-weathering rinds found on fanglomerate boulders (Fig. 8). It appears that mobilization of the fanglomerate boulders could ablate the weathering

Figure 8a. Weathering rinds missing from the Mission diamicton boulders in this boulder berm are replaced by lichen growth. Hammer in red circle for scale.

Figure 8b. Weathering rinds present on the fanglomerate deposits. Silver camera in red circle for scale.

rinds of fanglomerate boulders and form the deposits of the Mission diamicton.

The base of the Mission diamicton is not exposed in the main body of the fan but stream cuts expose approximately 4 m of the deposit on average. A 9.5 m maximum incision into the Mission diamicton by Mission Creek is present on the piedmont. Analysis of the topographic expression of the surrounding piedmont and of the Mission diamicton fan suggests a maximum deposit thickness of 13.5 m. The maximum thickness of the Mission diamicton is determined by measuring the maximum height of the compound morphologic lobes within the body of the piedmont fan deposits (Fig. 3).

The Mission diamicton is present from the piedmont to a distance of approximately 1500 m up Rattlesnake Creek. The narrow and confined topography appears to generally control an average width of 80 m within the Mission diamicton in Rattlesnake Canyon. Mission diamicton canyon deposits appear as fill terraces, at times locally on bedrock straths. Local geologic relationships of deposits are indicative of multiple debris flow sedimentary sequences.

Figure 9 depicts an outcrop within Rattlesnake Canyon where two debris flow deposits have apparently different geologic ages. The overlying debris flow sequence has a more youthful appearance and is part of the Mission diamicton. The underlying debris flow deposit is part

Figure 9a. Two debris flow deposits with apparent different geologic ages. Location in Rattlesnake Canyon on Rincon Formation. Viewing downstream of Rattlesnake Creek. Hammer in red ellipse for scale.

Figure 9b. Close-up photograph of the older debris flow deposit underlying the Mission diamicton and in contact with the Rincon Formation. Hammer in red ellipse for scale.

of an older debris flow deposit, not part of the Mission diamicton based upon greater induration and cementation, as well as distinct staining of the underlying debris flow sediments. This laterally discontinuous and localized debris flow deposit appears to be older than the overlying Mission diamicton based on the degree of sediment staining that is not present in the Mission diamicton. Both of these debris flow deposits may represent incision into the underlying, highly sheared, and fissile shale of the Rincon Formation. The Mission diamicton is deposited on both the strath of Rattlesnake Creek and on the older debris flow fill terrace within the canyon (Fig. 9). The stratigraphic relationships at the outcrop depicted in Figure 9 indicate basal scour occurred from the traveling debris flows of the Mission diamicton.

Alternatively, the debris flows of the Mission diamicton could be filling the paleo-stream channel topography at this location. Though the debris flows that were deposited as the Mission diamicton presumably had considerable shear strength and velocity in order to transport the large boulders found at distances up to 3 kilometers from source areas identified in this study. Therefore, the debris flows would likely have scoured the fissile shale of the Rincon Formation that would have been the paleo-topographic surface at the time the debris flows originated. Costa (1986) presents data of numerous documented debris flows that characteristically scour into underlying materials.

Costa (1986) documents that debris flows are able to deposit super-elevated sediments. Super-elevated deposits have inner-channel bend deposits at a lower elevation relative to outer-channel bend deposits. Evidence of super-elevation of the Mission diamicton is preserved within Rattlesnake Canyon and near the apex of fan deposits on the Santa Barbara piedmont. The fill terraces of Mission diamicton canyon deposits have subtle irregular surfaces (Fig. 10). Comparison of the inner bend and outer bend elevations of Mission diamicton deposits within Rattlesnake Canyon identifies locations of super-elevated fill terrace deposits (Fig. 10). The Mission diamicton displays large-scale super-elevation at the apex of piedmont fan deposits (Fig. 3). At this location, the Mission diamicton is super-elevated to nearby adjacent inner-bend deposits by over 12.2 meters.

Selting (2002) analyzed shaded relief digital images generated from a 3-meter grid digital elevation model and reports not observing super-elevation of Mission diamicton deposits. But Selting's (2002) geologic map of the Mission diamicton, similar to the geologic map presented by Urban (2000), includes locations where the Mission diamicton is super-elevated relative to adjacent deposits (Figs. 4 and 5).

The Mission diamicton terminates near the western edge of Skofield Park (Fig. 3). Although the Mission diamicton is not present beyond Skofield Park, landslide debris deposits with the similar clast and

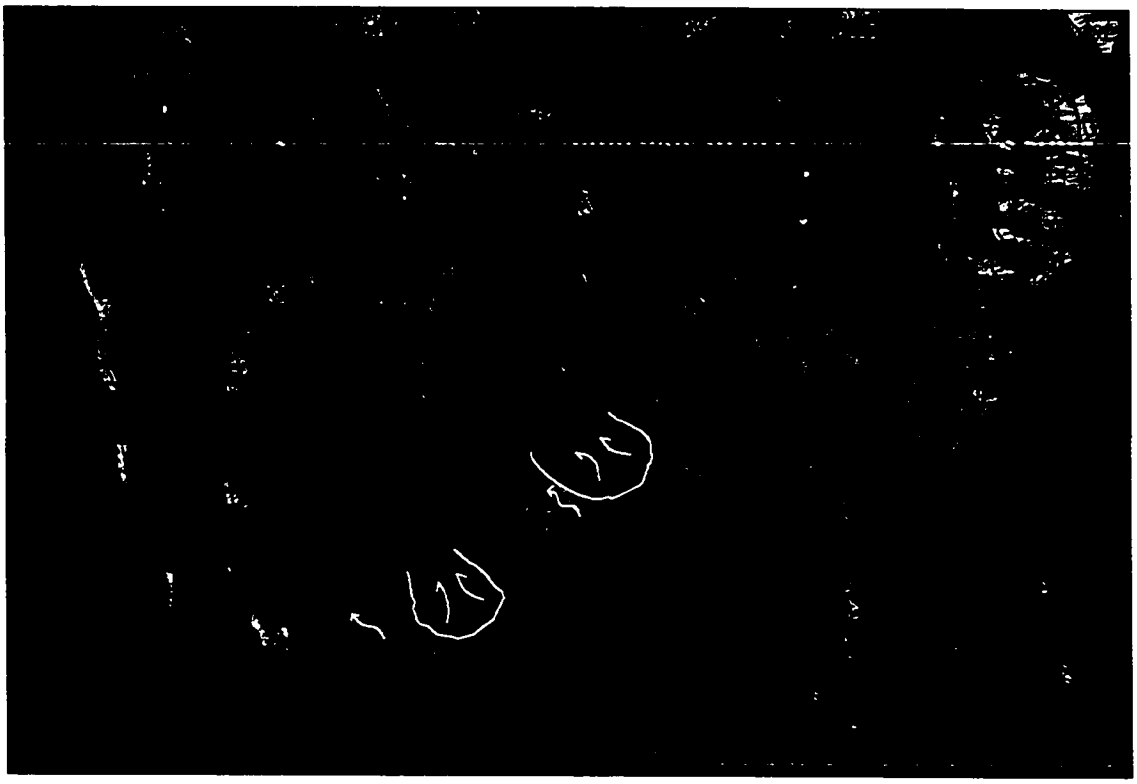

Figure 10. Photo-realistic render of Rattlesnake Canyon. Mission diamicton within green, other large evacuated regions of slope failures indicated by yellow, unnamed fault mapped by Gurrola (2002) indicated by red (no distinction made between concealed/unconcealed fault), Skofield landslide and dam deposits indicated by blue, and region of undifferentiated slope failures and landslide debris presumably related to the failure of the Skofield landslide dam indicated by purple. Topographic contours, streets, and man-made structures indicated by black lines.

matrix characteristics are present in the Skofield Park vicinity (Fig. 11). The lack of Mission diamicton beyond Skofield Park and further up Rattlesnake Canyon may be due to either lack of deposition beyond Skofield Park, erosion and removal of Mission diamicton, or lack of exposure because of burial by landslide debris deposits in this region. North of Skofield Park, the lack of exposure by burial from subsequent sediments is unlikely because of the thin veneer of sediments present in Rattlesnake Canyon. This thin veneer of stream sediments in Rattlesnake Canyon is probably associated with the steep rising gradient of Rattlesnake Creek and subsequent increased stream energy that facilitates sediment removal.

The Mission diamicton is traceable for approximately 240 meters up the drainage of Mission Creek, beyond the confluence with Rattlesnake Creek, before other debris flow deposits, not part of the Mission diamicton, originating from Mission Canyon appear stratigraphically adjacent to the Mission diamicton (Fig. 3). A boulder levee forms the lateral extent of the Mission diamicton up Mission Creek.

Geophysical Investigation

Because DTM volumetric calculations of the Mission diamicton and Skofield landslide did not suggest that the Skofield landslide was the

Figure 11. Coldwater Formation boulders in landslide debris at Skofield Park. These boulders have similar characteristics to the Mission diamicton surficial boulders with abated weathering rinds and lichen characteristically growing on the boulders. Rock hammer in red ellipse for scale.

only source contribution to the Mission diamicton development (Urban, 2002), the author conducted a geophysical investigation of the Mission diamicton to determine the thickness of the deposit. The subsurface data were utilized to create a three-dimensional model of Mission diamicton piedmont deposits in the DTM for volumetric calculations. The thickness of Mission diamicton deposits was unknown at the beginning of this study. Large quantities of subsurface data were required to determine the geometrical characteristics of the Mission diamicton and underlying geologic material's contact, for accurate three-dimensional volumetric calculations. Methods of subsurface exploration in defining the three-dimensional characteristics of the Mission diamicton piedmont deposits are limited to non-destructive subsurface investigation techniques because the debris fan is distributed throughout the City of Santa Barbara.

Geophysical Investigation Methods

Seismic refraction and resistivity surveys were performed in July 2002 and January 2003. The seismic refraction surveys included the use of a Geometrics, Inc. 24-channel Geode seismographs, geophone receivers, and sledge hammer seismic source. Seismic refraction data were recorded utilizing the Multiple Geode Operating System (MGOS) and

Single Geode Operating System (SGOS) developed by Geometrics, Inc. The locations of seismic refraction surveys are presented in Figure 3. Seismic refraction data were processed and analyzed with the Geometrics SeisImager seismic refraction data processing and analysis software.

Seismic refraction wavelet data were picked for first arrival times of P-waves and initial travel time curves were generated in the Pickwin module of SeisImager. First arrivals were chosen from seismic wavelet records, amplifying gain and analyzing cyclic background seismic noise when necessary to identify first arrivals on applicable seismic wavelets. First arrival picking is an interactive process in the Pickwin graphic user interface (GUI) environment.

After picking of first arrivals, travel-time curves were generated. Travel-time curves were analyzed for consistency of first arrival picks in the Plotrefa module of SeisImager. Minor editing of travel time curves by altering first arrival picks was necessary where background seismic noise obscured first arrivals. Analysis of first arrival picks was accomplished with the aid of travel time curves generated from first arrival data from shots within a spread. Travel time curves for respective spreads are presented in Appendix A. All of the original digital seismic refraction data is included on the CD-ROM that accompanies this thesis.

Two-way travel time analysis for a refractor dipping less than 10 degrees was accomplished for all seismic refraction spreads. The two-

way travel time refraction analysis was used, in collaboration with tomographic velocity analysis and borehole data, to determine refractor depth and geometry for three-dimensional modeling in the DTM. For the two-way travel time analysis, Microsoft Excel was used to make plots of travel time curves and calculate seismic velocities, depth to refractor, and refractor geometry for a simple two-layer velocity model. Figure 12 depicts the travel time curves generated for survey 1008 during this investigation and analyzed for a two-layer velocity model. Travel time curves and results of the two-way travel time analysis are presented in Appendix A.

The three-dimensional model of refractor geometry was input into the generated DTM of the study area and was then utilized to determine the volume of the Mission diamicton piedmont deposits. A discussion of the volumetric analysis method is presented in the volumetric calculations section of this thesis.

The two-way travel time analysis for a two or more layer model necessitates that the first arrivals of a shot have distinct crossover points along the travel time curves where changes in the slope of the curves occur. Some of the travel time curves for the two-way travel time analysis presented in Appendix A indicate that the travel time curves of first arrivals do not necessarily have discreet changes in slope or easily

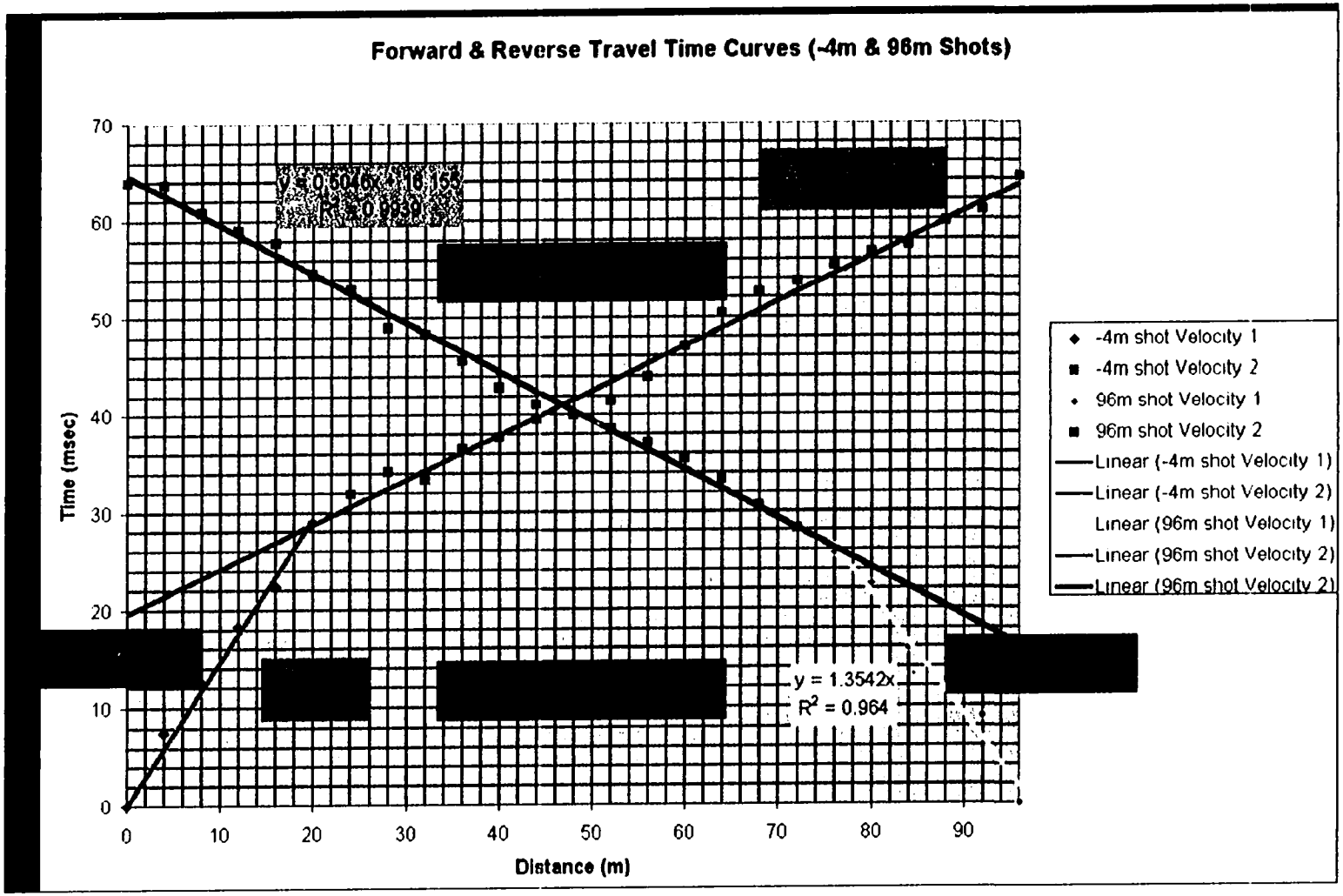

Figure 12. Two-way travel time analysis of a two-layer case velocity model for survey 1008. Calculated velocities for first layer (V1) and second layer (V2) and depths to refractor(Da and Db) are indicated on the graph.

identifiable crossover points. These curves indicate that the p-wave velocities increase gradually with depth.

Reynolds (1997) discusses the analysis and interpretation of seismic refraction data for sediments that would exhibit the effect of continuous velocity change. These sediment types would not exhibit discreet crossover points in travel time records for a seismic velocity layer. Reynolds (1997) further describes that it is not uncommon for sedimentary sequences in which grain sizes vary as a function of depth, such as fining upward or downward sequences, to experience continuous velocity changes. A classic debris flow sequence is inversely graded and thus one might anticipate a gradual increase in velocity when analyzing seismic refraction data to identify the thickness of debris flow deposits.

Some of the travel time curves either do not have distinct crossover points or the first cross-over point of a travel time curve indicates the first layer of the geophysical model is too thin, based on field observation and geomorphic expression, to represent the total thickness of the Mission diamicton. Therefore, a tomographic analysis of the seismic refraction data was done to aid in identifying the total thickness of the Mission diamicton. The tomographic analysis and velocity models are presented in Appendix A.

The tomographic analysis of the seismic refraction data was accomplished with the use of SeisImager seismic refraction processing

and analysis software developed by Geometrics, Inc. The first arrival picks and travel time curves developed during the two-way travel time analysis were used for tomographic analysis of seismic velocities. Travel time curves were inverted for a 10-layer seismic velocity model.

To identify the total thickness of the Mission diamicton where discreet crossover points are not readily identifiable on travel time curves, a combination of data was used to interpret the tomographic velocity models. The combination of highest p-wave velocities for the Mission diamicton, borehole data in the region of the piedmont deposits, and the measured p-wave velocity for the Monterey Formation determined from survey 1010 were used to identify the thickness of the Mission diamicton and interpret the tomographic velocity models.

Previous and current geologic maps indicate the presence of the More Ranch-Mission Ridge fault system in the study area (Dibblee, 1966 and 1986; Gurrola, 2002). Either main segments or splays from this fault system have been projected through the region of the Mission diamicton piedmont deposits by previous authors (Dibblee, 1986; Gurrola, 2002). The tomographic analysis was also used to examine evidence of geologic structure in the study area. A tomographic analysis of seismic refraction data can yield lateral changes in seismic velocities that may be correlative to fault offsets of geologic units in the region of the Mission diamicton.

Resistivity surveys were performed in late June of 2002 with the use of a Geometrics OhmMapper and data were recorded with a Geometrics DataMapper. The locations of the geophysical surveys are shown on Figure 3. Resistivity data were input into RES2DINV and RES2DMOD, developed by Geometrics, Inc., for processing resistivity data and developing resistivity models. Raw data were processed by removing abnormal spikes from data that are not representative of geologic features but are probably the result of inherent limitations, such as a temporary loss of electrical coupling between the transmitter, receiver, or ground surface, that occur during field data collection. The raw data model, pseudo-section, and resistivity model section are presented in Appendix B. Digital copies of the field collected resistivity data are included on the attached CD-ROM.

Geophysical Investigation Results

As part of the analysis of geophysical data, borehole data were acquired. Due to the unavailability or lack of data, borehole data to depths needed to identify the thickness of Mission diamicton could only be obtained from one hydrogeologic investigation (Hoover and Associates, 1984). The locations of boreholes and the logs of the boreholes are presented in Appendix C. The sediments in the boreholes identify the

cumulative thickness of Mission diamicton and fanglomerate materials, as well as depth to the Monterey Formation in some locations. The Mission diamicton and fanglomerate sediments were not properly distinguished at the time of the logging of the borings, probably due to the poor understanding of the regional geology at the time. Dibblee's (1986) geologic map, which would have been the current geologic map at the time the hydrogeologic investigation was performed, indicates that the Mission diamicton sediments were misinterpreted as fanglomerate or alluvial materials and thus accounts for the interpretation of the Mission diamicton being misinterpreted as fanglomerate material in boring logs.

Field mapping and seismic velocity analysis were used to identify the debris flow deposits associated with the Mission diamicton and distinguish diamicton from fanglomerate materials. A prominent seismic refractor is present at a depth less than the total thickness of deposits logged as fanglomerate materials. The differences in physical properties, which allow for the presence of the seismic refractor, indicate a change in geologic units across the seismic refractor. In locations where borehole logs encounter fanglomerate materials but seismic refraction data indicates the presence of a refractor at a depth shallower than the total thickness of logged fanglomerate materials, it is interpreted that the Mission diamicton overlays fanglomerate materials. This interpretation is based on the bulk velocity calculations, presented in Appendix D, that

indicate a change in geologic materials. The analysis of the seismic refraction data yields a variable thickness for the Mission diamicton piedmont deposits that range from approximately 6 to 13.5 meters. A summary of seismic velocities for the geologic materials encountered in the seismic refraction surveys is presented in Appendix A.

The seismic refraction velocities were analyzed to determine if the seismic refractor is related to the presence of ground water. The difference between direct arrival velocities, correlative with the first velocity layer from the surface, and refracted arrivals, correlative with the geologic materials underlying the first seismic velocity layer, is typically greater than 1000 meters/second. In order to establish that the velocity jump observed in travel time curves is related to a difference in geologic material properties and not the presence of ground water in a uniform geologic material, an analysis of bulk velocities from direct arrivals was accomplished to determine the velocity jump expected if unsaturated geologic materials of the Mission diamicton were saturated due to ground water.

Bulk velocity analysis calculations presented in Appendix D indicates that for an assumed porosity of 50 percent for the Mission diamicton sediments, a maximum velocity contrast of 200 meters/second is expected for P-waves transitioning from unsaturated to ground water saturated pore space. Costa (1986) has documented 20 to 80 percent air

volume for debris flows. It is assumed that a portion of the air volume, which becomes the void space of the debris flow deposit, is diminished at the time of deposition and subsequent void space is lost with consolidation of deposits. Therefore, the assumed 50 percent void space used in bulk velocity calculations is a reasonable estimate of void space in the Mission diamicton. Because the maximum velocity contrast of 200 m/s can be expected from ground water saturation of Mission diamicton sediments and the typical velocity contrast between the two primary velocity layers of interest is typically greater than 1000 m/s, the velocity calculations presented in Appendix D demonstrate that the refractor is not due to ground water saturation but rather to a change in geologic materials. It is interpreted that the change in geologic materials is the contact between Mission diamicton and different underlying geologic materials.

The tomographic analysis of data identifies intermediate velocities not distinguishable in travel time analysis for a two-layer velocity model. The tomographic velocity analysis also provides insight into the thickness of the Mission diamicton when p-wave velocities are gradually increasing through the thickness of the Mission diamicton. Additionally, interpreting intermediate seismic velocity layers with consideration to borehole data allows for insight into the geologic structure of the region

when seismic velocities can be correlated to geologic features exposed in nearby outcrops.

The tomographic velocity models for seismic refraction surveys 1006 and 1008 have lateral velocity changes that are correlative to the regional geologic structure of the study area. The Mission diamicton is located on the western portion of the Mission Ridge anticline. The Mission Ridge anticline is a westerly propagating anticlinal fold related to More Ranch-Mission Ridge thrust faulting (Gurrola, 1999). The tomographic velocity models are consistent geologic thrust fault propagation fold models proposed by Gurrola (1999) and Gurrola and Keller (1997) for the Mission Ridge anticline. Stream cuts expose splays of the More Ranch fault in Mission Creek. Mission Creek stream cuts expose fault offsets of the Monterey Formation that are correlative to velocity offsets observed in the tomographic velocity model for survey 1008. The tomographic velocity model for survey 1008 is presented in Figure 13. Figure 14 depicts the clearly exposed structural relationships and style of the More Ranch Fault in a sea cliff exposure at a Santa Barbara beach southeast of the study area. Fanglomerate velocity offsets in tomographic models are interpreted based on faulting offset observed in weak bedding of fanglomerate materials in stream cuts.

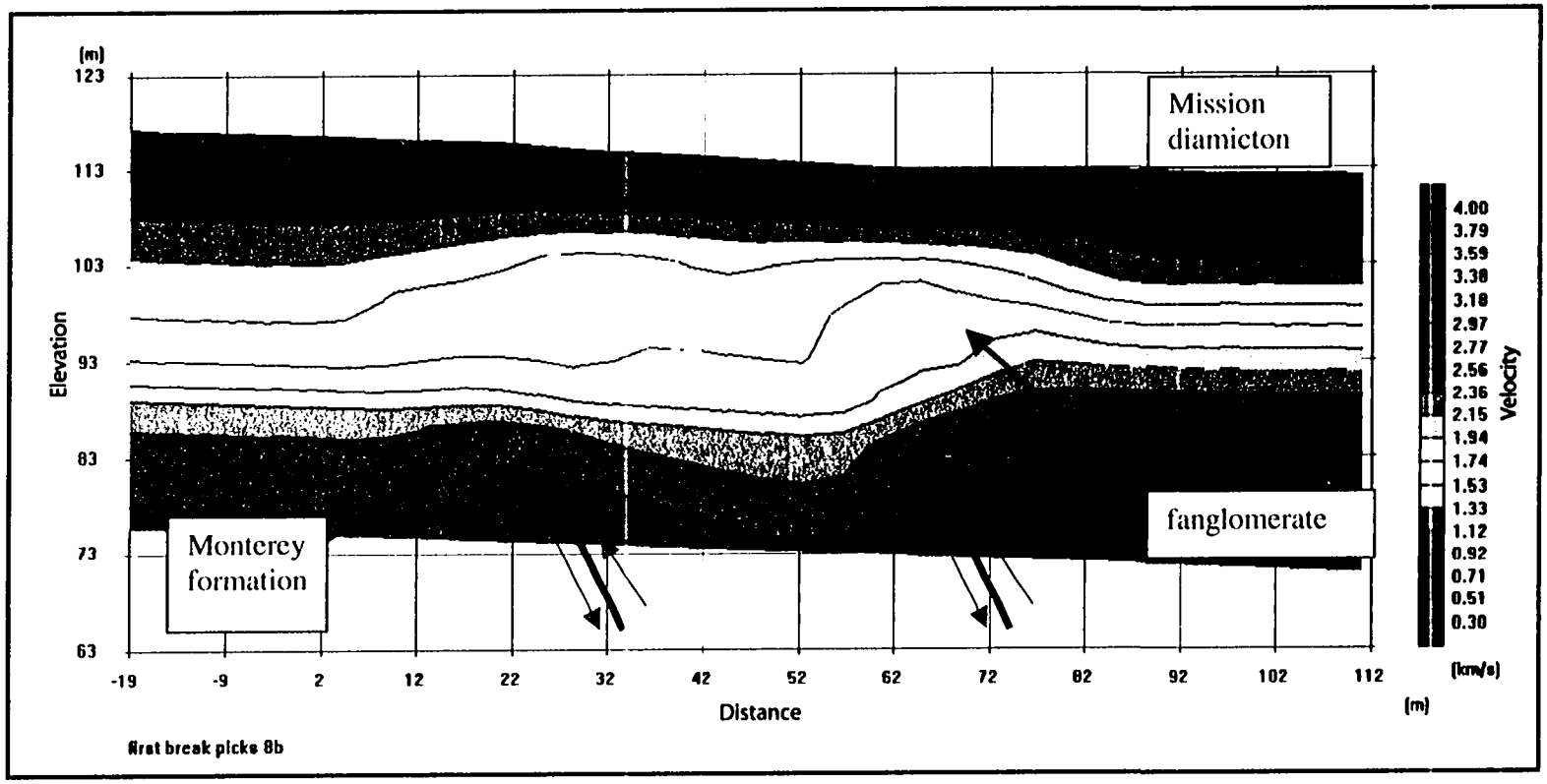

Figure 13. Tomographic analysis velocity model for survey 1008. Survey trends approximately N036E from right to left. More Ranch-Mission Ridge fault locations (indicated in red) are interpreted from lateral velocity changes that are not observed in velocity models where faults are not anticipated. Length and number of discreet faults are unknown.

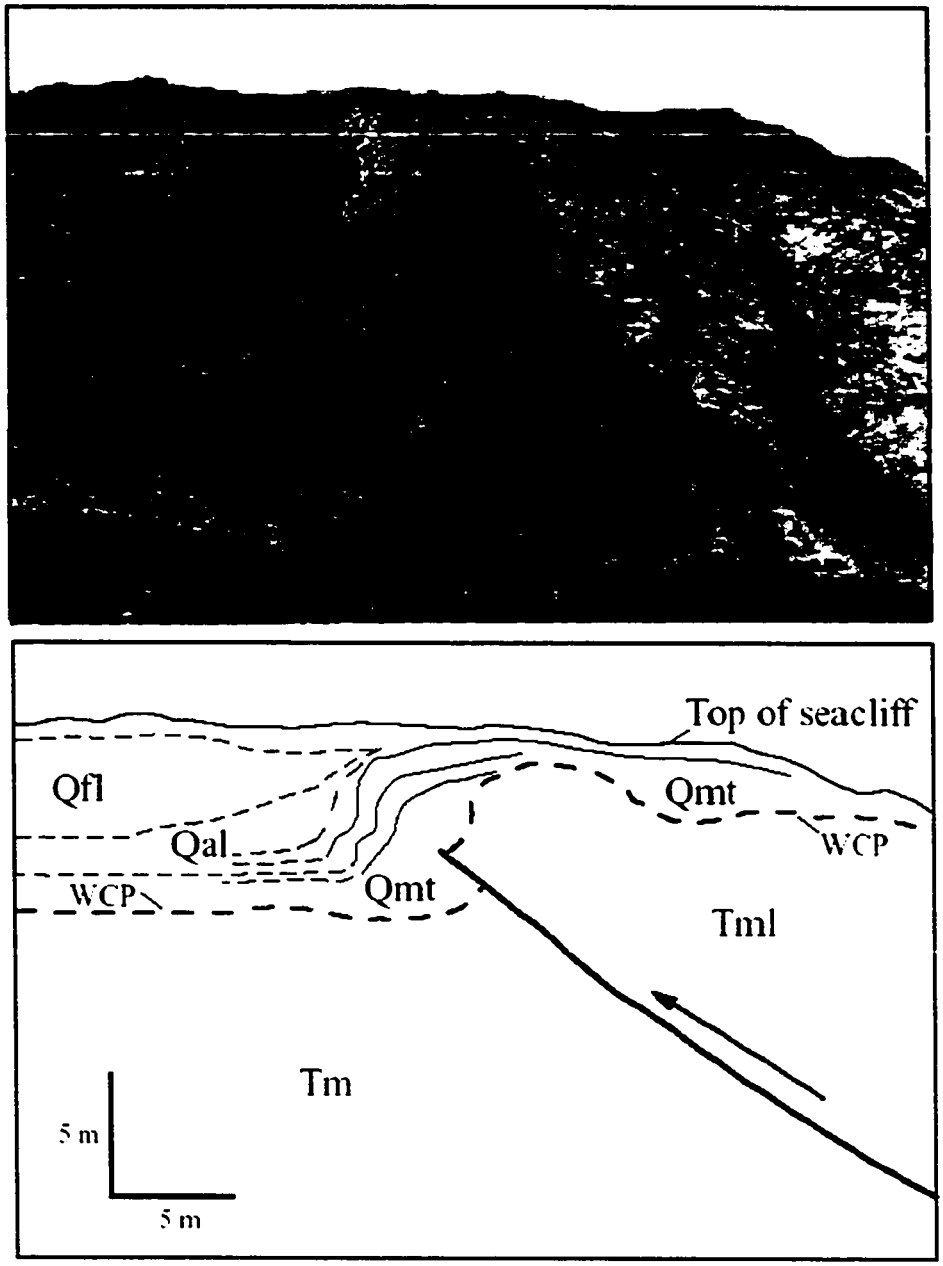

Figure 14. Photograph and sketch of the More Ranch fault sea cliff exposure at Ellwood Beach southeast of the study area. The drape anticline folds Quaternary marine terrace (Qmt), alluvial (Qal) and fluvial (Qfl) sediments. The wave-cut platform (WCP) on top of Tertiary Monterey Formation (Tm and Tml-lower member) is vertically offset about 6 m. Figure 14 provided by Dr. Edward Keller at the University of California at Santa Barbara.

An alternative to the faulting interpretation of the tomographic velocity models is that sedimentologic differences are responsible for the lateral velocity changes. The sedimentologic interpretation is not likely because velocity models in regions where faults are not anticipated, such as survey 1009, do not depict dramatic velocity changes as observed in surveys 1006 and 1008. The tomographic velocity model for seismic refraction survey 1009 displays velocity layers of the fanglomerate exposed in Mission Creek stream cuts along the eastern margin of the Mission diamicton piedmont deposits. And, the topographic modifier, Mission Creek, which could have been responsible for sedimentologic re-working in the region where the seismic refraction surveys are located, is known to have remained along the eastern portion of the Mission diamicton piedmont deposits, away from the body of the debris flow fan. Paleo-stream channels present along Mission Ridge document the paleo-location of Mission Creek along the eastern portion of the Mission diamicton and the westward propagation of Mission Ridge (Fig. 15). Therefore, it is unlikely that sedimentologic reworking is responsible for the lateral velocity changes in tomographic velocity models in the vicinities of projected faults.

Figure 15. Mission Creek paleo-channels (figure from Gurrola, 2002). The uplift of Mission Ridge and subsequent deflection of Mission Creek to the west, as well as lack of Mission diamicton deposits in the Mission Creek paleo-channels, indicates Mission Ridge was present prior to deposition of the Mission diamicton. Yellow stars refer to ^{21}Ne sample site location. Green arrow indicates anticline and direction of plunge. Red lines indicate fault locations. Dark blue line indicates modern stream location. Light blue indicates defeated stream locations. Qf refers to quaternary alluvial fans with the number 1 referring to the youngest fan and the number 5 refers to the oldest fan. Qf_4 (fanglomerate) is located to the north and south of Qf_1 (Mission diamicton piedmont deposits) suggesting Qf_4 (fanglomerate) is under the Mission diamicton. The fanglomerate is identified in both borehole data and geophysical data collected during this investigation.

Skofield Landslide Region and Rattlesnake Canyon Slope Failures

The Mission diamicton deposits terminate at the region of Skofield Park in Rattlesnake Canyon (Fig. 10). Aerial photographs of the study area were used to locate potential source area contributions to the Mission diamicton. A list of aerial photographs is presented in Table 3.

The Skofield landslide was originally identified by Urban (1999) and later an additional region of landsliding just north of, and adjacent to, the Skofield landslide was identified by Urban (2000). An aerial photograph of the study area depicting the distinct head scarps of the Skofield landslide and area of undifferentiated slope failures just north of the Skofield landslide is presented in Figure 16.

Morphology

At the termination of the Mission diamicton, aerial-photo analysis of this region indicates the presence of a large steep arcuate scarp (maximum height of 53 m) on the southeast side of Rattlesnake Canyon and encompassing Skofield Park (Fig. 16). This area has been interpreted as having the presence of a large compound and complex landslide, termed the Skofield landslide (Urban, 1999). Urban (2000 and 2002) also describes a region of slope failure just north of the large landslide complex (Fig. 16).

Table 3. Aerial photographs reviewed during this investigation.

Flight	Date	Scale	Frames
C-311	1928	1:18,000	B10 to B12; C11 to C13
C-430	1929	1:24,000	B33 to B35; C42 to C44
C-24989	1965	1:12,000	28 to 30; 35 to 38; 43 to 46
HB-QR	1970	1:48,000	33 to 34
PW-55010	1995	1:12,000	82 to 86; 104 to 107
PW-SB-10	1997	1:24,000	50 to 53; 27 to 30; 92 to 93

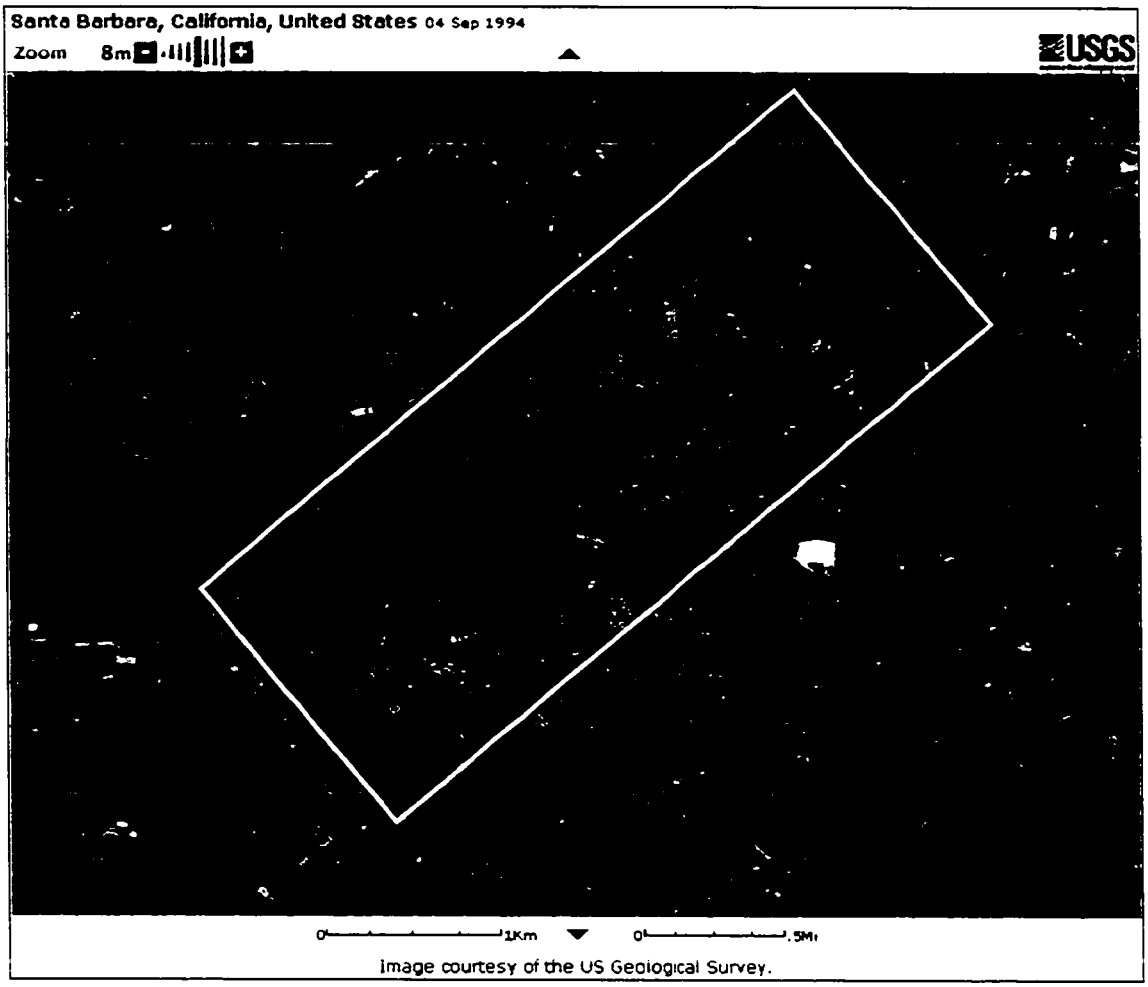

Figure 16. Aerial photograph depicting the Skofield landslide region. Study area region indicated within yellow rectangle. Note the northeast trend of canyon slopes that is used to infer an interpreted paleoslope reconstruction in the region of slope failures just north of the Skofield landslide region indicated by red arcuate line.

The Skofield landslide and nearby region of slope failure is recognizable by a series of steep arcuate head scarps (Figs. 16 and 17). The steep arcuate head scarps decrease in slope gradient to moderately steep slopes. The slope gradient change is resultant from head scarp degradation. The moderately steep slopes change into gentle to very gentle slopes with several subtle but slope truncating body scarps (Figs. 17 and 18). The gentle slopes are segmented by body scarps and are interpreted to be the tops of landslide blocks. Urban's (2000) analysis of aerial-photos, photo-realistic rendering of the DTM, and field observations also indicated the presence of body scarps within the Skofield landslide.

Selting (2002) also recognized the presence of scarps by morphologic analysis and interpretation of the 3-meter grid DEM (Fig. 19). However, Selting (2002) interpreted the location of landslide scarps that are actually the morphologic expression of engineering cuts related to the construction of a parking lot at Skofield Park, Los Canoas Road, or horse corrals built near the beginning the 20th century by local vaqueros (Fig. 19). In addition, Selting (2002) misinterprets the Skofield landslide body geometry as a result of analyzing exaggerated cross-sections (Fig. 19b).

The Skofield landslide body is comprised of multiple landslide blocks that are segmented by body scarps. Cross-sections of the Skofield

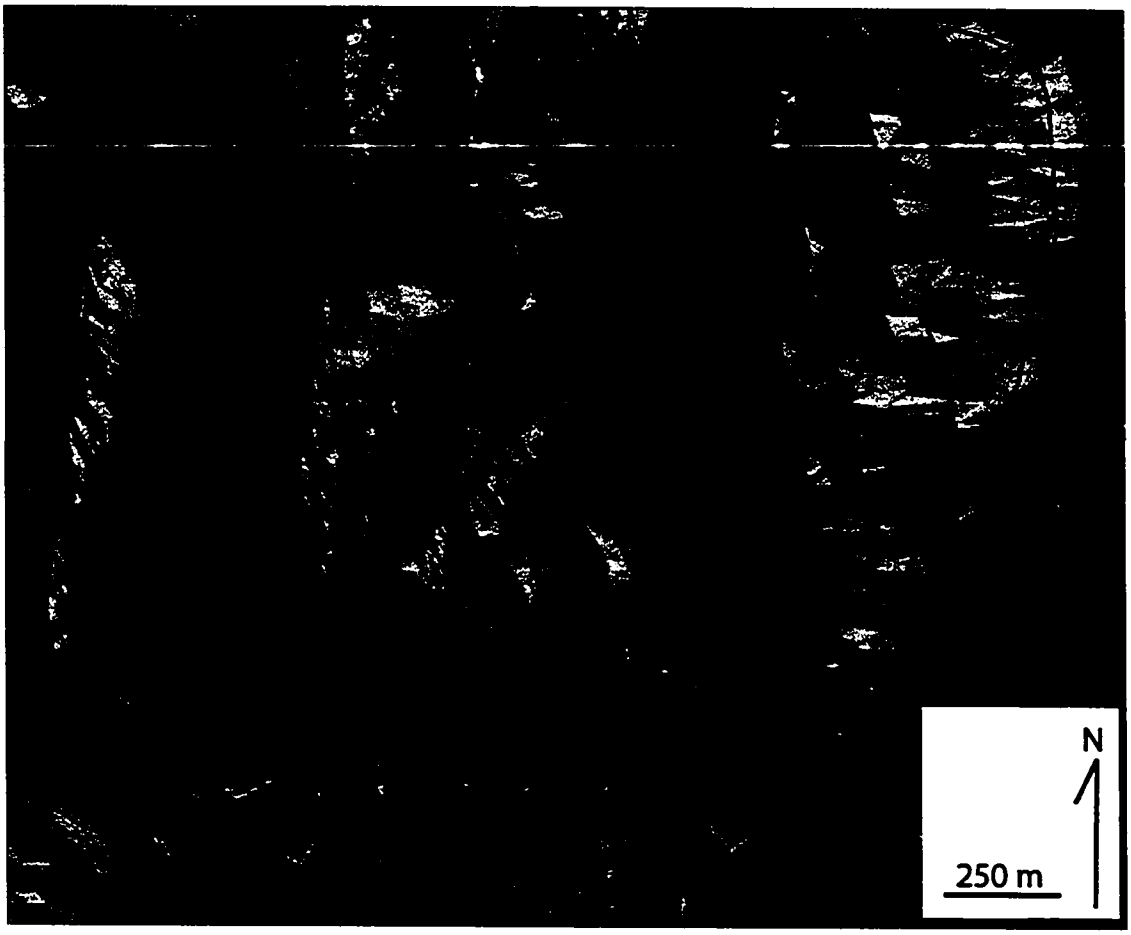

Figure 17. Photo-realistic render of the Skofield landslide region. Landslide and landslide deposits depicted within blue regions. Unnamed fault mapped by Gurrola (2002) indicated by red line with no distinction between concealed/unconcealed. Tick points for cross-sections in Figures 18 and 25 indicated with green.

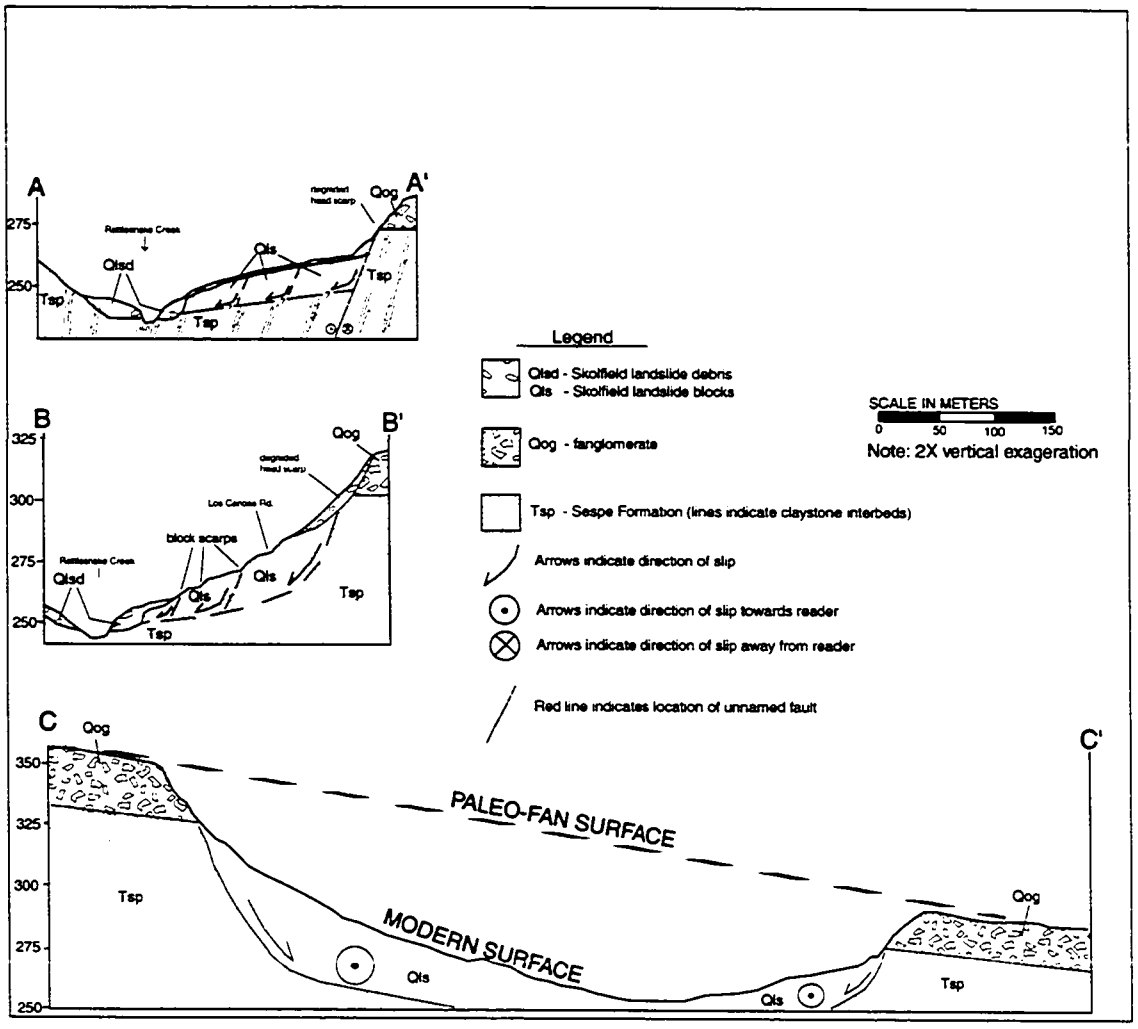

Figure 18. Diagrammatic cross-sections of the Skofield landslide region. Landslide debris has similar sedimentologic characteristics as the spatially higher fanglomerate deposits (see sections A and B). Basal failure plane of the Skofield landslide is unknown.

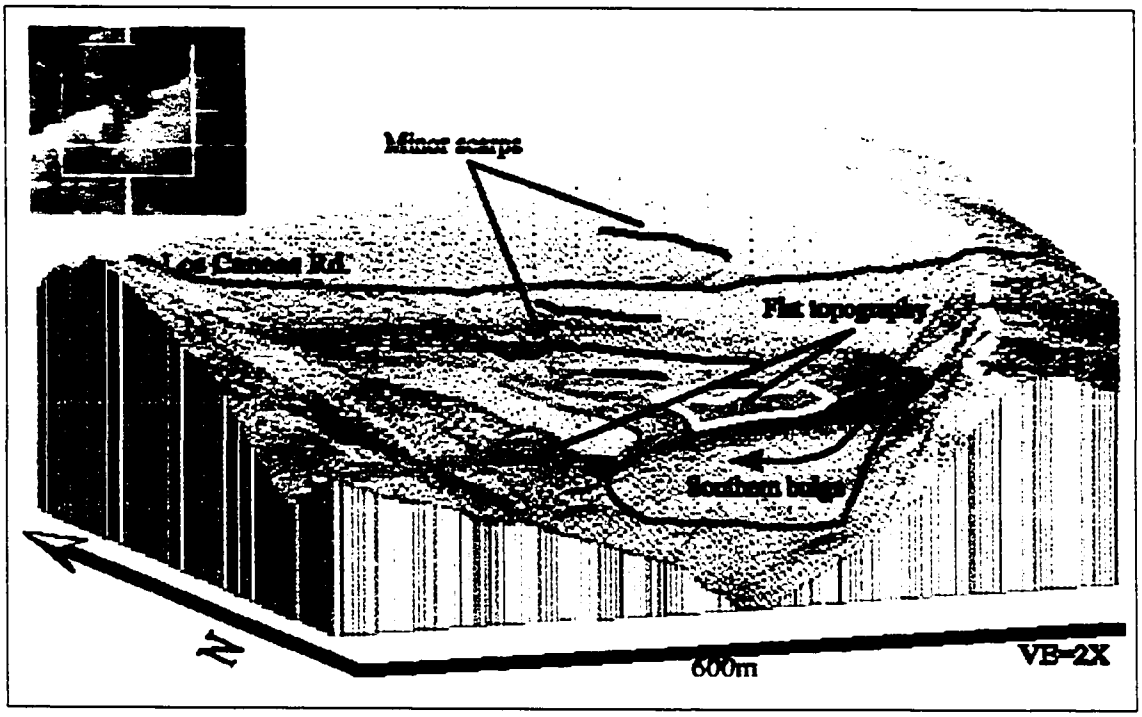

Figure 19a. Digital elevation model of Skofield landslide region. Selting (2002) interprets locations of scarps are either not expressed in field conditions or are actually man-made morphologic features. The two blue lines below Los Canoas Road are man-made features related to Los Canoas Road and parking lot cut slopes at Skofield Park. Figure from Selting (2002).

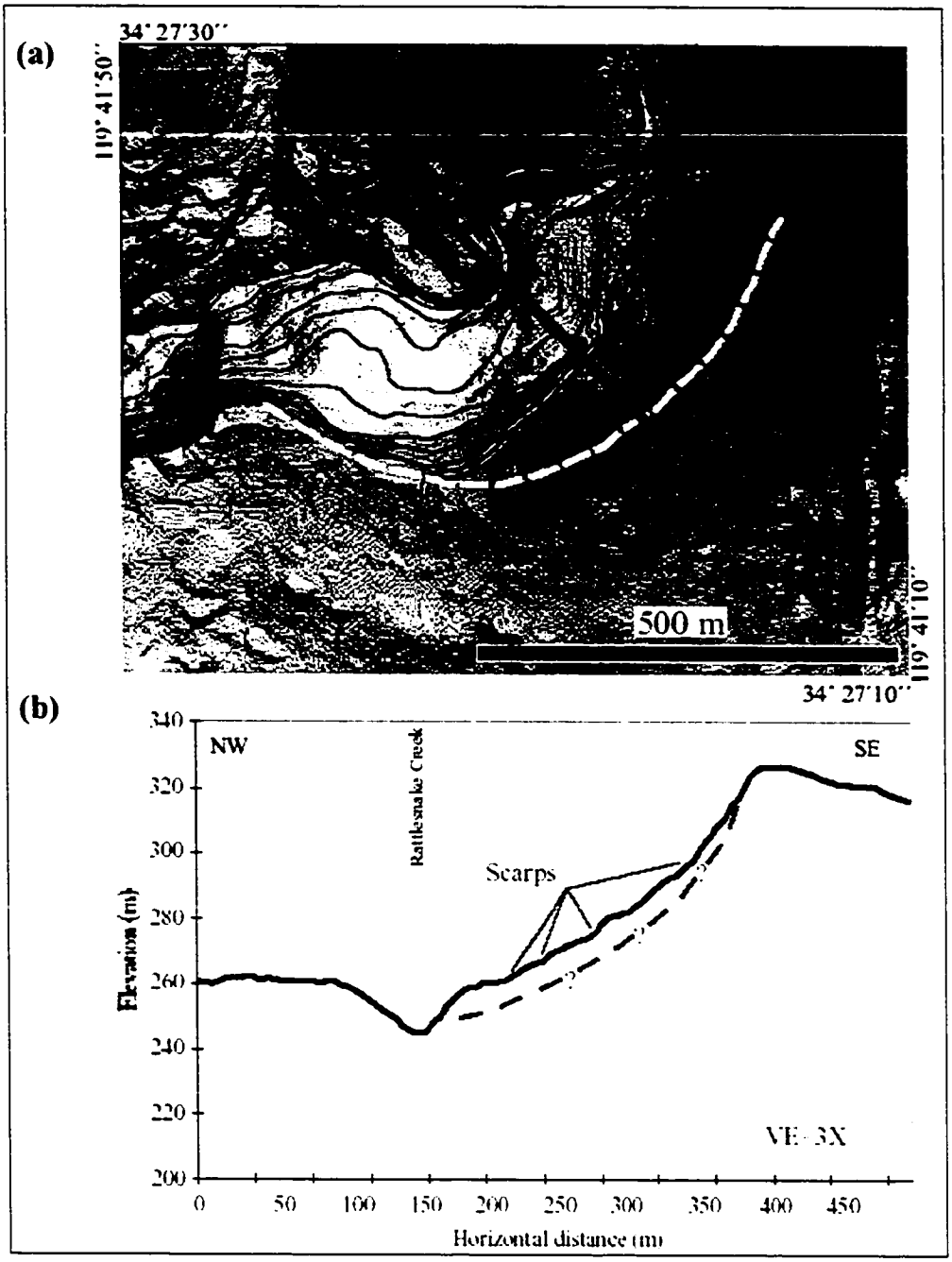

Figure 19b: Selting (2002) exaggerated cross-sections. Over-exaggerated vertical section depicts some scarps that are not observed in the field or are man-made features related to Los Canoas Road and the Skofield Park parking lot. Figure from Selting (2002).

landslide illustrate that the landslide blocks do not have back rotated bodies typical of rotational landslides (Fig. 18). The lack of back rotation within internal landslide blocks supports the interpretation that translational movement dominates the Skofield landslide.

Geologic Mapping

A previously published geologic map by Dibblee (1986) and a recent geologic map by Minor et al. (2002) indicate that the Sespe Formation is overlain by Quaternary fanglomerate in the Skofield landslide region (Fig. 20). A geologic map including the Skofield landslide region developed during this thesis work is presented in Figure 3.

Outcrops of interbedded gray to buff sandstone and reddish-brown siltstone and mudstone beds of the Sespe formation are present at the base of Skofield landslide. Bedding at these outcrops measured by Urban (2000) and Selting (2001) coincide with bedding orientations measured by Dibblee (1986) and Minor et al. (2002). No indication of a slip surface has been observed in the vicinity of the Skofield landslide. Bedding orientations within a rotational landslide would not be expected to be congruent with bedding orientations outside of the body of the landslide. However, the congruent orientation of bedding to regional bedding attitudes and lack of slip surface at the Skofield landslide

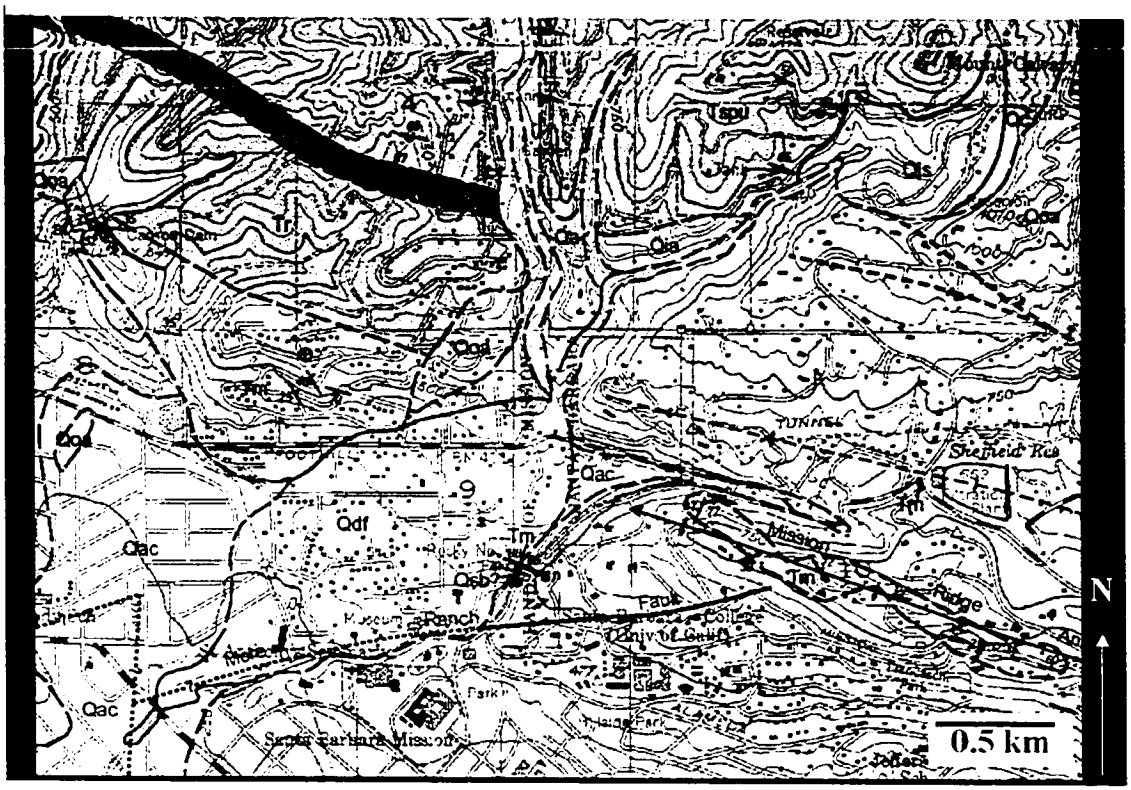

Figure 20. Study area region of the Preliminary Geologic Map of the Santa Barbara Coastal Plain, Santa Barbara County, California (Minor et al., 2002). Geologic units from oldest to youngest include: Tspu – Sespe Formation; Tv – Vaqueros Formation; Tr – Rincon Formation; Tm – Monterey Formation; Qoa – Older alluvium [fanglomerate as named by Dibblee (1986)]; Qac – Young alluvium; Qls – landslide (Skofield landslide); Qdf – debris flow deposits (Mission diamicton).

should not eliminate consideration of a bedrock failure plane(s). If the dominant displacement of the Skofield landslide is by translation to the north or northwest, the bedding orientations within the body of the landslide may preserve a resemblance to regional bedding if translation direction is perpendicular to the east–west bedding strike.

Several geologic features have relationships to the Skofield landslide. The southern terminus of the Skofield landslide appears to be bound by an unnamed fault mapped by Gurrola (2002). Gurrola (personal communication, 2003) states that this unnamed fault has significant sinistral displacement within a zone of transpressional deformation.

The Sespe formation in the region of the Skofield landslide, as well as outcrops throughout Rattlesnake Canyon, has ubiquitous joints observable in outcrop. Joint and bedding orientations from Sespe formation outcrops in Rattlesnake Canyon were measured according the selection method discussed by Nickelsen and Hough (1967). An equal area stereonet projection of joint and bedding orientations collected during the field investigation of this study is presented in Figure 21. Representative samples of joints were collected from measurement stations. Joint set samples were obtained by collecting rock samples from both sides of a joint set and scribing spatial orientation directly onto samples for later re-orientation. These joint sets were tested for

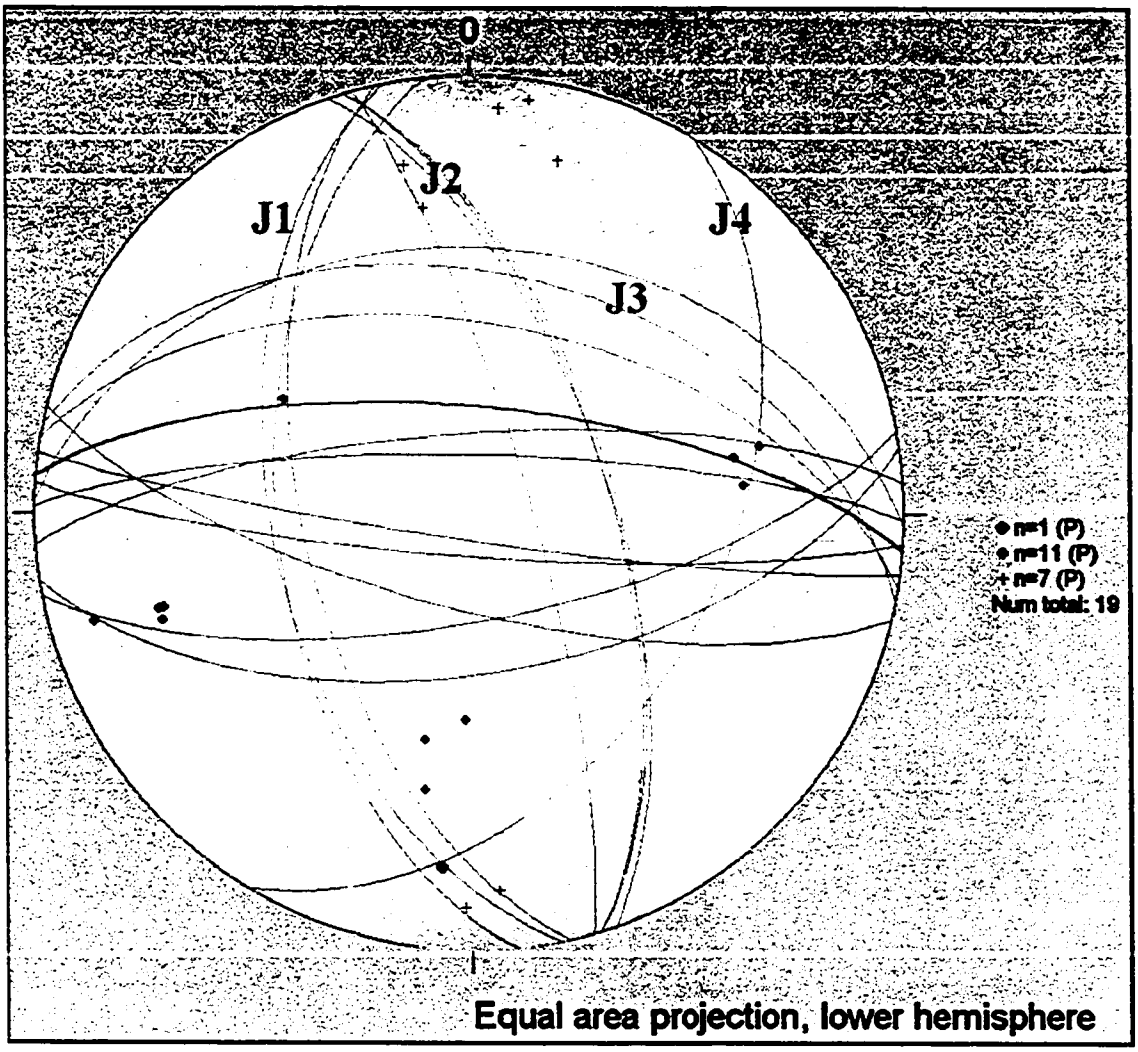

Figure 21. Stereonet projection of discontinuity orientations. Blue great circles and dots indicate joint sets and respective poles. Black great circles and crosses (+) indicate bedding plane orientations and respective poles. Red great circle and dot indicates the orientation of the unnamed fault mapped by Gurrola (2002). Yellow shaded circle is a 30-degree cone of friction determined by Markland's Test for the friction angle of discontinuities. With respect to slopes in Rattlesnake Canyon and underlain with Sespe Formation bedrock, slopes exceeding the dip of joint sets J1/J3, J2/J3, and possibly J3/J4, wedge failure is anticipated. Planar failure is anticipated for slopes exceeding dip of joint set J3.

friction angle according to the Markland's Test described by Hoek and Bray (1981). Table 4 depicts the friction angles of discontinuities determined according to Markland's Test. The results of the discontinuity analysis were used in the geohazard analysis for slope failure and landslide dam formation in Rattlesnake Canyon discussed later in the Geohazard Evaluation section in this thesis.

Overlying the Sespe Formation, an inactive fanglomerate alluvial fan displays similar sedimentary characteristics to the Mission diamicton. Landis (2002) dated the fanglomerate fan as mid- to late-Pleistocene by cosmogenic dating techniques. Both the fanglomerate and Mission diamicton contain poorly sorted coarse deposits with predominately arkosic sandstone boulders and cobbles (Fig. 22). Though the fanglomerate and Mission diamicton are both typically matrix supported, the percent of matrix present in the fanglomerate is generally less than matrix present in the Mission diamicton based on qualitative assessment of field outcrops. Fanglomerate clasts are predominately sub-angular with few angular clasts. Mission diamicton clasts are predominately sub-rounded with fewer sub-angular clasts than the similar fanglomerate materials. There is a subtle increase in rounding of Mission diamicton clasts as compared to fanglomerate materials. Qualitative field observations note an increase in rounding of Mission

Table 4. Friction angles of Sespe Formation discontinuities as determined according to Markland's Test. Refer to Figure 21 for graphical depiction of joint set orientations.

	Joint Set	**Friction Angle (degrees)**		
Sespe Formation Discontinuities	J1	30	37	34
	J2	34	33	30
	J3	35	30	34
	J4	31	30	33

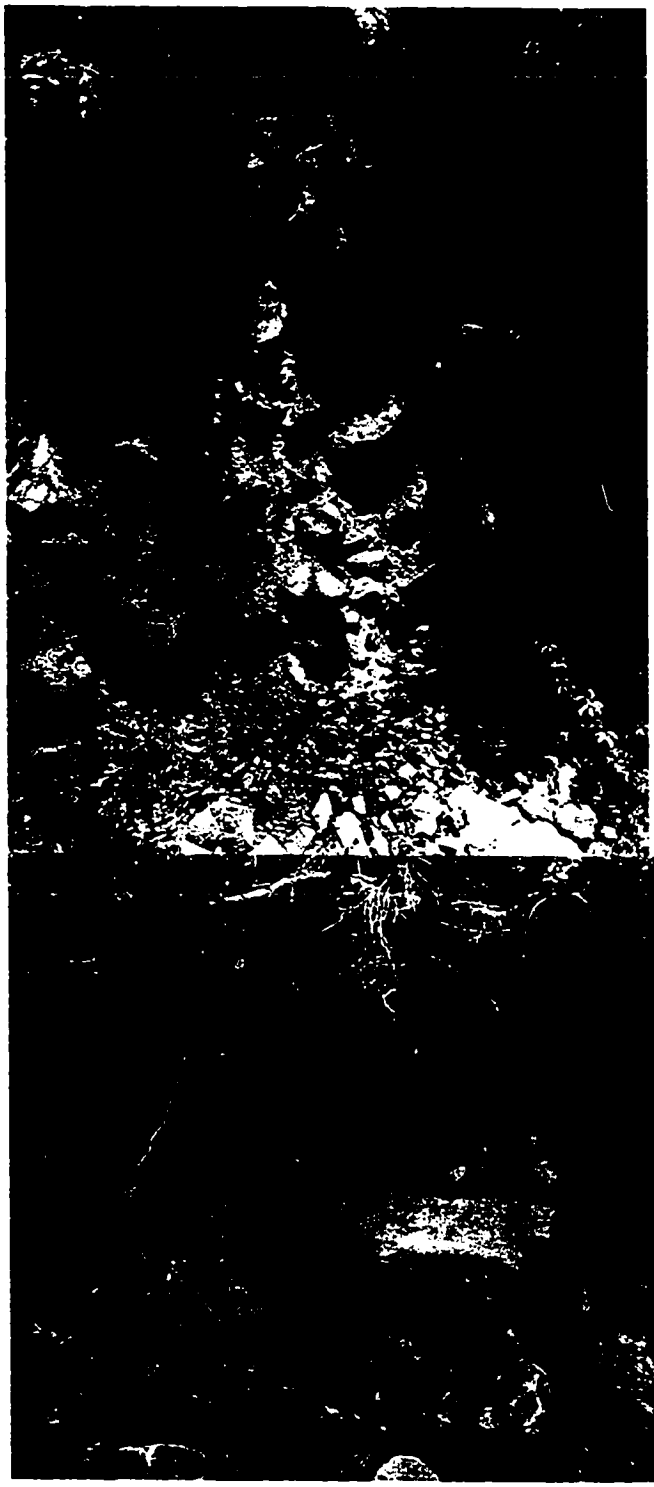

Figure 22. Fanglomerate source material and Mission diamicton deposits: (a) fanglomerate on the left and (b) Mission diamicton below. Fanglomerate materials have a higher clast to matrix ratio than the Mission diamicton. Angularity of clasts is higher in fanglomerate materials than the Mission diamicton. Transport of fanglomerate materials could produce the sedimentologic characteristics of the Mission diamicton.

diamicton clasts with increasing distance from the Skofield landslide region.

On the north side of Rattlesnake Canyon and opposite the Skofield landslide is a terrace comprised of material similar to displaced fanglomerate found on and around the Skofield landslide. The presence of large boulders scattered on this terrace resembles the Mission diamicton. Though this deposit appears similar to the Mission diamicton, characteristic debris flow features are lacking. Spatially, these deposits are not at the same elevation as the base of fanglomerate deposits and Sespe Formation contact in this region (Fig. 18). Therefore, these deposits are interpreted to be remnants of landslide debris associated with the Skofield landslide. Because the landslide debris is present on both sides of Rattlesnake Canyon, the Skofield landslide is interpreted to be the remnants of a landslide dam.

During mapping of the Skofield landslide, a fine-grained sandy silt deposit with visible pieces of charcoal was identified near the northern terminus of the Skofield landslide body (Fig. 3). The simplified stratigraphic section and photograph of this outcrop are presented in Figure E1. The outcrop exposes Sespe Formation bedrock overlain by landslide debris derived from the fanglomerate, overlain by the fine-grained sandy silt with charcoal, and mantled by more fanglomerate derived landslide debris. The fine-grained charcoal bearing deposits lack

the landslide debris characteristics of over- and underlying landslide debris but appear to have a fluvial origin. These deposits may represent deposits that settled during the temporary formation of an impounded lake behind the Skofield landslide dam.

Selting (2002) reports a red clay deposit just upstream of the Skofield landslide dam and interprets this geologic material as lake deposits from the landslide dam identified by this study. Field observation of the outcrop reported by Selting (2002) indicates that the red clay is soil and colluvium derived from the Sespe Formation.

North of the Skofield landslide body is a region of undifferentiated slope failures with a subtle arcuate head scarp but lacking an easily distinguishable landslide body (Figs. 16 and 17). There are a few reasons why a morphologically distinct landslide body is not present in this region. One reason is that the landslide body may be obscured due to burial by subsequent head scarp degradation that is present in this region or the landslide body was subsequently removed from the region by a secondary geologic process. Another reason for lack of a distinguishable landslide body is that an individual landslide body did not exist due to the mode of slope failure, such as debris sliding or multiple compound landslides.

Though a distinguishable landslide body is not present in the region of slope failures north of the Skofield landslide, fanglomerate

materials displaced from the fan on the ridges of Rattlesnake Canyon are scattered at the base of Rattlesnake Canyon. These displaced materials are likely the remnants of landslide debris from this region of slope failure that have not been removed from the canyon by secondary processes such as erosion or the failure of the landslide dam discussed in this document.

Other forms of slope failure are identified in Rattlesnake Canyon (Fig. 10). Of importance to understanding the origins of the Mission diamicton, there are two large landslide bodies between the Skofield landslide region and the confluence of Mission and Rattlesnake creeks (Fig. 10). These two large bedrock landslides have a significant amount of exhumed landslide debris based on qualitative estimate of evacuated volume depicted in the photo-realistic rendering images produced from the DTM and the landslide debris from these two landslides was not observed in Rattlesnake Canyon. The large volume of exhumed landslide debris from these landslides could have easily blocked the drainage of Rattlesnake Creek, thus forming one or more landslide dams. The failure of these landslide dams may have produced the debris flows that are part of the Mission diamicton.

Geophysical Investigation of the Skofield Landslide

Geologic mapping and sedimentologic evidence identifies the Skofield landslide region as a source area of the Mission diamicton deposits. To evaluate the geohazard posed by slope failures and landslide dam formation in Rattlesnake Canyon to the City of Santa Barbara, an understanding of the kinematics by which the Skofield landslide formed as well as modes of other failures in Rattlesnake Canyon is needed to evaluate potential for future failure types. To identify structural features such as geologic offsets or shear zones that define the kinematics of the Skofield landslide, a ground penetrating radar (GPR) geophysical investigation of the landslide body was undertaken.

In March 2003, ground penetrating radar (GPR) surveys of the Skofield landslide were accomplished within regions of suspected kinematic indicators, such as the Skofield landslide body scarps. The GPR surveys were oriented perpendicular to morphologic body scarps and head scarps as well as parallel to the interpreted direction of dominant displacement. Data collected during the GPR surveys and developed GPR survey cross-sections are presented in Appendix F.

The GPR surveys were used to identify subsurface displacements of strong reflectors. The body scarp and GPR cross-section investigated in survey 03-03-A is depicted in Figure 23. For the GPR surveys, a

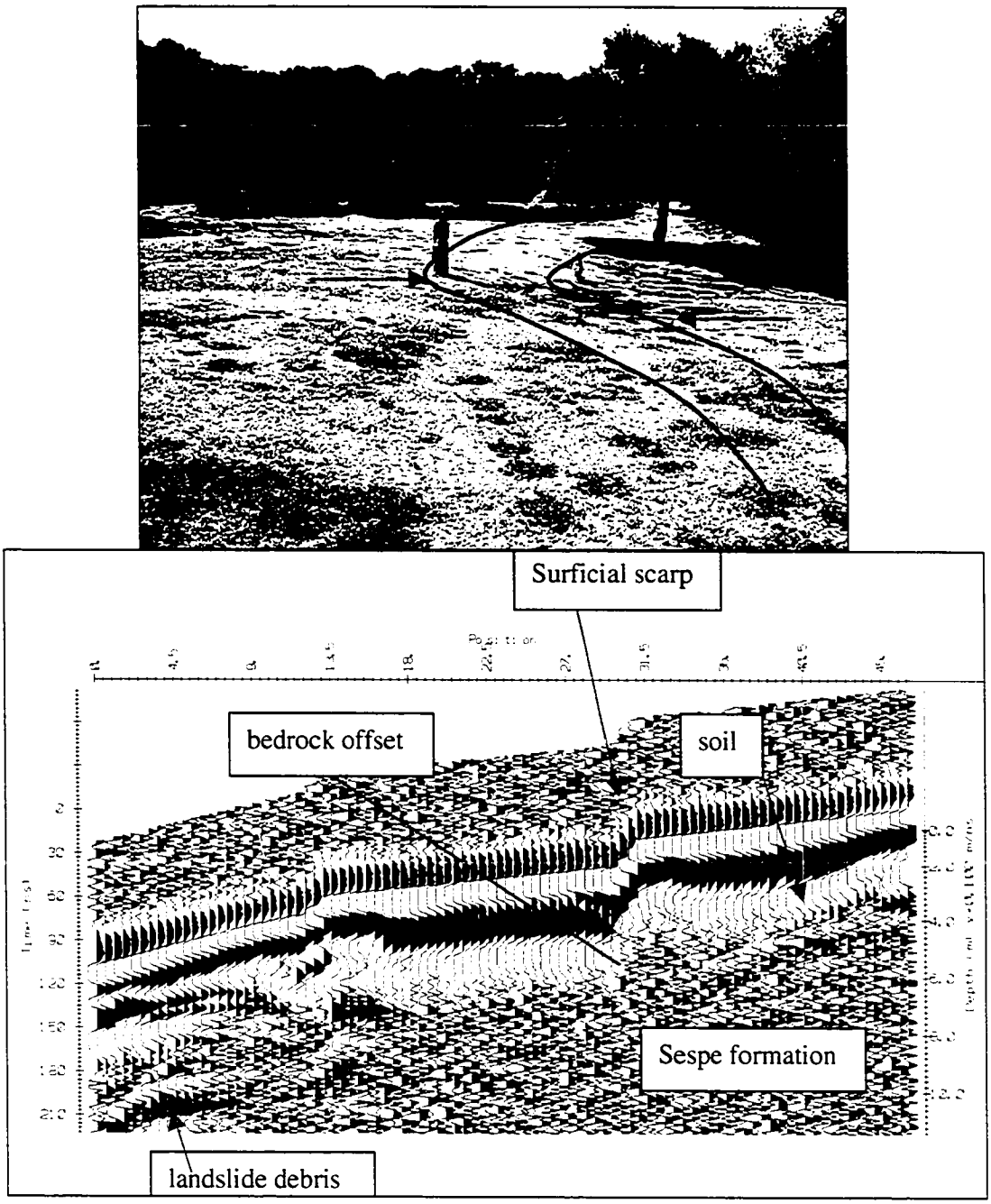

Figure 23. Surficial photograph of the location of GPR survey number 03-03-A and GPR cross-section. In the photograph, the red curvilinear arc and arrow on topside of scarp, blue curvilinear arc and arrow on downside of scarp. Scarp is approximately 1 meter in vertical height.

strong reflector is at a depth marking the top of Sespe formation bedrock under landslide debris. The southern portion of the Skofield landslide head scarp was also surveyed with GPR to identify potential subsurface displacements in body scarps and the region of the head scarp. The terrain on which surveys 03-03-B and 03-03-C were conducted is depicted in Figure 24. Displacements of strong reflectors at the anticipated depth of the Sespe Formation are interpreted as bedrock offsets related to the formation of the Skofield landslide; supporting the identification of the Skofield landslide and interpretation that rockslide slip surfaces are subsurface and the modern topographic surface is not the paleo-failure plane.

The geomorphic expression, geologic field relationships, and analysis of the GPR data, indicate that the Skofield landslide is a compound and composite landslide bound by an unnamed fault to the south and dominated by translated rockslide blocks according to the Varnes classification scheme (Varnes, 1978). Cross-sections of the Skofield landslide are presented in Figure 18. The narrow and confined geometry of Rattlesnake Canyon and the large Skofield landslide indicates that the Skofield landslide largely translated during initial failure in the Sespe Formation and formed a landslide dam in Rattlesnake Canyon.

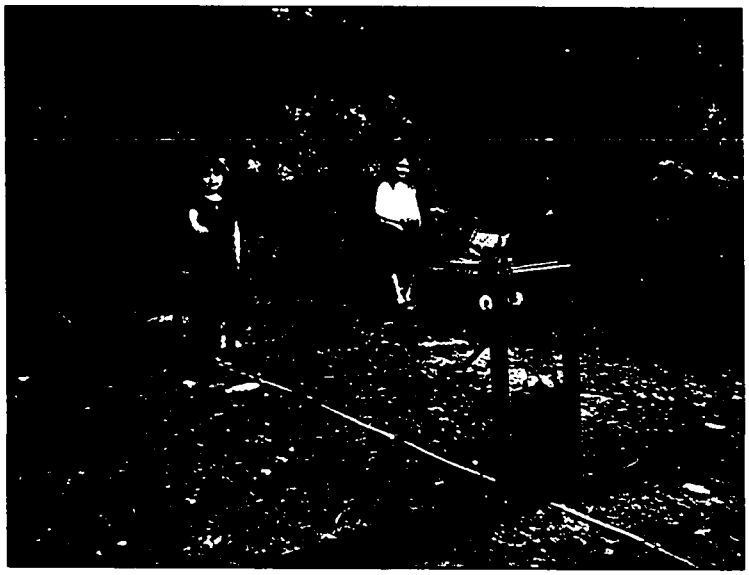

Figure 24. Surficial photograph of the location of GPR survey number 03-03-C.

Selting (2002) presents cross-sections of the Skofield landslide used to interpret that the dominant kinematics of the Skofield landslide was rotation. Selting's (2002) cross-sections, vertically exaggerated, give the false impression that the geometry of the Skofield landslide would be consistent with rotational landsliding (Fig. 19). A more representative geometry of topographic conditions are the cross-sections presented in this report. The cross-sections in Figure 18 indicate that rotation is not consistent with geometric characteristics of the Skofield landslide. Though the cross-sections depicted in Figure 18 are vertically exaggerated two times, it is identifiable that the geometric constraints of Rattlesnake Canyon and the size of the Skofield landslide indicate that a rotational failure in the Sespe formation is less likely than translational slip. Rattlesnake Canyon can accommodate a translational landslide the size of the Skofield landslide, but not a rotational landslide of the same size. If the Skofield landslide was dominantly rotational, then the radius of moment for rotation would need to extend to such heights that the Skofield landslide would be classified as translational for geometric reasons.

The kinematics of the Skofield landslide are interpreted as complex rocksliding of Sespe Formation blocks that initiated mobilization of the overlying fanglomerate materials into a debris slide. The debris sliding of

fanglomerate materials formed the arcuate scarp that is characteristic of the Skofield landslide. Figure 25 depicts the interpreted kinematics of failure for the Skofield landslide. The landslide debris of fanglomerate materials and Sespe formation bedrock became the source material for the Mission diamicton debris flows.

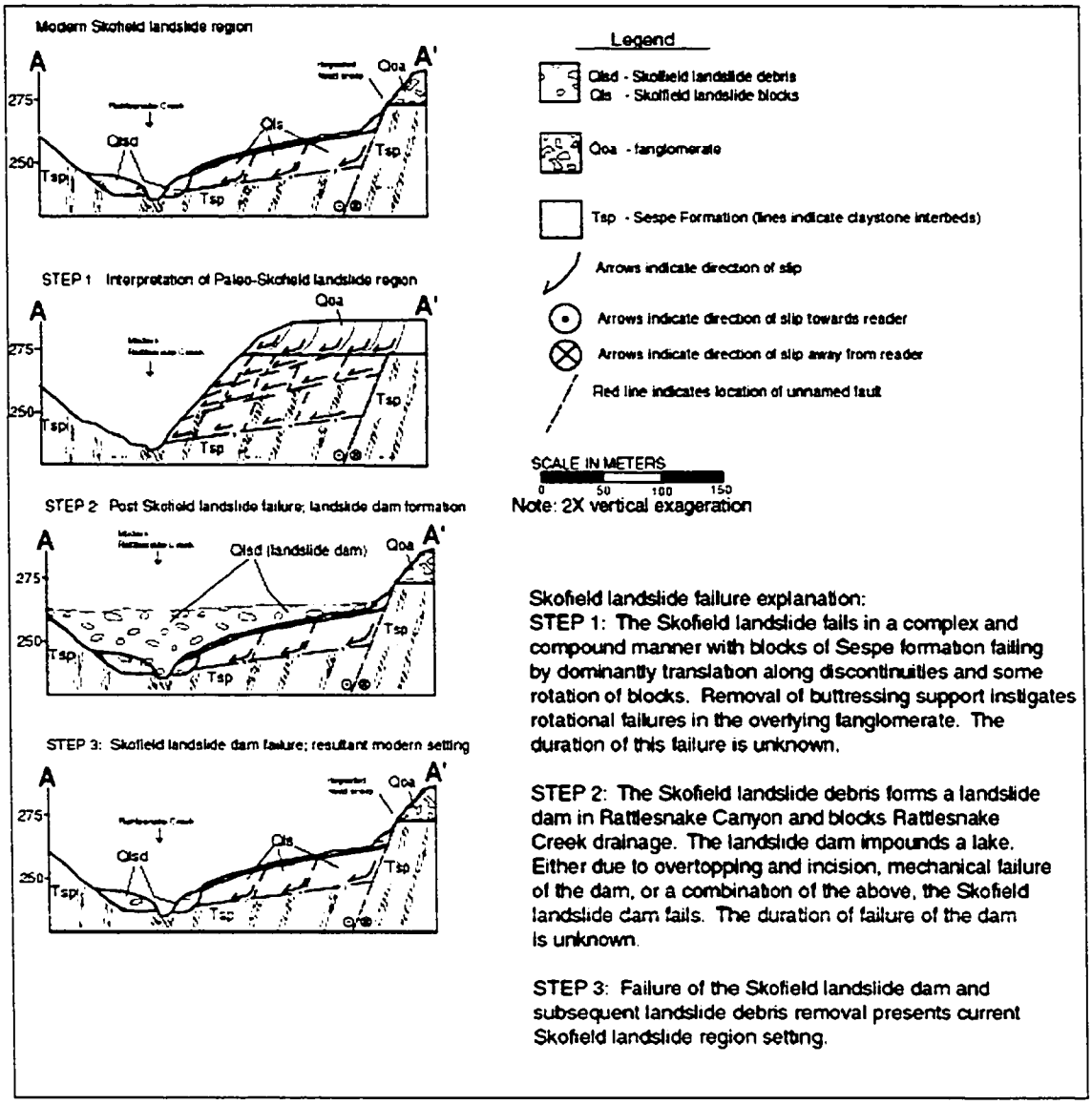

Figure 25. Diagrammatic cross-sections of the Skofield landslide failure. Section A to A' is located on Figure 17. The diagrammatic cross-sections illustrate the compound and complex kinematics of the Skofield landslide failure and the formation of the Skofield landslide dam.

HYPOTHESIS OF THE MISSION DIAMICTON ORIGIN

The southern flank of the Santa Ynez range, north of Santa Barbara, is characterized by narrow canyons with steep topography, factors which Costa and Schuster (1988) describe as contributors to increased susceptibility of landslide dam formation. Steep topography increases landslide susceptibility and narrow canyons are easier to block the drainage by slope failure. As a landslide dam impounds water, a build up of pore pressures in the landslide dam may lead to dam failure or water may spill over-top the dam and lead to rapid down-cutting, and ultimately dam failure (Costa and Schuster, 1988). Debris flows may form from landslide debris and water of the failed landslide dam, and have been documented to cause extensive loss of life and property (Costa and Schuster, 1988). Evans and DeGraff (1997) estimate that almost half of all fatalities resulting from major landslide disasters of the twentieth century are related to landslide dam failures.

Geologic mapping, geomorphic, and sedimentologic evidence indicates that the Skofield landslide region is a source area for the Mission diamicton. Thus, this study concludes that the Skofield landslide formed a landslide dam in Rattlesnake Canyon, blocking drainage of Rattlesnake Creek and forming a temporary lake. Evidence

of the potential lake deposits exists near the Skofield landslide. Charcoal samples were extracted from a sandy clay horizon stratigraphically above stream deposits and below Skofield landslide debris. This outcrop, from which charcoal samples were collected for radiocarbon dating, is presented in Figure E1 in Appendix E. The Skofield landslide dam had failed either due to internal failure of the landslide dam or over-topping and rapid down cutting of the landslide dam. Selting (2002) presents a longitudinal profile of Rattlesnake Canyon that depicts a nickpoint at the location of the Skofield landslide dam and interprets that the nickpoint indicates over-topping and incision of the landslide dam had occurred. The nickpoint, however, could be the result of ground deformation along the unnamed fault that is mapped in this region (Figs. 3, 10, and 17). The failure of the Skofield landslide dam resulted in a debris flow event with multiple large volume debris flows originating from landslide debris in the Skofield region and floodwaters from the release of the temporary lake.

Costa and Schuster (1988) document that 50 percent of documented landslide dams fail within the first week of formation and 90 percent of landslide dams fail within the first year of formation. Costa and Schuster (1988) describe case histories in which many landslide dam failures and the release of waters from temporary lakes produce a

series of landslides resultant from the rapid drawdown of a temporary lake.

The failure of the Skofield landslide dam released the water of the temporary lake and most likely resulted in rapid drawdown of the temporary lake that left unsupported and saturated slopes with a presumably lower shear strength. The slopes in the region where the temporary lake once existed would then have failed and contributed additional source material to the debris flows that traveled down Rattlesnake Canyon. This region of slope failure is depicted as the area just north of the Skofield landslide in Figure 17. The debris flows that flowed through Rattlesnake Canyon must have been fast traveling to produce the super-elevated deposits in the northern portion of the piedmont deposits (Fig. 3).

To test this geologic history interpretation for the origin of the Mission diamicton, a volumetric analysis of the Mission diamicton piedmont deposits and the Skofield landslide region was undertaken.

Testing the Hypothesis of the Mission Diamicton Origins: Volumetric Calculations

The Mission diamicton is a series of debris flow deposits that are largely deposited on the Santa Barbara piedmont. To test the validity that the bulk of the Mission diamicton originated as debris flows from

the failure of the Skofield landslide dam, a volumetric analysis of Mission diamicton deposits and the Skofield landslide region was accomplished.

Volumetric calculations of the hypothesized source, the Skofield landslide, and the debris flow fan were performed by Urban (2000 and 2002) and Selting (2001). Initial volumetric calculations by Urban (2000) estimated the Mission diamicton to be 9.13×10^6 m^3 based upon an estimated average thickness of 9 m and areal extent of 1.01×10^6 m^2 determined in the AutoDesk Land Development R2 GIS environment. Selting (2001) re-mapped the Mission diamicton and Skofield landslide and performed volumetric calculations that substantiated Urban's (2000) initial mapping and preliminary volumetric calculations. Selting (2001) also calculated a volume of 9.1×10^6 m^3 for the Mission debris flow based on remapped boundaries and an estimated average thickness of 9.3 meters. Selting (2002) later presents a total volume for the Mission diamicton as 10.92×10^6 $m^3 \pm 20\%$ using different geometries for the unknown paleosurface on which the Mission diamicton was deposited.

Preliminary volumetric calculations for material from the Skofield landslide initially proposed by Urban (2000) indicate that the Skofield landslide was the dominant source of sediment to the debris flow fan. Urban (2000) generated preliminary volumetric calculations of the Skofield landslide. Five topographic profiles of the Skofield landslide were analyzed and the estimated cross-sectional areas for material were

averaged. The average cross-sectional area of exhumed material was multiplied by the length of the straight line as measured between the lateral extents of the head scarp crown. This preliminary calculation method imploring fundamental integral calculus methods for an over-estimation yields an overestimate volume of approximately 7.89 x 10^6 m^3 of exhumed landslide debris from the Skofield landslide. The preliminary volumetric calculation method by Urban (2000) is the maximum amount of exhumed landslide materials from the Skofield landslide alone. Subsequent or improved calculations must have smaller exhumed volumes for the Skofield landslide.

Selting (2000) later calculated the Skofield landslide material using a MATLAB program written by C. Marcinkovich and reports an exhumed volume of 8.8 x 10^6 m^3. Selting (2000 and 2002) does not report the method by which this volumetric calculation was performed so an independent verification cannot be made. Selting (2002) presented an additional volumetric calculation using a method traditionally used for field estimation of ellipsoid volumes and estimated an exhumed volume of 9.9 x 10^6 m^3 for the Skofield landslide represented as a half-ellipsoid. Selting's (2001 and 2002) calculations are larger than should be anticipated from the Skofield landslide based on over-estimation calculations initially performed by Urban (2000). The over-estimation method is based on integral calculus and the approximation of area.

Urban (2000) approximated the maximum cross-sectional exhumed area of the Skofield landslide and multiplied the area by the distance between headscarp crown termination points.

The geometry of the Skofield landslide is not accurately depicted as a half ellipsoid. Selting (2002) misinterpreted the half-ellipsoid geometry from the over-exaggerated profiles generated in the landslide region (Fig. 18). Even if this geometry were correct, the exhumed landslide materials from the Skofield landslide would only be 50 to 60 percent of a half-ellipsoid for this calculation to be a more appropriate approximation of the volume of exhumed landslide debris. This interpretation is based on the assumption that the cross-sectional area of exhumed material resembles a quarter-ellipsoid rather than a half-ellipsoid. Interestingly, 50 percent, or a quarter ellipsoid, of Selting's (2002) is equal to 4.95×10^6 m^3. This quarter ellipsoid volume more closely matches the 3.7×10^6 m^3 volume determined by the three-dimensional volumetric analysis of the Skofield landslide presented by Urban (2002).

Utilizing the AutoDesk Land Development R2 GIS environment, Urban (2002) generated digital terrain models (DTMs) for differing paleosurface interpretations on which the debris flow fan is deposited and generated volumes ranging between 10.3×10^6 m^3 to 23.0×10^6 m^3. Utilizing the AutoDesk Land Development R2 GIS environment for volumetric calculations, Urban (2002) reports an exhumed volume from

the Skofield landslide of 3.7×10^6 m^3. It should be noted that the AutoDesk Land Development R2 GIS environment is commonly used in the civil engineering and geotechnical engineering industry to routinely perform cut-and-fill volumetric calculations for earthwork projects.

The completed field map of the Mission diamicton and Skofield landslide was digitized for volumetric and spatial analysis. A digital terrain model (DTM) of the subject area was generated in AutoDesk's Land Development R2 GIS environment. With the aid of a computer-processing platform, new volumetric calculations presented in this study were performed utilizing the DTM. Volumetric calculations in the Land Development R2 environment utilizing the DTM account for detailed topographic effects, allow multiple methods of performing calculations to test validity, and allow ease of calculating multiple paleosurface interpretations. Volumetric calculations utilizing the DEM of previous studies were abandoned due to reasons explained earlier in this thesis, such as the incomplete topographic data used to construct the 3-meter grid DEM.

Mission Diamicton Volumetric Calculations

The basal surface of the Mission diamicton identified in geophysical surveys was utilized to generate a digital terrain model TIN of

the paleosurface on which the Mission diamicton is deposited. The basal surface of the Mission diamicton is higher in elevation in the eastern portion of the study area and dips to the southwest. The trend of the surface identified in seismic refraction surveys 1001 through 1005 were used to define the east to west dip of the paleosurface on which the Mission diamicton was deposited. The north to south apparent dip of the paleosurface is defined in the volumetric analysis by seismic refraction surveys 1006 through 1009. The paleosurface on which the Mission diamicton was deposited was defined in the DTM by connecting the trends of the paleosurface identified from the seismic refraction surveys. The paleosurface in the region south of the large morphologic lobes of the piedmont deposits was modeled by joining the basal contact of the Mission diamicton mapped in stream cuts to contacts with alluvium to the west. The entire paleosurface on which the Mission diamicton was deposited as well as the present day topographic surface were modeled as a triangulated irregular networks (TINs), respectively.

Each TIN, one for the paleosurface of deposition and one for the present day topographic surface, was used to calculate the volume between surfaces, which is the total volume of Mission diamicton deposits. Because the areal extent of this area is large and the size of triangles used to model the topographic surfaces is small, it is not feasible to depict the TINs generated in this analysis as a presentable

figure. Therefore, all digital files used in the volumetric analysis are included on the CD-ROM accompanying this thesis.

The result of a volumetric calculation for the Mission diamicton piedmont deposits based on the geophysical data is 8.71 x 10^6 m^3. Because this volumetric analysis utilizes the complete topographic data set to account for topographic effects on volumetric calculations and the geometry of the paleosurface on which the Mission diamicton is defined by the geophysical investigation of this study, this is the most accurate volumetric calculation of the Mission diamicton.

The complex geometry of Rattlesnake Canyon and lack of 3-dimensional information regarding geologic contacts makes digital terrain modeling of the Mission diamicton canyon deposits impractical. Therefore, a generic volumetric analysis of the Mission diamicton canyon deposits is accomplished by using a general terrace fill geometry observed throughout Rattlesnake Canyon. The resultant volume of Mission diamicton deposits in Rattlesnake Canyon is approximately 0.5 x 10^6 m^3. The volumetric calculation of the Mission diamicton canyon deposits is presented in Table 5.

The total volume of the Mission diamicton deposits (9.21 x 10^6 m^3) is greater than the exhumed material calculations of 3.7 x 10^6 m^3 for the Skofield landslide alone, indicating the entire region of landsliding, including the Skofield landslide and areas to the north, has a closer

Table 5. Mission diamicton canyon deposits calculation.

Mission diamicton canyon deposits calculation	Measurements (average) in meters		
	Width	Depth	Length
	80	4	1500
	Volume = 480,000 cubic meters ~500,000 cubic meters		

volumetric match to the calculated volume of the Mission diamicton. A discussion of the landslide volumetric calculations is presented below. A summary of the volumetric calculations is shown in Table 6.

Source Area Volumetric Calculations

The evidence of a remnant landslide dam, lack of landslide debris equivalent to exhumed material from the Skofield landslide in the Skofield Park region, termination of Mission diamicton, and similarities between Mission diamicton and potential fanglomerate source sediments prompts further investigation of the Skofield landslide as a source area of the Mission diamicton.

A paleosurface interpretation of the Skofield landslide and nearby slope failure region was created as a 3-dimensional surface modeled as a TIN for volumetric analysis (Fig. 26). The paleosurface of the Skofield landslide is interpreted from analysis of a topographic profile of the Skofield landslide as well as general trends within Rattlesnake Canyon (Figs. 16, 17, and 18). The paleosurface of the slope failures just north of the Skofield landslide is based on the general trend of Rattlesnake Canyon (Fig. 16).

Table 6. Summary of volumetric analysis results. Volumes are reported in cubic meters. Volumetric calculations are reported in the chronological order in which accomplished and reported. Volumes reported in this thesis that includes identification of Mission diamicton thickness is indicated in **bold**.

Mission Diamicton					
Author	**Date**	**Method**	**Piedmont**	**Canyon**	**Total Volume**
Urban	2000	Estimated thickness based on field relationships	9.1×10^6	n/a	9.1×10^6
Selting	2001	Assumed thickness	9.1×10^6	n/a	9.1×10^6
Selting	2002	Geometric postulation	n/a	n/a	10.92×10^6 $\pm$20%
Urban	**2003**	**Thickness identification & 3-D modeling**	**8.71×10^6**	**0.5×10^6**	**9.21×10^6**
SOURCE AREAS					
Skofield Landslide					
Author	**Date**	**Method**	**Total Volume**		
Urban	2000	Cross-Section Area; Over-estimate integration	7.89×10^6		
Selting	2001	Matlab program	8.8×10^6		
Selting	2002	Half-ellipsoid	9.88×10^6 (note that 60 % of a half-ellipsoid more closely resembles landslide geometry which makes this calculation yield 5.93×10^6)		
Urban	**2003**	**Geologic Analysis & 3-D modeling**	**3.7×10^6**		
Slope Failures Associated with Skofield Landslide Dam Failure					
Urban	**2003**		**Geologic Analysis & 3-D modeling**	**6.6×10^6**	

Urban, 2003	**Mission Diamicton**	**Skofield Landslide & Slope Failures**
TOTAL VOLUME	**9.21×10^6**	**10.3×10^6**

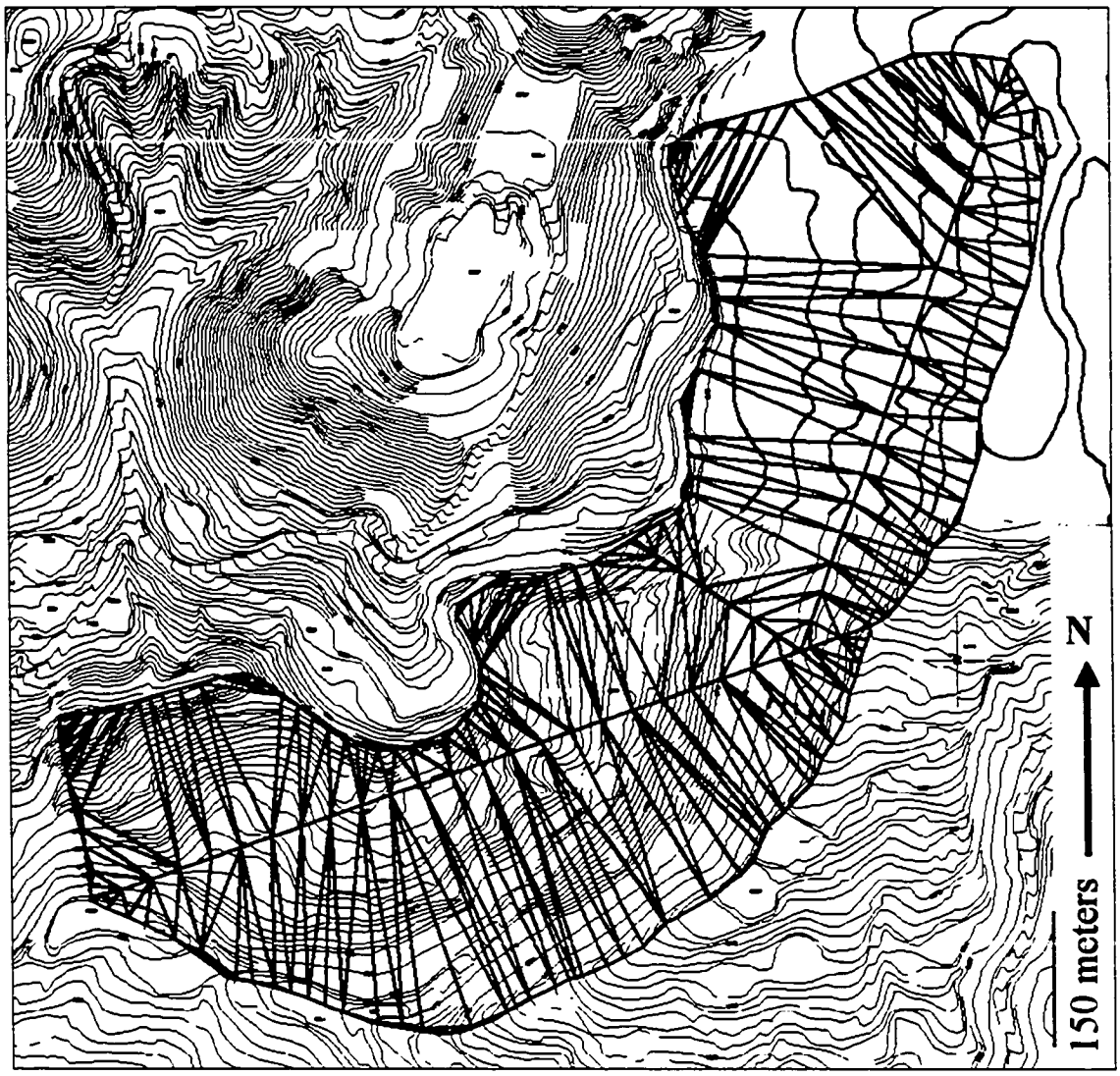

Figure 26. Triangulated-Irregular-Network (TIN) of the Skofield landslide region. Topographic contours indicated by black lines. USGS topographic contour intervals, approximately 12 meters (40 feet), digitized from USGS Santa Barbara Quadrangle are indicated by red lines. The TIN is indicated by blue lines networking into triangles that represent the three-dimensional paleo-topographic surface. The TIN depicts the paleo-topographic surface interpreted for the Skofield landslide region prior to slope failures.

The paleosurface geometry of the Skofield landslide region is a series of connecting lines that form 3-dimensional triangles used to depict paleo-topography (Fig. 26). Modeling of the paleo-topography in this region begins with connecting a straight line between the termination points of the crown of the Skofield landslide headscarp. The line plunges to the southwest from the top of slopes at the northeast head scarp crown to the southwest head scarp crown. The existing topography along the head scarp crown was joined to this line. The top of this new slope was then joined to the bottom of the mapped landslide body along Rattlesnake Creek.

The paleo-topography of the region of slope failures just north of the Skofield landslide was joined to the Skofield landslide paleo-topography (Fig. 26). The paleoslope of the nearby region of slope failures just north of the Skofield landslide was generated by joining a line from the headscarp crown in the north to the paleo-topographic surface of the Skofield landslide. The trend of this line is oriented with the general trend of Rattlesnake Canyon to the north of the slope failure region. Again, the existing topography along the head scarp crown was joined to this line. The top of this new slope was then joined to the bottom of slopes in Rattlesnake Creek.

A summary of the volumetric analysis of the Skofield landslide region is presented in Table 6. The total volume of exhumed landslide

debris from the Skofield landslide region includes landslide debris from the Skofield landslide and nearby slope failures to the north. The total exhumed landslide debris calculated in the three-dimensional volumetric analysis is 10.3×10^6 m^3.

Volumetric Analysis Discussion

The volumetric analysis of the Mission diamicton and Skofield landslide supports the hypothesis that the Mission diamicton was sourced largely from the Skofield landslide region. The total volume of the Mission diamicton deposits is determined to be approximately 9.21×10^6 m^3. The total volume of exhumed landslide debris from the Skofield landslide and nearby region is calculated at 10.3×10^6 m^3. The volumetric discrepancy between the primary source and depositional areas is 1.09×10^6 m^3.

The exhumed landslide debris volume calculation should be interpreted as the maximum amount of landslide debris from this region that could contribute to the total volume of the Mission diamicton. Any modification to the interpreted paleo-topography in the Skofield landslide area that would account for gullies typical of the Rattlesnake Canyon slopes would slightly decrease the total exhumed landslide debris volume and more closely match the volume calculated for the Mission diamicton.

Therefore, it is possible that the vast majority of source material for the Mission diamicton originated from the Skofield landslide region.

However, during the field investigation portions of this study, other large landslides were identified in Rattlesnake Canyon. These large landslides have exhumed landslide debris that is not present in the vicinity of their respective failures. Also, the large volume of debris that would have been produced from these slope failures could have each easily blocked the Rattlesnake Creek drainage and formed multiple landslide dams. Failure of these landslide dams would have presumably produced debris flows with sediment loads that have now been carried out onto the Santa Barbara piedmont and are now part of the Mission diamicton.

AGE OF THE MISSION DIAMICTON AND SKOFIELD LANDSLIDE

The absolute age of the Mission diamicton is not known. Cosmogenic isotope dating of several boulders performed by Landis (2002) yielded erroneous age values based upon age constraints of the piedmont fan on which the Mission diamicton rests and the eastern margin of Mission Ridge (Keller, 2001 personal commun.).

Selting and Urban (2001) indicate that the Mission debris flow is younger than the presence of Mission Ridge (Fig. 3). The Mission Ridge geomorphic feature is being formed by uplift and faulting associated with fault propagation for the More Ranch-Mission Ridge fault system. By calculations of regional folding and uplift rates of marine terraces, Gurrola (1999) estimates that Mission Ridge was in place by 45 ka. Keller (1999) documents an abandoned paleochannel of Mission Creek exists between the Santa Barbara Mission and Rocky Nook Park (Fig. 15). The lack of debris flow deposits in this paleochannel is evidence that Mission Ridge had already been in place and Mission Creek was diverted to its current position due to the westerly propagating Mission Ridge.

Based on the geophysical investigation of this study, the paleosurface on which the Mission diamicton rests is approximately half

of the elevation of the portions of Mission Ridge just to the east (Fig. 15). The orientation of the geologic contact between the Mission diamicton and underlying fanglomerate deposits is not congruent with the slope of the modern day topographic surface of the Mission Ridge or piedmont regions outside of the study area (Fig. 27). If the Mission diamicton were deposited at the early stages of the Mission Ridge development, then the geologic contact between the Mission diamicton and underlying fanglomerate deposits should have the generally same orientation as the modern topographic surfaces expressed in nearby portions of Mission Ridge. This assumption is based on the idea that the deformation to the modern topographic surface, produced by Mission Ridge uplift, would be replicated in underlying geologic contacts that had the same orientation as the topographic surface prior to deformation. The slope of the geologic contact between the Mission diamicton and underlying geologic materials is not congruent with the modern topography of nearby Mission Ridge regions.

The incongruent geologic contact between the Mission diamicton and topographic slope of nearby portions of Mission Ridge argues that the Mission diamicton was deposited on a topographic surface which was very near the elevation of the geologic contact between the Mission diamicton and underlying materials. These geometric and geologic relationships argue that the Mission diamicton is actually less than 22.5

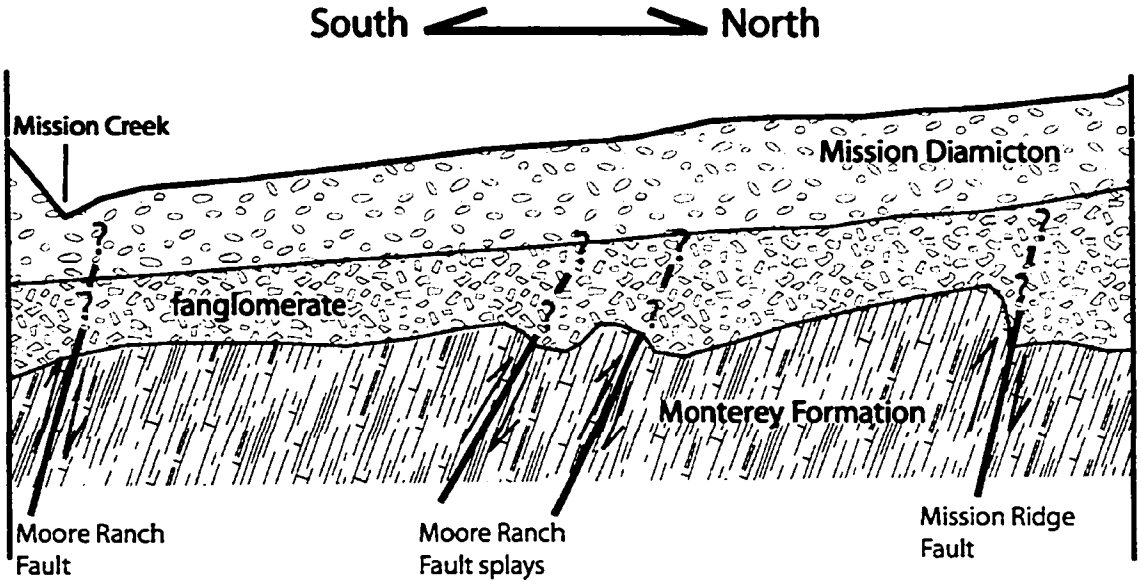

Figure 27. Diagrammatic cross-section of the Mission diamicton piedmont region. The figure is not to scale. The cross-section depicts general stratigraphic and structural relationships identified by analysis of a combination of data including field relationships, geophysical surveys, and borehole information. The areal average thickness of the Mission diamicton is 8.7 meters. Fault locations are identified by geophysical investigation and analysis accomplished during this study.

ka. Interestingly, Bianchin (a Santa Barbara Engineering Geologist consultant) reports that a series of large landslides from a regionally nearby site were carbon dated and their formation was between 22 to 19 ka (2002, personal communication). This suggests a regional slope failure event at about this time. Borchardt et al. (1982) and Schlemon (1980) describe an A2 soil horizon in the Point Conception region to the west of Santa Barbara, with physical properties characteristic of a diamicton, which is thought to have originated from a mudflow approximately 1,000 years ago. The presence of the Point Conception diamicton may indicate climatic and/or seismic conditions conducive to mudflow and debris flow initiation at this time.

Additional evidence that the Mission diamicton is much younger than 45 ka is the pristine morphology of the debris fan comprised of the Mission diamicton and the weakly developed soils from the Mission diamicton (Figs. 4 and Appendix E). The Mission diamicton piedmont deposits compose a debris flow fan with pristine morphology depicting debris flow lobes. In addition, weak A horizon soils have developed on the Mission diamicton. Keller (2002 personal commun.) believes that the weakly developed soils indicate that the Mission diamicton is less than 10 ka.

Modern historical records do not document the occurrence of the geologic processes such as a large volume debris flows in the region

where the Mission diamicton is now deposited. No reports indicating a large landslide or a debris flow exist from written records as early as 1782 when the settlement of non-indigenous people to the Santa Barbara region began (Selting and Urban, 2001). The age of the Mission diamicton is interpreted as younger than 45 ka but older than 1748 A.D. Weakly developed soils suggest that the Mission diamicton may be Holocene in age.

Radiocarbon Dating

Constraining the age of the Mission diamicton is important for understanding and evaluating the geologic hazards posed by the deposit to the City of Santa Barbara and nearby regions. The benefits of absolute dating the Mission diamicton include further constraining the depositional age of the deposits, which can then be used to assess paleo-environmental conditions that influenced the genesis of the deposits. Paleo-environmental conditions that may have influenced the genesis of the Mission diamicton include the climatic regime(s), seismic inputs, and/or external perturbations such as a fire.

Because of the importance in further constraining the age of the Mission diamicton in terms of evaluating the geologic hazards posed by the deposits, field collection of charcoal samples for radiocarbon dating was accomplished. A total of 10 samples of sediment, two samples with

visible charcoal pieces, were collected from the Mission diamicton and Skofield landslide debris. Bulk samples of Mission diamicton sediment were collected to pick microscopic pieces of charcoal. Because of costs associated with radiometric dating, only two of the samples could undergo absolute dating. The two samples to be dated were chosen based on geologic relationships that could best constrain the age of the Skofield landslide failure and one debris flow levee in the Mission diamicton.

At the two chosen sample locations, visible pieces of detrital charcoal were collected. At one location, a charcoal sample was collected from a sandy clay horizon interpreted to be deposits from a temporary lake and are stratigraphically just below Skofield landslide debris. At a second location a sample was collected from a debris flow levee deposited directly on Sespe formation bedrock and just downstream of the Skofield landslide. Photographs and diagrammatic cross-sections of sample locations are presented in Appendix E.

Laboratory Procedure for Preparing Radiocarbon Dating Samples

The laboratory procedure for preparing samples for microscopic charcoal extraction is included in Appendix E.

Radiocarbon Dating Results

The charcoal samples were dated using radiometric methods and results provided by the Center for Accelerator Mass Spectrometry (CAMS), Lawrence Livermore National Laboratory, Livermore, California. The U. S. Geological Survey provided funding for radiometric dating of the charcoal samples collected by the author. Table 7 is a copy of the official U. S. Geological Survey report for the ^{14}C dates of the collected charcoal samples. Sample 02-01-03-A1-K was collected from lacustrine deposits stratigraphically above and below landslide debris near the toe of the Skofield landslide and is reported as an age of 1000 ± 40 years. Sample 01-20-03-B1-H was collected within a singular debris flow deposit of a channel levee downstream of the Skofield landslide in Rattlesnake Canyon and is reported as an age of 1460 ± 40 years.

The radiocarbon dates were calibrated by Gurrola (2004 personal commun.) utilizing the OxCAL radiocarbon calibration program. Sample 02-01-03-A1-K is dated to have originated with a 95.4 percent probability between 970 and 1160 AD. Sample 01-20-03-B1-H is dated to have originated with a 95.4 percent probability between 530 and 670 AD.

Table 7. Radiometric Carbon Dates

WW	Sample ID	Material	Region	δ13C	^{14}C AGE	±	DATED ON
4506	01-20-03-B1-H	charcoal	Santa Barbara	-25	1460	40	10/29/2003
4507	02-01-03-A1-K	charcoal	Santa Barbara	-25	1000	40	10/29/2003

Notes:

- Samples were processed at the 14C laboratory of the U. S. Geological Survey in Reston, Virginia.
- 14C ages were determined at the Center for Accelerator Mass Spectrometry (CAMS), Lawrence Livermore National Laboratory, Livermore, California.
- The quoted age is in radiocarbon years (BP) using the Libby half life of 5568 years.
- The WW number is the identification assigned to a sample by the USGS 14C laboratory.
- Values reported for δ13C are the assumed values according to Stuiver and Polach (Radiocarbon, v.19, p. 355, 1977) when given without decimal places. Values measured for the material itself are given with a single decimal place.

Comments or questions may be referred to:
Jack McGeehin
U. S. Geological Survey
MS 926A National Center
Reston, VA 20192

Radiocarbon Dating Discussion

The radiometric carbon dating ages of the Mission diamicton charcoal samples imply a young age for the formation of the Skofield landslide and at least a bulk of the Mission diamicton. The radiometric ages of the charcoal samples place the origin of sample 02-01-03-A1-K with a 95.4 percent probability between 970 and 1160 AD and sample 01-20-03-B1-H with a 95.4 percent probability between 530 and 670 AD. Because of the relatively small age range of the dated samples (± 40 years), the radiocarbon dates can be interpreted as reliable.

There are multiple ways of interpreting the radiometric carbon dates with respect to the age of the Mission diamicton and the age of the formation of the Skofield landslide. To understand the discrepancy between the two reported ages of the dated samples, it is best to discuss the samples individually.

Sample 02-01-03-A1-K was collected from a charcoal bearing sandy clay horizon within landslide debris near the toe of the Skofield landslide. The site outcrop is depicted in Figure E1 and is located at the northern area of the Skofield landslide (Fig. 3). This site location has macroscopic pieces of charcoal contained within this sandy clay horizon. It is interpreted that an absolute date obtained from this horizon would best constrain the age of landsliding in the Skofield landslide region. This interpretation is based on that the sandy clay horizon from which

sample 02-01-03-A1-K was collected is constrained stratigraphically above and below by landslide debris. Therefore, some of the landsliding in the Skofield landslide region is older and some of the landsliding is younger than 1000 ± 40 years.

The charcoal-bearing sandy clay horizon from which sample 02-01-03-A1-K was collected is constrained between landslide debris and is congruent with the landslide dam hypothesis proposed as the source of the bulk of the Mission diamicton. One interpretation, and the favored interpretation by the author, is that the charcoal-bearing horizon is the remnants of a lake deposit. An episode of landsliding occurred prior to the deposition of the charcoal-bearing zone from which sample 02-01-03-A1-K was collected. The inclusion of clay and charcoal in this deposit implies that longevity of the lake allowed deposition of these particles. The failure of the landslide dam would have left unsupported and saturated slopes with a presumably lower effective shear strength. The failure of these weakened slopes is evident by the landslide debris overlying the charcoal-bearing sandy clay horizon that is interpreted to be landslide dam lake deposits. A second interpretation is that the sandy clay horizon was deposited in bulk with the over- and underlying landslide debris. This interpretation is unlikely because of the stratification of the sandy clay horizon. It would seem that bulk deposition of the over- and underlying landslide debris and the sandy

clay horizon would not preserve the sandy clay horizon but rather entrain the horizon within the landslide debris.

Sample 01-20-03-B1-H was collected within a singular channel levee debris flow deposit downstream of the Skofield landslide. Sample 01-20-03-B1-H is reported as an age of 1460 ± 40 years. The sample is approximately 460 years older than sample 02-01-03-A1-K. It is important to stress the importance that microscopic charcoal sample 01-20-03-B1-H was extracted from a bulk sediment sample that was collected from a singular channel levee deposit. The bulk of the Mission diamicton is comprised of a multitude of debris flow deposits with evidence of stratigraphic separation between depositional sequences (Figure 7). Sample 01-20-03-B1-H was extracted from one debris flow deposit of the many debris flow sequences that comprise the Mission diamicton.

The 460 ± 40 year separation between the radiometric dated charcoal samples implies that the debris flow history of the Mission diamicton and the relationship to the Skofield landslide was a relatively long- lived feature. The age separation and fact that the debris flow deposit age is older than the sample collected from the sandy clay horizon between Skofield landslide debris suggests that the debris flow history of the Mission diamicton is not limited to a singular catastrophic event but to numerous and sometimes voluminous debris flows

separated in time throughout centuries. The 460 ± 40 year age difference between samples can be resolved by any of the following explanations:

1) The Skofield landslide formed a dam and impounded drainage, forming a lake approximately 1000 ± 40 years ago. Debris flows were generated from the failure of the dam, and one such debris flow contained a piece of charcoal with an age of 1460 ± 40 years. The charcoal contained within the debris flow is approximately 460 ± 40 years older than the debris flow deposit.
2) The Skofield landslide formed a landslide dam that failed episodically. The formation of the Skofield landslide is older than 1460 ± 40 years and is constrained by sample 01-20-03-B1-H. A temporary lake formed at least 1000 ± 40 years ago as signified by sample 02-01-03-A1-K. Failure of at least a portion of the dam resulted in draining of the lake and subsequent landslide debris buried the sandy clay lake deposits.
3) The Skofield landslide dam was a long-lived feature that provided debris flows that range in age at least 460 ± 40 years.
4) The Skofield landslide was a progressive and dynamic feature that formed at least 1460 ± 40 years ago and provided a source for debris flow material. At approximately 1000 ± 40 years ago, the Skofield landslide dam was in place and a temporary lake formed

that allowed for fine sediment and charcoal to be deposited. Subsequent slope failure in the Skofield landslide region occurred as evident by the landslide debris stratigraphically higher than the sandy clay horizon.

The age discrepancy between the sample collected from the Skofield landslide region and the sample collected downstream from the debris flow deposit does not indicate that the Skofield landslide and Mission diamicton are unrelated. The radiometric carbon dates indicate that the timing of landsliding and debris flow genesis is not necessarily as simple as a singular catastrophic event, but instead is a series of debris flow events episodically dispersed over at least four centuries.

The two radiometric carbon dates provide insight into the age and duration of the Mission diamicton and Skofield landslide origins. However, more numerous radiometric dating of samples dispersed spatially and stratigraphically throughout the Mission diamicton and Skofield landslide region could provide more insight and constraints on the timing of landsliding, dam formation, and debris flow events.

The ages of the samples indicate that the formation of a landslide dam in the Skofield landslide region and debris flows of the Mission diamicton were occurring at the time when indigenous people, the Chumash, were in the area. No known reports or heritage of a story indicate a singular large catastrophic landslide or debris flow event that

would be characterized by the entire Mission diamicton if the deposit represents a single debris flow event. Though documentation of a Chumash story or report of a singular debris flow event does not exclude the possibility of such an event, the radiocarbon dates can be explained by multiple debris flow events that may have occurred episodically over an unknown duration of at least 400 years. These debris flows may be either related to one landslide dam and episodic failure over an unknown duration in time, multiple individual landslide dam failures and resultant debris flows, or a combination two.

The combination of the young age of the Mission diamicton and the Point Conception diamicton, described by Borchardt et al. (1982) and Shlemon (1980) suggest regional conditions were conducive to slope failure and debris flow initiation. Both diamictons have similar ages of approximately 1,000 years old. The presence of the two diamictons suggests that either climatic or seismic conditions conducive to slope failure were available in the Transverse geomorphic provenance at this time. Moreover, evidence of the two young debris flow events in the region indicates a geohazard warranting evaluation.

GEOLOGIC HAZARDS EVALUATION

The Mission diamicton represents a complex of large volume debris flows that originated as the result of the failure of a landslide dam formed by the Skofield landslide. The geohazards that are identified by this study and posed by the Mission diamicton include: slope failure, landslide dam formation and failure, and debris flows resultant of the failure of landslide dams. Residential development and public infrastructure of both the City and County of Santa Barbara are within the immediate boundaries of the geologically related features, the Mission diamicton and Skofield landslide region. Over 300 residential homes and public infrastructure is now within the approximate 1 square kilometer region of the Mission diamicton piedmont deposits (Fig. 3). Numerous residential homes within Rattlesnake Canyon are located on debris flow fill terraces and on, or located within, regions of potential slope failure.

Urban (1999) suggests that the evidence for a debris flow fan and genesis from the failure of a natural landslide dam at Skofield Park indicates a geohazard to the city of Santa Barbara that has not been evaluated in the region. A modern natural landslide dam in nearby Los

Positas Creek has been documented by Keller (1999). Evans and DeGraff (1997) estimate that almost half of all fatalities resulting from major landslide disasters of the twentieth century are related to natural landslide dam failures. Because the Santa Barbara region has now been identified as having a history of landslide dam formation, which can affect the life and property of humans, the need to evaluate the geologic hazards posed by the Mission diamicton is mandatory.

Slope Stability Geohazard Evaluation Method

Geohazard evaluation requires identification of geologic phenomenon occurring (or may occur) in a region that can or may affect or cause effect on inhabitants. As part of this investigation, an evaluation of the geohazards posed by the Mission diamicton through field identification of geologic hazards and collection of data was necessary.

As described in the Rattlesnake Canyon Geologic Mapping section of this thesis, the Sespe Formation in Rattlesnake Canyon has ubiquitous joints (fractures) observable in outcrop. Rock slope failures are identifiable in Rattlesnake Canyon and failure in the Sespe Formation has allowed mobilization of overlying fanglomerate deposits. Figure 28 depicts such a modern rockslide where overlying fanglomerate

Figure 28. Modern rockslide that enables mobilization of overlying fanglomerate materials. Notice the fanglomerate and Sespe Formation debris that now blocks a portion of the Rattlesnake Creek drainage.

has been mobilized and the cumulative debris from the slope failure has blocked a portion of the Rattlesnake Creek drainage.

Sespe Formation Rockslide Analysis

A field reconnaissance collection of joint and bedding orientations was accomplished according to the methods of Nickelsen and Hough (1967). An equal area stereonet projection of joint and bedding orientations and the cone of friction determined for discontinuities is presented in Figure 21.

The cone of friction for discontinuities was determined by collecting representative samples of joints where discontinuity orientations were measured. Rock samples from both sides of a joint set were collected and spatial orientation information was scribed directly onto samples for later re-orientation. The samples were collected by hammer and chisel. Samples were immediately placed in polyethylene bags to preserve field conditions of moisture content. Though, some fracture samples had visible water flowing from fractures in the field, these conditions could not be preserved given the sampling methodology.

The discontinuity samples were then tested for friction angle according to the Markland's Test described by Hoek and Bray (1981). The results of this analysis is presented in Table 4. Each discontinuity

set had at least one sample that has a minimum friction angle value of 30 degrees. Therefore, a cone of friction of 30 degrees is used in the geohazard analysis of rock slope stability for all of the discontinuity sets. An equal area stereonet projection of the discontinuities and cone of friction allows the direct observation that there is the potential for wedge and planar failure of the Sespe Formation within Rattlesnake Canyon. The geometric relationships conducive for each type of failure, either wedge or planar, with respect to discontinuity sets was queried in ESRI's ArcView 3.2 GIS environment to identify all slopes within Rattlesnake Canyon with appropriate slope angles and aspects conducive to rock slope failure. The query code input into this analysis is presented in Figure 29.

Fanglomerate Landslide Analysis

An analysis of landslide potential for fanglomerate materials was also accomplished for evaluating slope failure potential. Because modern debris slides were evident in 1995 aerial photographs after severe rainstorms, a limit equilibrium slope stability analysis of circular and irregular shaped failure surfaces was accomplished. Geotechnical data from geotechnical consultant reports were collected at the City of Santa Barbara Public Works offices for properties located in Rattlesnake

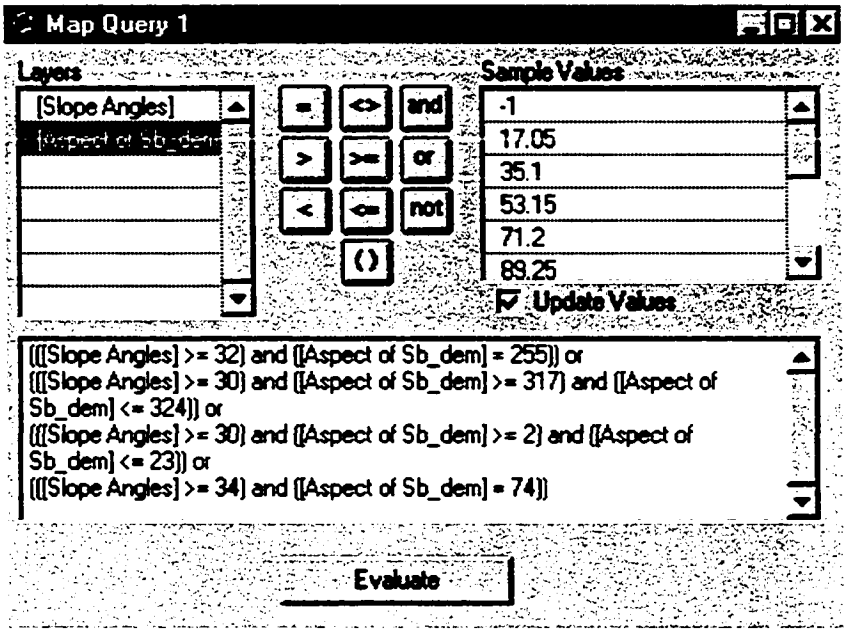

Figure 29. Query dialog box for ESRI's ArcView 3.2 geographic information system used in spatial analysis to identify all unfavorable slope orientations utilizing limit equilibrium slope stability analysis results. The results of the method of slices limit equilibrium analysis of fanglomerate materials are presented in Appendix G.

Canyon. A summary of the geotechnical data is presented in Table 1.

The fanglomerate materials in Rattlesnake Canyon were analyzed according to limit equilibrium slope stability methods utilizing the Bishop method for circular failures and the Janbu method for random failure surface geometries. The pre- and post-processor STEDwin 2.74, developed by Harold Van Aller, was used for inputting geotechnical data and slope geometries as well as generating the graphical presentation of the results of the stability analyses. STEDwin utilizes the slope stability analysis software PC STABL, developed by Purdue University, which is a computer program for solving two-dimensional limiting equilibrium slope stability methods. PC STABL and STEDwin are commonly used software programs in the geotechnical and engineering geology professions for the analysis of slope stability and therefore have a history of testing for validity of output results.

Fabricated slopes consisting of geotechnical data obtained from geotechnical consultant data for the fanglomerate were input into STEDwin for analysis. For geohazard evaluation purposes, the most conservative estimation of the level of geohazard or identification of slope failure potential using the weakest shear strength of the geologic materials was used in this analysis. Slope angles for the fanglomerate materials were increased and analyzed for both Janbu and Bishop methods, respectively, until the factor of safety became less than one (1).

At a slope angle when the factor of safety became less than one, the driving forces have become greater than the resisting forces to slope failure and therefore the slope is in a state of disequilibria. The slope angle for which the fanglomerate materials are in a state where forces driving slope movement exceed forces resisting slope movement, and therefore critical state of failure, is determined to be 30 degrees. The slope stability analyses graphical depictions and respective output files, that depict the constraining of a 30-degree slope as critically oriented for fanglomerate materials, are presented in Appendix G. A query in ESRI's GIS program, ArcView 3.2, identifies all slopes at or exceeding 30 degrees in the fanglomerate materials and identifies locations of all slopes that are at or exceeding their respective critical orientation for failure.

Both the results of the rockslide analysis of the Sespe Formation and limit equilibrium methods analysis of fanglomerate materials were queried in the ArcView GIS environment to identify all slopes within Rattlesnake Canyon on the 3-meter grid DEM that are either at or exceeding their respective critical orientations for failure. The spatial distribution of slopes that are at or exceeding their critical orientation for failure as determined by this analysis is presented in Figure 30.

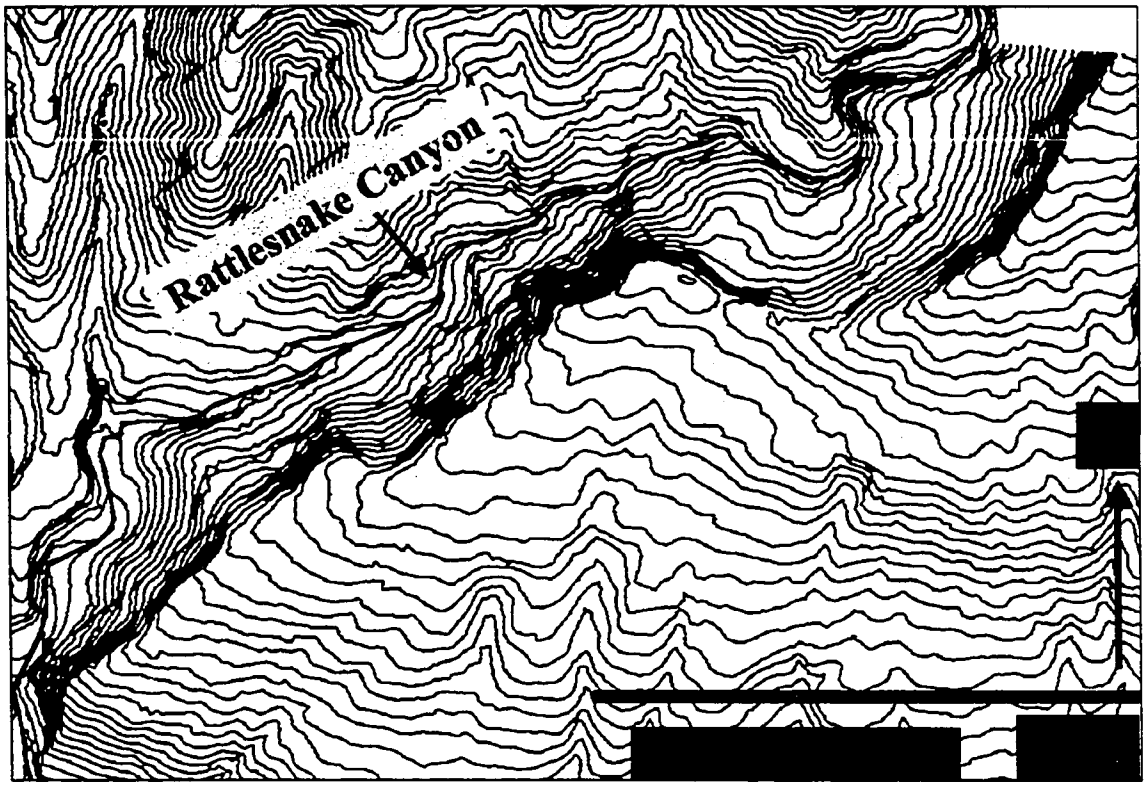

Figure 30a. Geographic information system (GIS) analysis of critically oriented slopes in Rattlesnake Canyon. Red zones are locations where slopes are at or exceeding the critical orientations according to the discontinuity limit equilibrium slope stability analysis presented in Figure 21 and Appendix G.

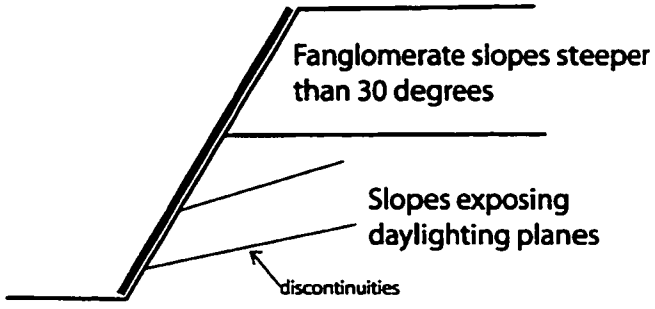

Figure 30b. Diagrammatic cross-sectional sketch of slopes orientations identified as red zones in Figure 30a.

Slope Stability Geohazard Evaluation Limitations

Though the geohazard evaluation of slope failure potential in Rattlesnake Canyon identifies various regions with slopes that are either at or exceeding their critical orientation for failure, there are a few limitations to this method of slope stability geohazard evaluation. The slope stability analysis of fanglomerate slopes is limited by the type and availability of geotechnical data on the fanglomerate materials. Geotechnical data available for the fanglomerate materials at the City of Santa Barbara Public Works is from only two site locations. The limitation that this presents in the slope stability analysis is that the available geotechnical data do not accurately characterize the distribution of shear strength for the fanglomerate materials throughout Rattlesnake Canyon. Also, the samples from which density and shear strength information were used in the analysis were at depths less than the total depth of the fanglomerate slopes analyzed for stability. If samples were collected at varying depths and their appropriate geotechnical information are input into the stability analysis, the global slope stability analysis results will change.

Though there is the limitation of the amount of sampling used in the analysis of the fanglomerate slope stability analysis, it is the belief of the author that the slope stability analysis presented herein is a good first order approximation to the stability of slopes in Rattlesnake Canyon.

The slope stability analysis and identification of slopes at or exceeding their critical orientation for failure identifies that slopes in Rattlesnake Canyon warrant the need for further investigation of the slope failure geohazard.

Another limitation to the slope stability analysis of Rattlesnake Canyon is within the spatial analysis of slopes at or exceeding critical orientations. As described in the discussion of digital modeling and the inherent digital flaws in the 3-meter DEM, there are some topographic surfaces that are likely misrepresented by the DEM. The spatial identification of slopes at or exceeding critical orientation presented in Figure 26 utilizes the digital data of the 3-meter grid DEM. As such, there is an inherent limitation to the spatial analysis of critically oriented slopes using the 3-meter DEM digital data set. The errors that this is likely to produce are that changes in slope orientation less than the 3-meter resolution of the dataset will not be identified. Though, for gross spatial identification of slope stability analysis results, the identification of critically oriented slopes is justifiable.

Geohazard Evaluation Discussion

The slope stability geohazard evaluation identifies slopes that are either at or exceeding their respective critical orientations for failure. The identification of slope failure potential in Rattlesnake Canyon indicates

that the potential for landslide dam formation exists and subsequently geologic events represented by the Mission debris flow and cumulative Mission diamicton have a modern potential to occur. Rattlesnake Canyon, as well as the vast majority of canyons in the Santa Ynez mountain range, is narrow and confined with steep slopes. Narrow and confined canyons with steep slopes are conditions which Costa and Schuster (1988) identify as conditions that are conducive to the formation of landslide dams.

CONCLUSIONS

Origin of the Mission Diamicton

Geomorphic, geologic, and volumetric evidence indicates the Mission diamicton was formed as a result of debris flow processes at least in part due to a large debris flow event related to the failure of a landslide dam. The Skofield landslide and at least two other large volume landslides in Rattlesnake Canyon indicate that there is a history of landslide dams formation in the steep and confined reaches of the canyon.

Sedimentologic and geophysical data indicates that the bulk of sediments within the debris flow fan resulted from a single geologic event. The youthful and similar appearance of all exposed sediments of the Mission diamicton sediments indicate a correlative origin though multiple debris flow sequences indicates multiple debris flows separated by unknown duration in time. The similar outcrop appearance indicates that Mission diamicton sediments have an origin related in geologic time.

The Mission diamicton is a morphologically distinct feature in the Santa Barbara region. The evidence presented in this study indicates the Mission diamicton was largely, if not entirely, derived from a massive and catastrophic debris flow event. Geomorphic evidence from a high-

resolution digital terrain model of the debris flow fan indicates large volume debris flow lobes were formed during genesis of the fan.

The large morphologic lobes represent the minimum size of depositional debris flow lobes. Each of these respective pulses or events indicates a large supply of sediment involved and warrants sources able to supply large volumes of material for each pulse or event. Sediment within the Mission diamicton is similar and therefore warrants the need for a similar source area or areas to provide sediments for the Mission diamicton.

Geologic mapping and sedimentary evidence indicates source material contributing to the Mission diamicton originated from Rattlesnake Canyon. The lack of Mission diamicton beyond the Skofield landslide suggests an association between these two geologic and geomorphic features. At the Skofield landslide, evidence of landslide debris interpreted to be remnants of a landslide dam and similar sedimentary signatures between Mission diamicton and exhumed fanglomerate landslide debris indicates further relationship between the geologic features.

This study identifies that the Mission diamicton sediments are debris flow deposits that have been contributed by the failure of a landslide dam. The Skofield landslide failed in Rattlesnake Canyon and blocked the drainage of Rattlesnake Creek. A temporary lake impounded

upstream of the Skofield landslide dam. Then, the landslide dam failed either as the result of internal failure of the dam or to overtopping of the dam. The landslide dam failure allowed removal of landslide debris and water in the form of debris flows that traveled down Rattlesnake Canyon and onto the Santa Barbara piedmont. Removal of the impounded lake would have exposed saturated slopes; with a presumably lower shear strength that is commonly experienced with the rapid drawdown of modern dams. Subsequently, slopes in the region where the temporary lake existed had failed and contributed additional material to the Mission diamicton sediments in the form of debris flows.

Volumetric calculations accomplished in a 3-dimensional digital terrain model in collaboration with identification of the thickness and geometrical relationships of the Mission diamicton indicate the Skofield landslide dam and nearby region of slope failures contributed the bulk of sediment in the form of debris flows to the Mission diamicton. The formation of the Skofield landslide dam, the landslide dam failure, and resultant debris flows is a geologic event constrained to the name of the *Mission debris flow.*

This study identifies landslide regions in Rattlesnake Canyon including the Skofield landslide, two additional large bedrock body landslides, and two large debris slides. The exhumed landslide debris materials from the two large bedrock body landslides are not present in

Rattlesnake Canyon. These two landslides could have also formed landslide dams because of their characteristic large volume of exhumed materials could easily have filled the cross-sectional area needed to block drainage in Rattlesnake canyon. And presumably these two landslide dams would have resulted in similar debris flow events as represented by the failure of the Skofield landslide dam. It is presumed that the additional large volume landslides contributed source materials to the cumulative Mission diamicton sediments.

The additional large volume landslides in Rattlesnake Canyon with exhumed materials not present in the canyon presumably contributed the additional source materials to provide resolution of volumetric disparity between the Mission diamicton deposits and Skofield landslide region source area. These additional large landslides would have also formed landslide dams that failed, allowing debris flows to travel through Rattlesnake Canyon and onto the Santa Barbara piedmont to contribute to the cumulative *Mission diamicton.*

Geohazards

Geologic and geomorphic evidence indicates the Mission diamicton is a debris flow process dominated fan. Evidence indicates that the failure of a landslide dam at Skofield Park generated a massive debris flow event that contributed to the bulk of Mission diamicton deposits and

is now deposited over a surface area of approximately 1 square kilometer. This event is termed the Mission debris flow and contributes a portion of the entire Mission diamicton.

This debris flow fan is now the location of over 300 homes to residents of the city of Santa Barbara. And residential development has spread not only into Rattlesnake Canyon but other narrow and steep canyons as well. Geologic evidence indicates that natural landslide dam and associated debris flow geohazards are unevaluated for these residents and the surrounding region. If the failure of a natural landslide dam and debris flow event occurred of the same magnitude of the hypothesized Skofield landslide and Mission diamicton and if advanced warning to residents of Santa Barbara did not occur, a catastrophic event with extensive loss of life and property could occur. Geohazards to the City and County of Santa Barbara including slope failures, landslide dam formation and failure, and debris flows in the region of the Rattlesnake Canyon and the Santa Barbara piedmont just north of the Santa Barbara Mission are identified by this study. A quantitative risk assessment of the slope failure and associated geologic processes geohazards was accomplished for the study area using field collected discontinuity data and available geologic or geotechnical consultant report data. Evidence indicates that slope failure in Rattlesnake Canyon is controlled by unfavorable discontinuity

orientations in the Sespe Formation and unfavorable slope orientations in fanglomerate materials. The geohazard risk assessment identifies regions in Rattlesnake Canyon that are either at or exceeding their respective critical orientations for slope failure.

Because of the narrow and confined characteristic of Rattlesnake Canyon, even small volume landslides can block drainage of Rattlesnake Creek and form landslide dams. If unmitigated, these landslide dams will fail and result in debris flows that can travel long distances onto the Santa Barbara piedmont where residents of the city live today. Further work including modeling of slope failure potential with an expanded database of appropriate borehole data is warranted in the region of Rattlesnake Canyon. Because of the regional geologic structure generally trends east-west in the coastal region of Santa Barbara, an extension of the quantitative geohazard assessment method developed by this study is warranted and possible for regions beyond the study area of this thesis project.

REFERENCES

Borchardt, G., Rice, S., and Treiman, J., 1982, Mudflow deposition and horizonation in Holocene soils near Point Conception, California [unpublished paper] available at: http://www.soiltectonics.com/mudflow.htm

Costa, J.E., 1986, Physical Geomorphology of Debris Flows, in Costa, J.E., and Fleisher, P.J., eds., Developments and applications of geomorphology: Berlin; New York, Springer-Verlag, p.372.

Costa, J.E., and Schuster, R.L., 1988, The formation and failure of natural dams: Dept. of Interior, U.S. Geological Survey; Books and Open File Reports distributor, 87-392.

Dibblee, T.W., Ehrenspeck, H.E., and United States Forest Service. Los Padres National Forest. Los Padres National Forest, 1986, Geologic Map of the Santa Barbara Quadrangle, Santa Barbara County, California: Thomas Wilson Dibblee Jr. Geological Foundation, 1:24,000.

Evans, S.G., and DeGraff, J.V., 1997, Major landslide disasters of the millennium: GSA 1997 annual meeting, Abstracts with Programs, v. 29, no.6, p. 285.

Gurrola, L.D. and Keller, E. A., 1997, Tectonic geomorphology of the Santa Barbara fold belt, western Transverse Ranges, California: Geological Society of America, 1997 Abstracts with Programs, v. 29, no. 6, p. 344-345.

Gurrola, L.D., Keller, E.A., Trecker, M.A., Hartleb, R.D., and Dibblee, T.W., 1999, Active folding and buried reverse faulting of the Santa Barbara fold belt, California, Coast Geological Society Field Trip Guide Book.

Gurrola, L.D., Selting, A., Keller, E., Tierney, T., Hartleb, R., Trecker, M., and Dibblee, T., 2001, Neotectonics of the Santa Barbara fold belt, California: 2001 Geological Society of America Cordilleran Section Annual Meeting Field Guide.

Gurrola, L.D., 2002, Digital Elevation, Topographic, and Tectonic Geomorphology Map of the Eastern Santa Barbara Fold Belt, Santa

Barbara, California, [Dissertation map]: University of California at Santa Barbara.

Hoek, E. and Bray, J.W., 1981, Rock Slope Engineering. 3rd edn. London: Institution of Mining and Metallurgy, p. 402.

Hoover and Associates, 1984, Summary of Monitoring Well Construction, Mission Canyon Wastewater Facilities Project, available at the City of Santa Barbara Public Works Department.

Keller, E.A., 1999, The natural history of Mission Creek: A story of earthquakes and debris flows, available at the Santa Barbara Natural History Museum, p.8.

Landis, G., Gurrola, L., Selting, A., and Mills-Herring, L. 2002, Evaluation of cosmogenic 21Ne surface exposure ages from a mid-late Pleistocene alluvial fan and Holocene Debris Flow, Santa Barbara, California: Geological Society of America 2002 Annual Meeting Abstracts.

Minor, S., Kellogg, K., Stanley, R., Stone, P., Powell, C., Gurrola, L., Selting, A., and Brandt, T., 2002, Preliminary Geologic Map of the Santa Barbara Coastal Plain Area, Santa Barbara County, California: U.S. Geological Survey Open File Report 02-136.

Nickelsen, R. and Hough, V., 1967, Jointing in the Appalachian Plateau of Pennsylvania: Geological Society of America Bulletin, v.78, p.609-630.

Reynolds, J.M., 1997, Applied Seismology, in An Introduction to Applied and Environmental Geophysics. West Sussex: John Wiley & Sons, Ltd, p. 796.

Shlemon, R.J., 1980, Soil-stratigraphy of the proposed LNG site, Little Cojo Bay, Santa Barbara County, California. Report submitted to Dames & Moore (Los Angeles) on behalf of Western LNG Terminal Associates (Los Angeles), Dames and Moore Job No. 00011-168-02, 26 p.

Selting, A.J., 2000, Morphology, Process and Hazard of the Mission debris flow: Paper associated with comprehensive exam project. University of California at Santa Barbara.

Selting, A.J., 2002, The Mission debris flow: an example of debris flow initiation by the failure of a prehistoric landslide dam in Santa Barbara, California [Masters thesis]: University of California at Santa Barbara.

Selting, A. and Urban, R.J., 2001. Investigation of the Mission Debris Flow Deposit, Santa Barbara, California: 2001 Geological Society of America Cordilleran Section Annual Meeting Field Guide.

Urban, R.J., 1999, Preliminary report of the Santa Barbara massive debris flow and associated natural landslide dam, Santa Barbara, California [unpublished undergraduate individual project thesis]: University of California at Santa Barbara.

Urban R.J., 2000, The Santa Barbara catastrophic debris flow and associated natural landslide dam failure [unpublished undergraduate individual project thesis]: University of California at Santa Barbara.

Urban, R.J., 2002, The Massive Mission Debris Flow and Skofield Landslide, Santa Barbara, California: Association of Engineering Geologists Program with Abstracts 2002 Annual Meeting.

Urban, R.J., 2003, The Debris Flow Origin of the Mission Diamicton and Associated Geohazards to the City of Santa Barbara, Santa Barbara County, California. Presentation to the San Francisco Section of the Association of Engineering Geologists.

Varnes, D.J., 1978, Slope Movement and Types and Processes. In Landslides: Analysis and Control, Transportation Research Board, National Academy of Sciences, Washington, D.C., Special Report 176, Chapter 2, 1978.

APPENDIX A

SEISMIC REFRACTION DATA AND ANALYSIS

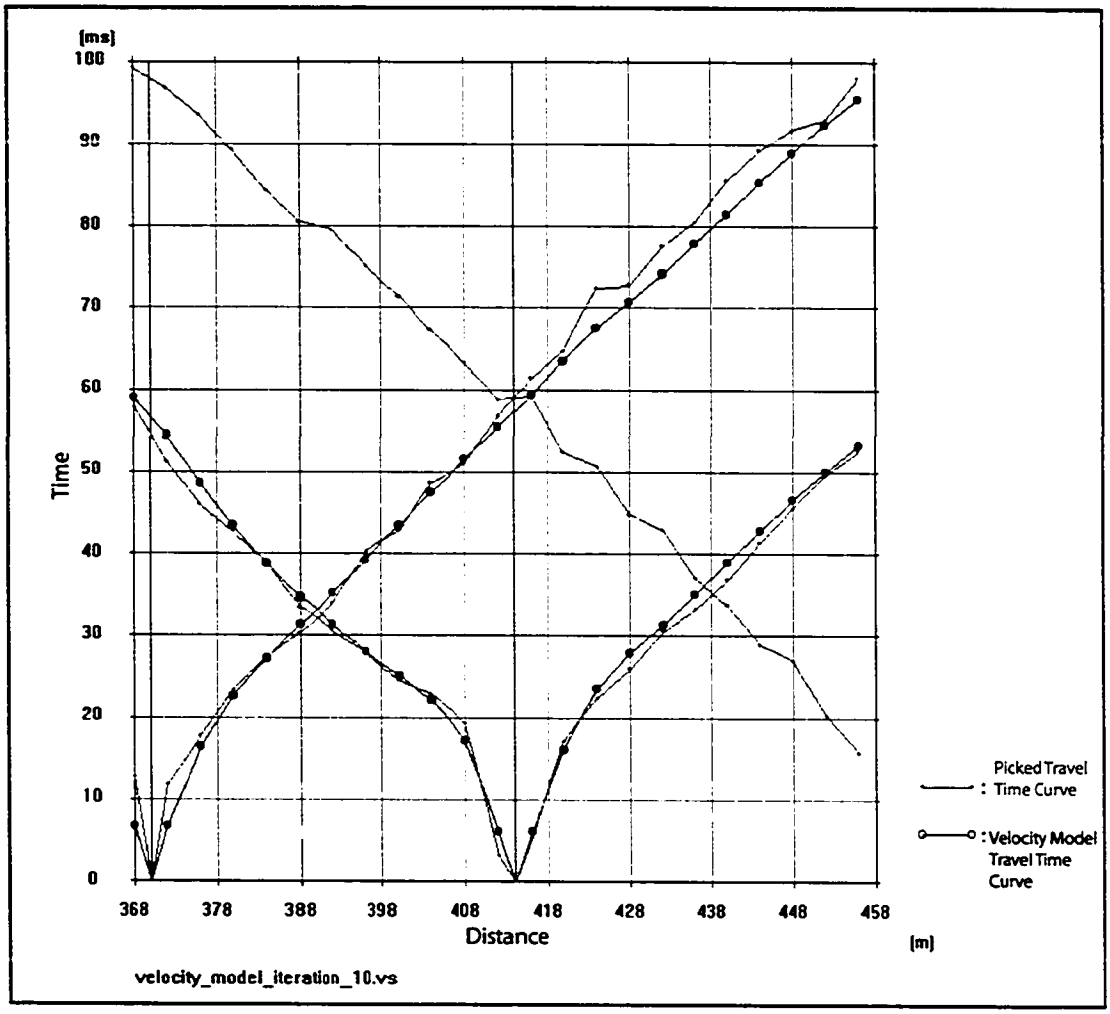

Figure A1. Tomographic analysis travel time curves for survey 1001.

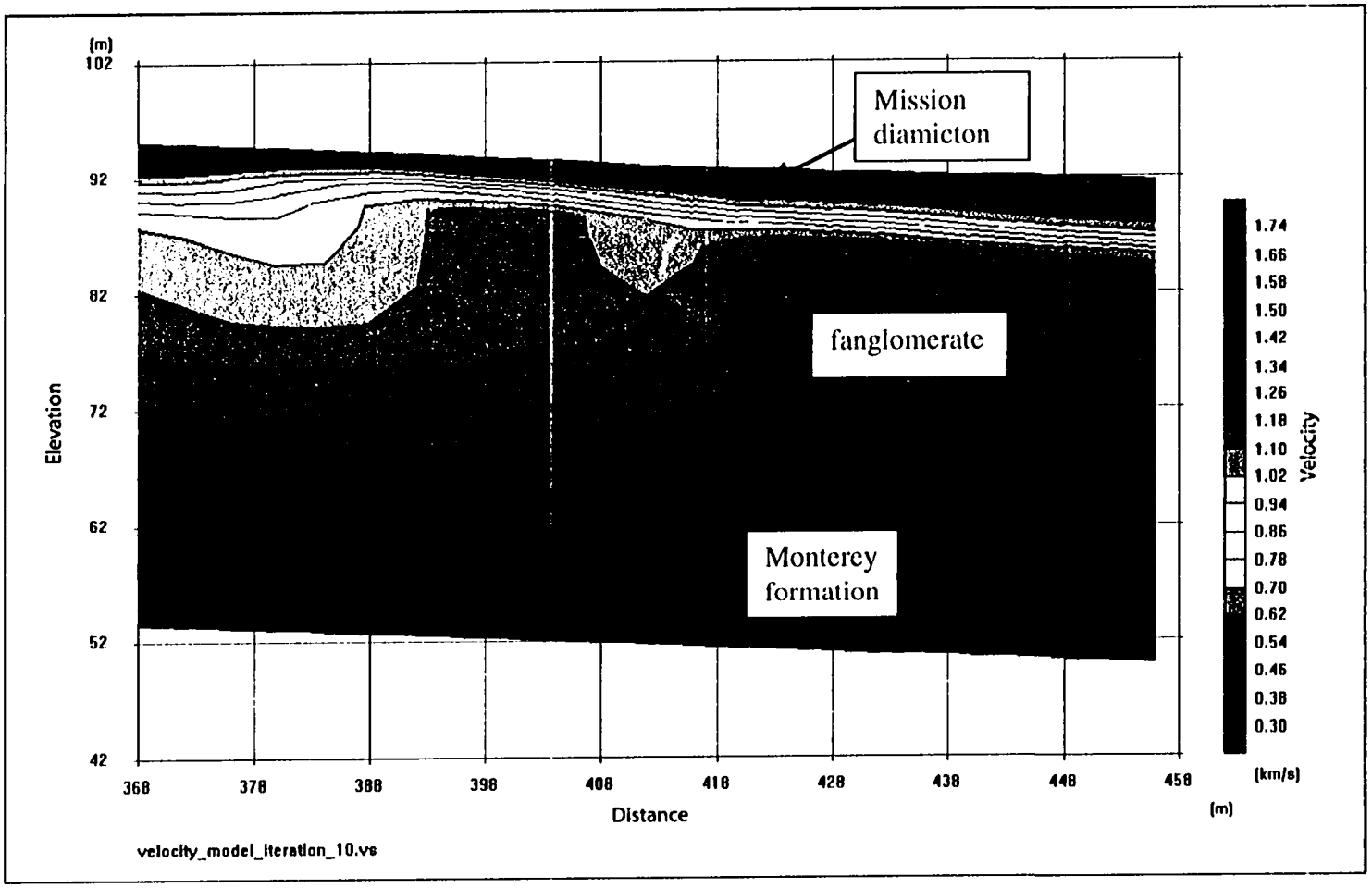

Figure A2. Tomographic analysis velocity model for survey 1001. Survey trends approximately N090E from right to left.

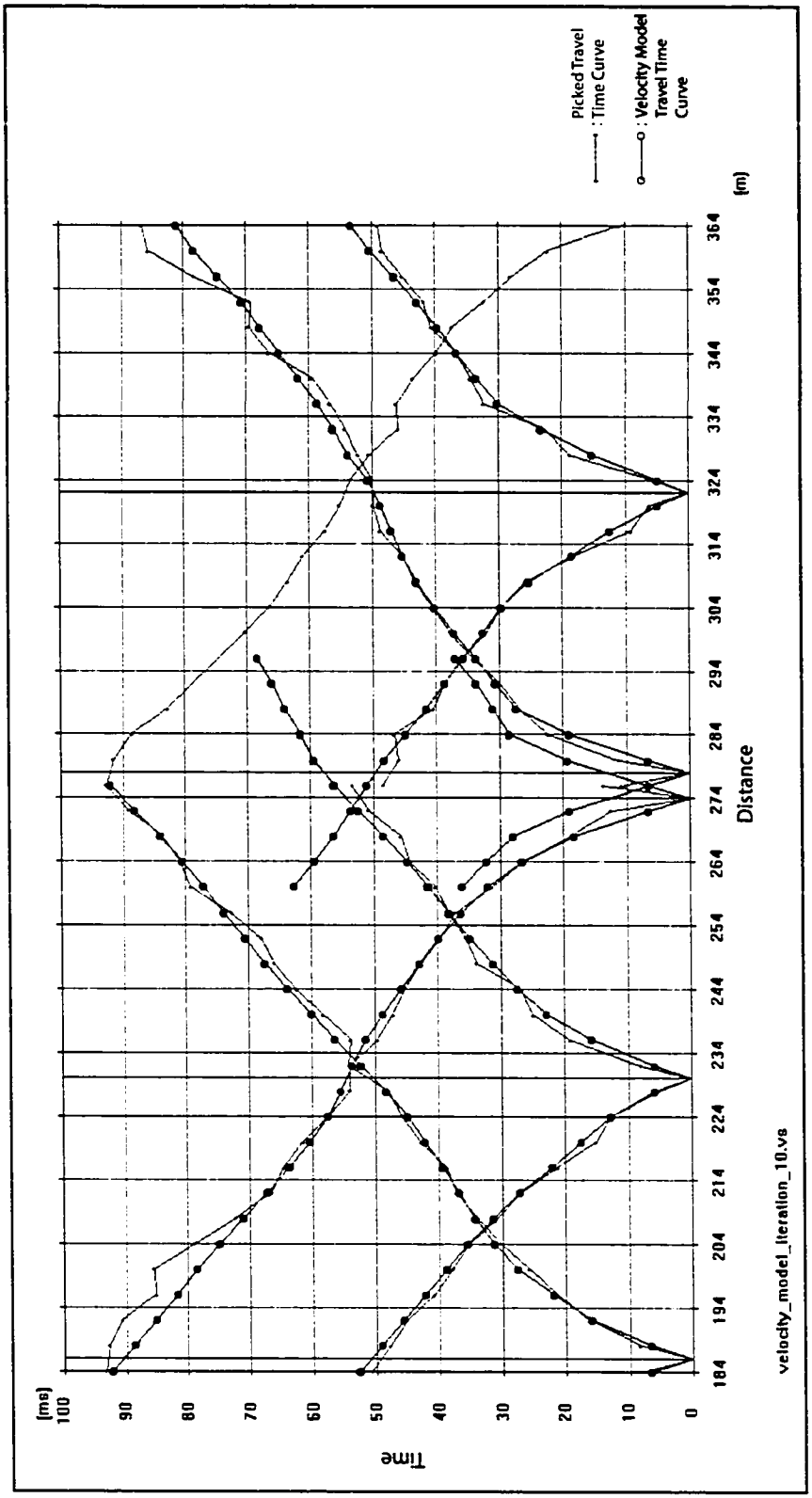

Figure A3. Tomographic analysis travel time curves for surveys 1002 and 1003.

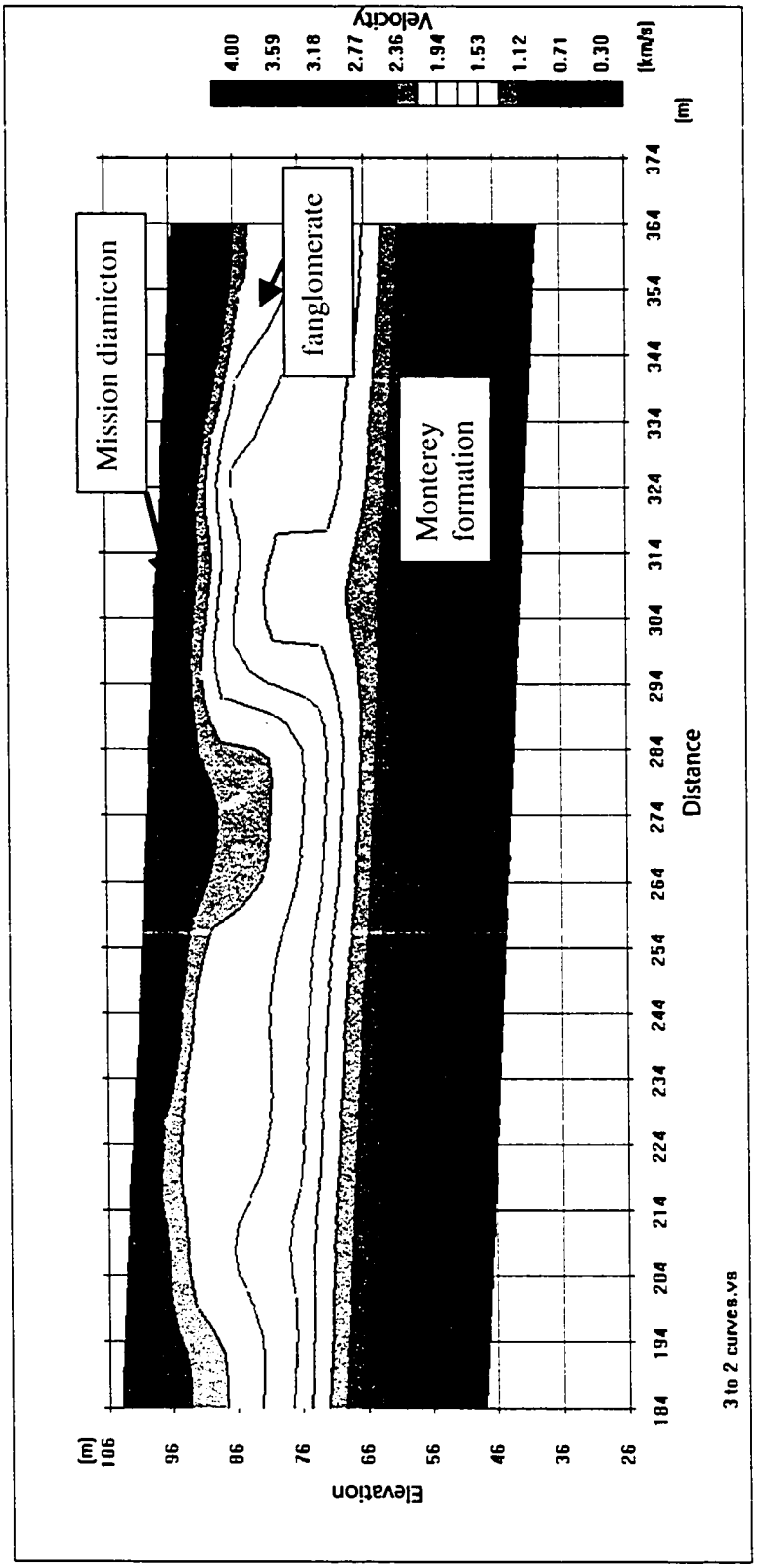

Figure A4. Tomographic analysis velocity model for surveys 1002 and 1003. Survey trends approximately N090E from right to left.

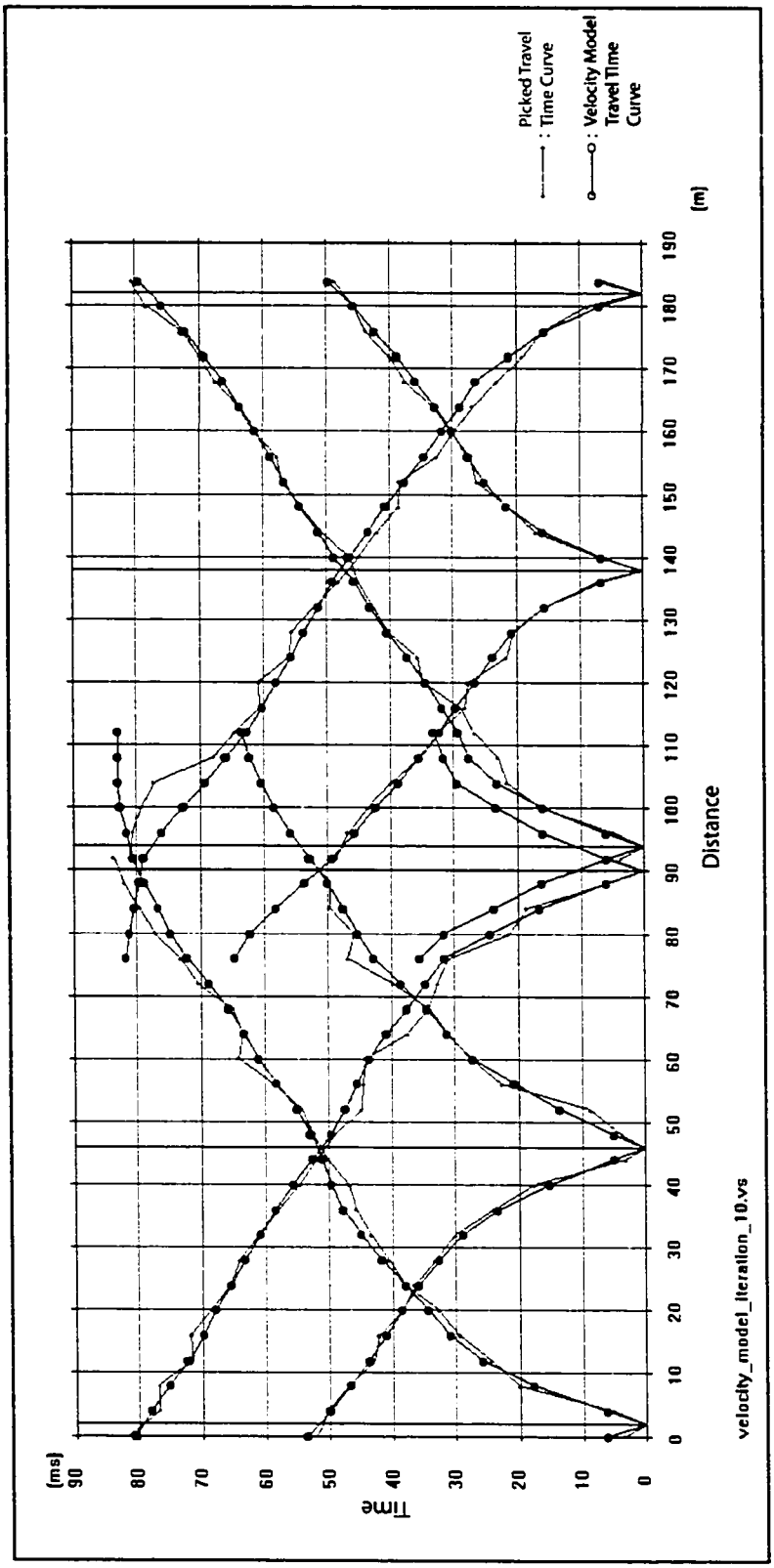

Figure A5. Tomographic analysis travel time curves for surveys 1004 and 1005.

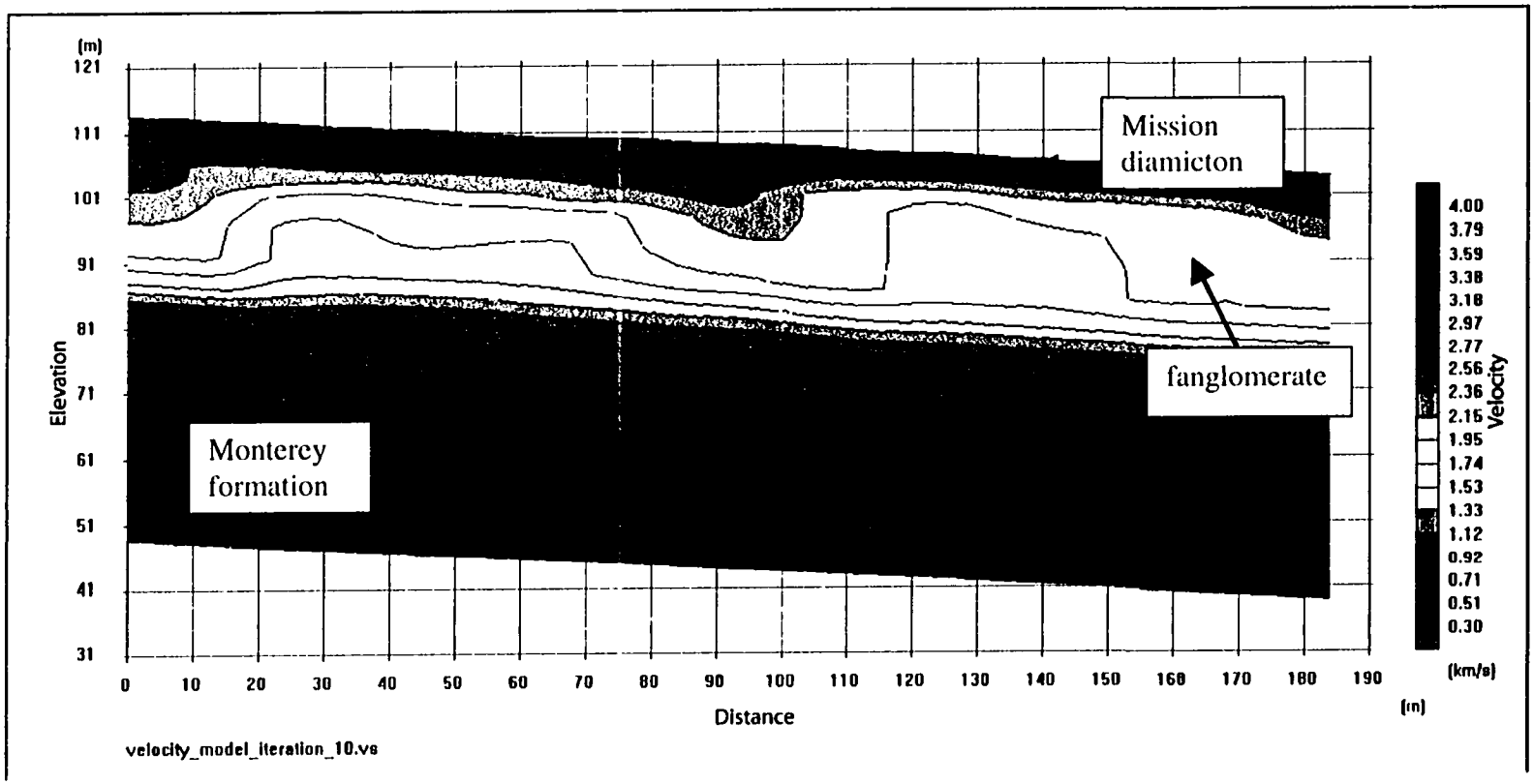

Figure A6. Tomographic analysis velocity model for surveys 1004 and 1005. Survey trends approximately N090E from right to left.

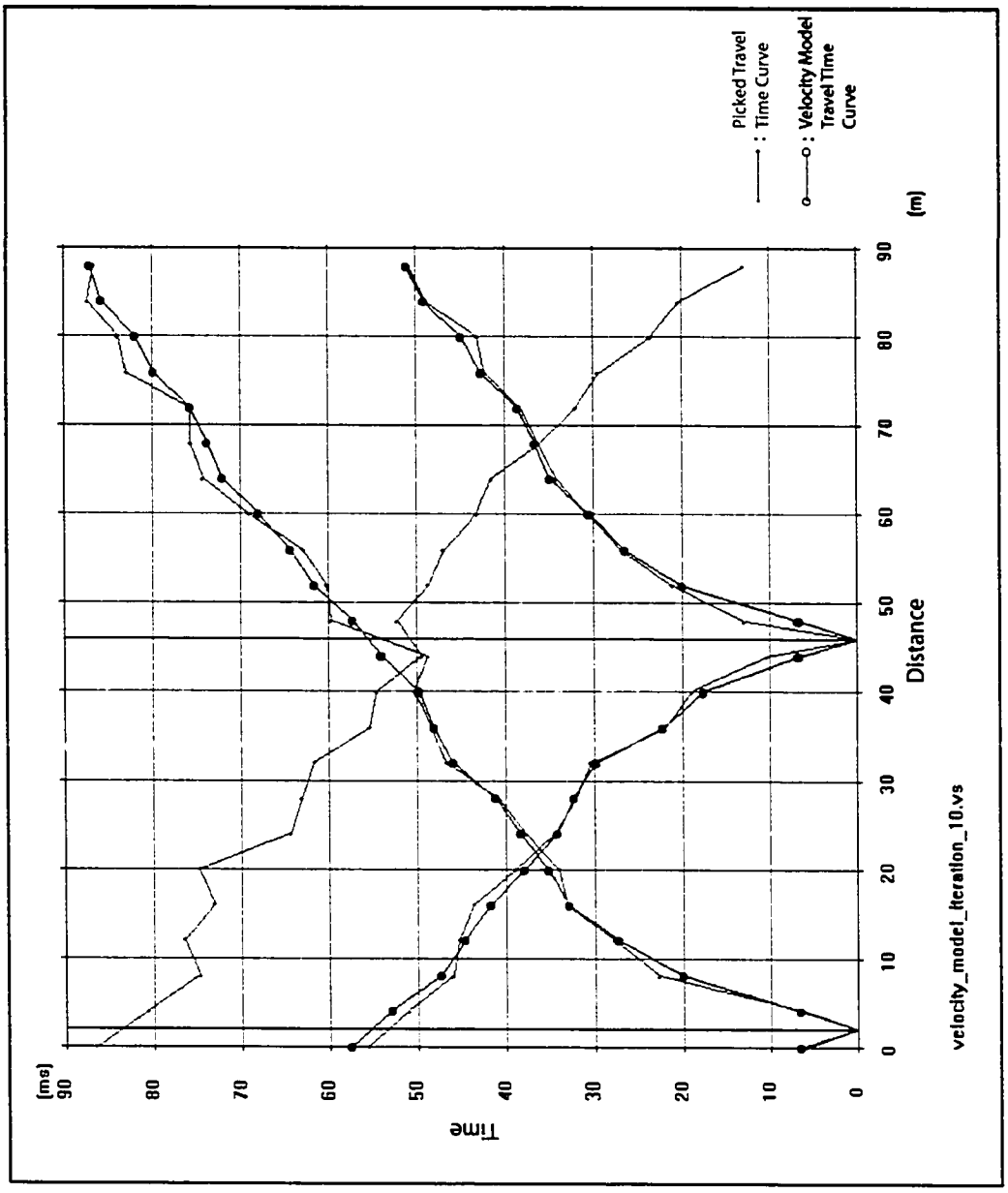

Figure A7. Tomographic analysis travel time curves for survey 1006.

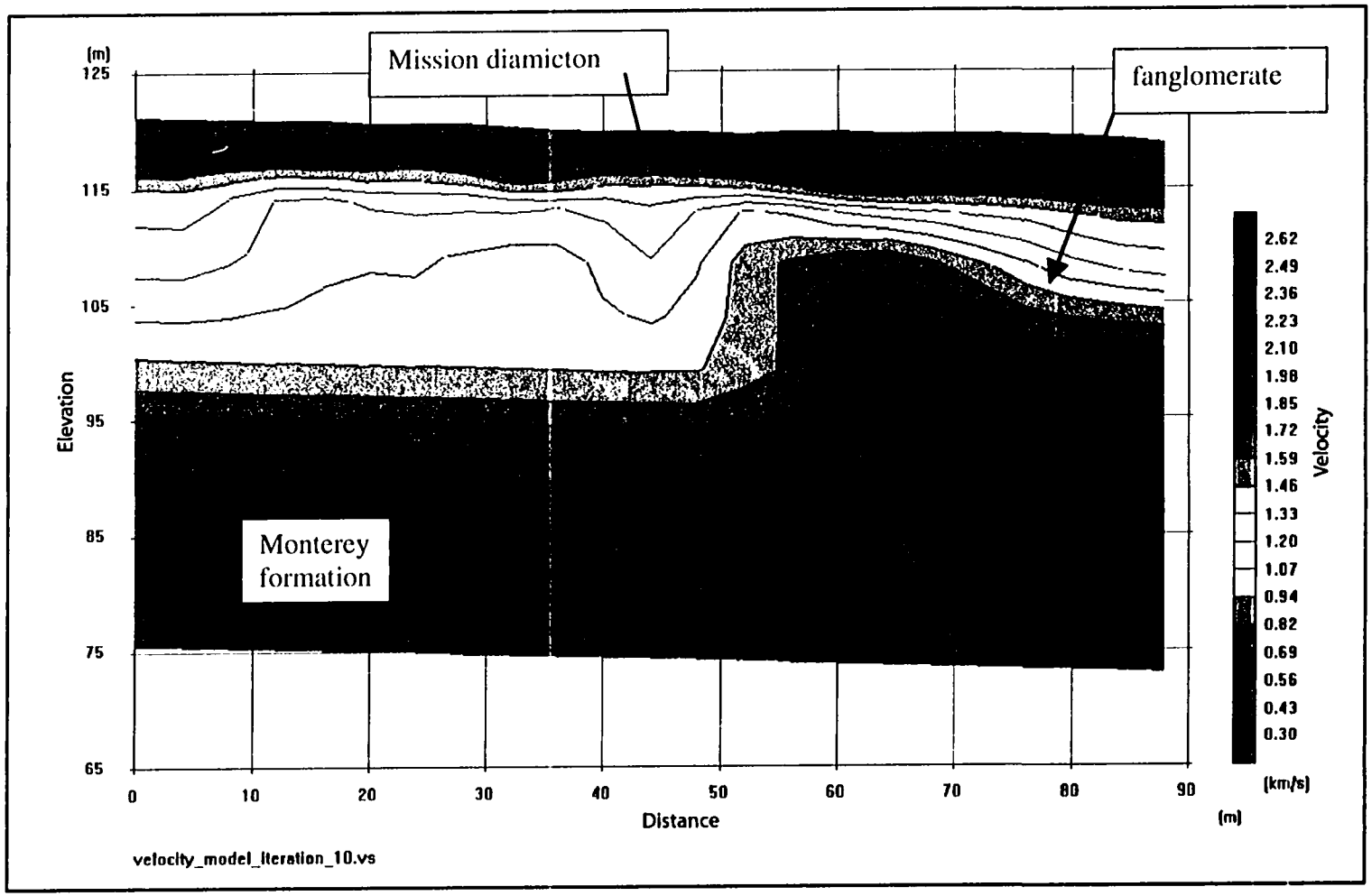

Figure A8. Tomographic analysis velocity model for survey 1006. Survey trends approximately due north from right to left.

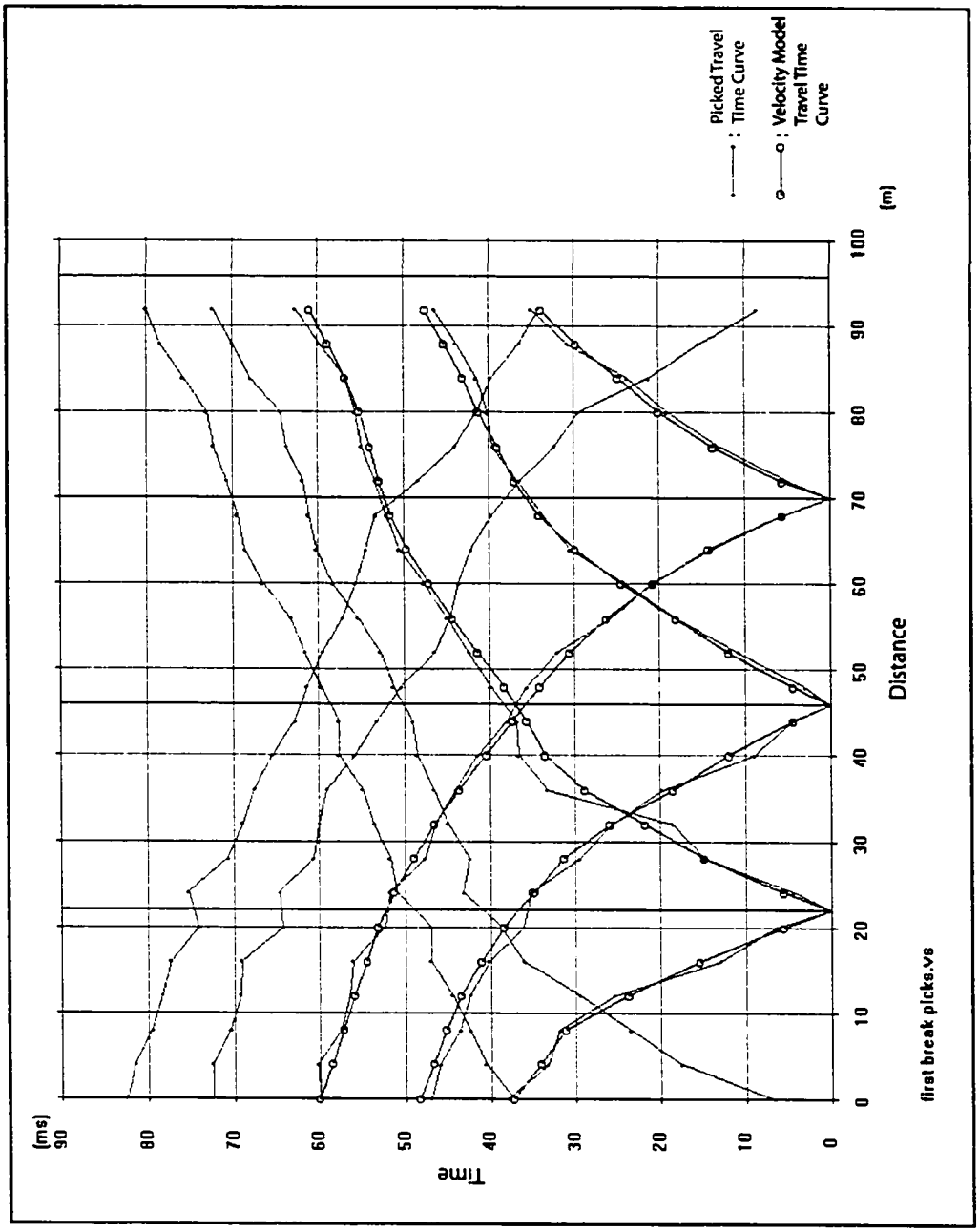

Figure A9. Tomographic analysis travel time curves for survey 1007.

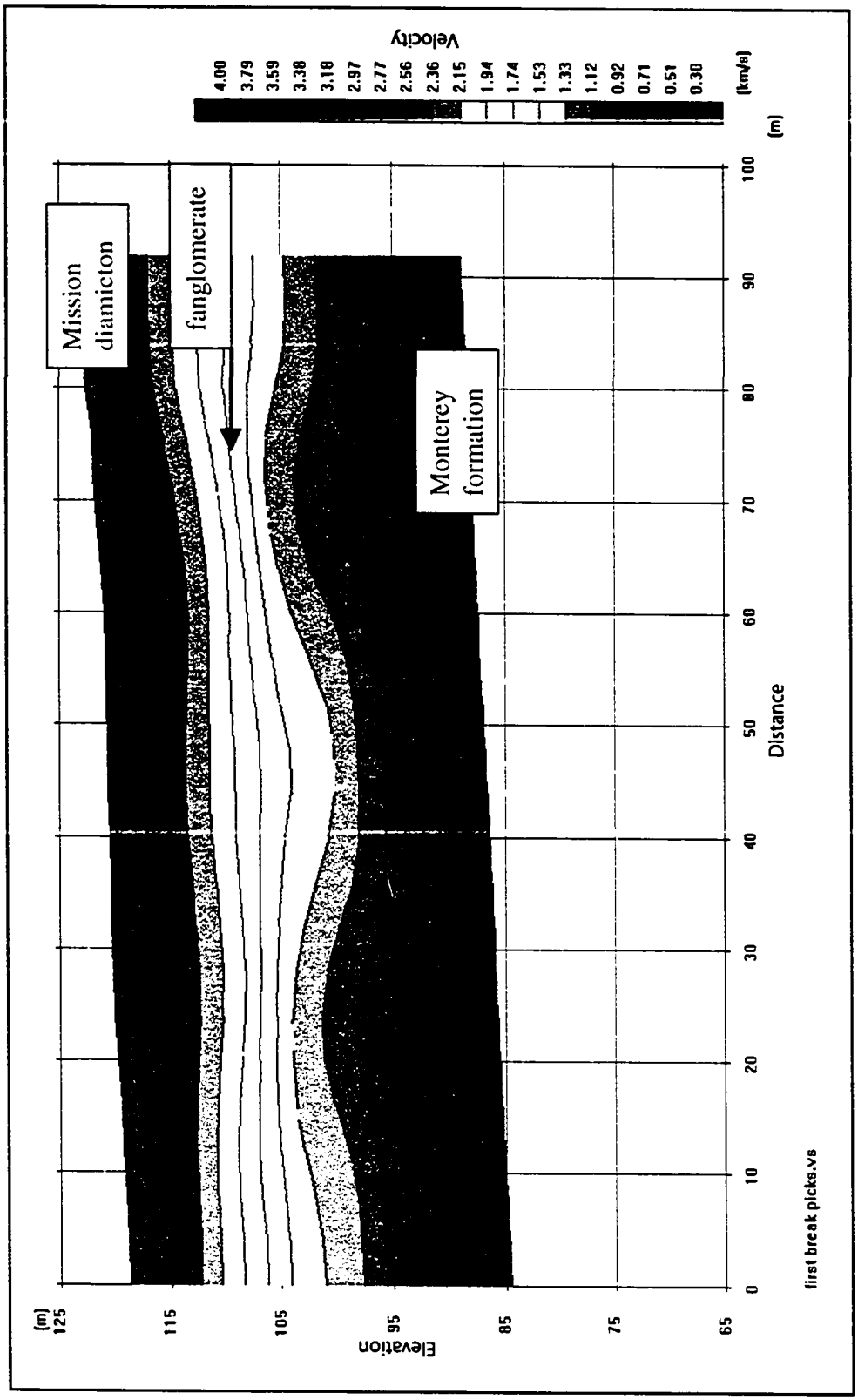

Figure A10. Tomographic analysis velocity model for survey 1007. Survey trends approximately N008E from left to right.

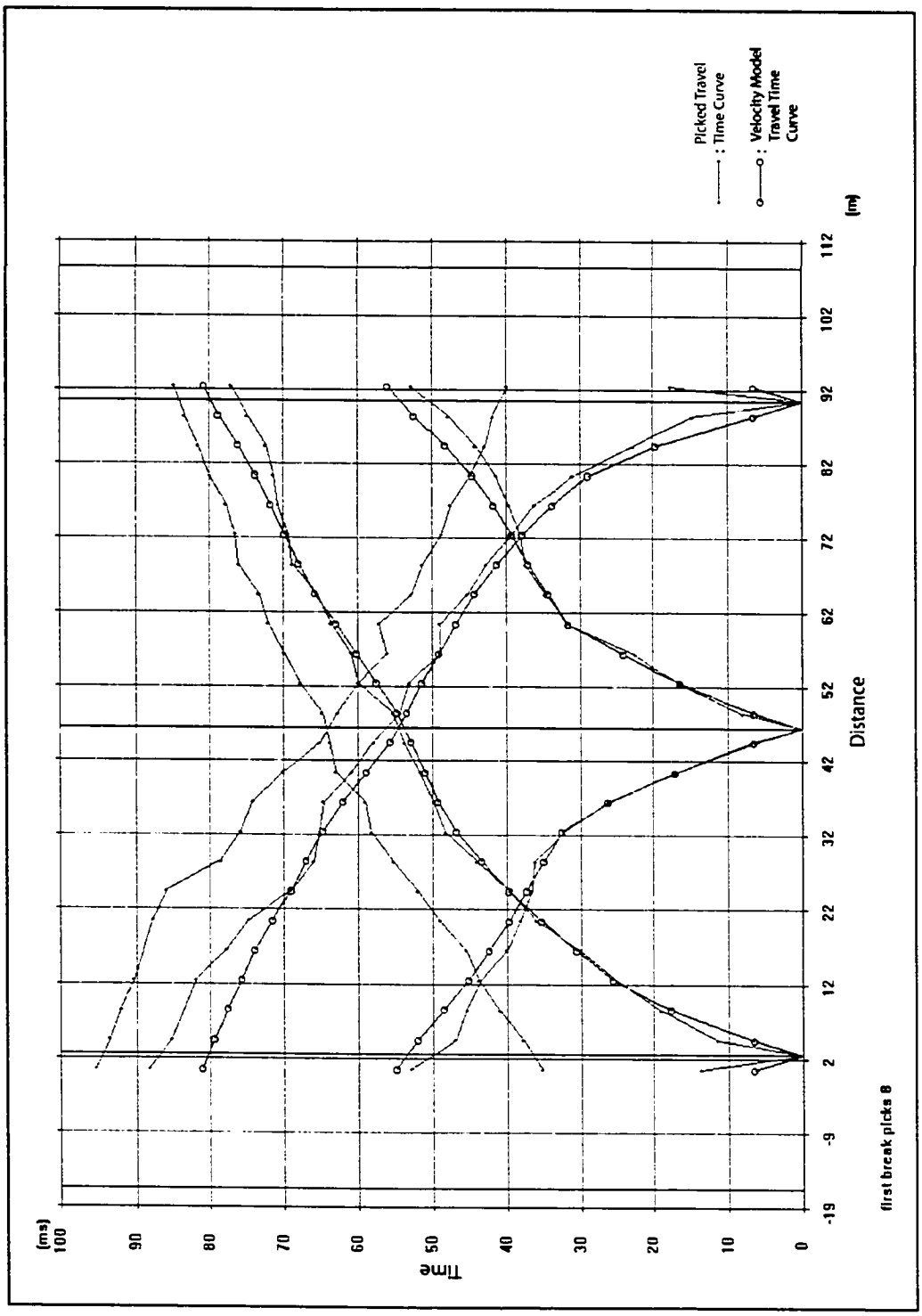

Figure A11. Tomographic analysis travel time curves for survey 1008.

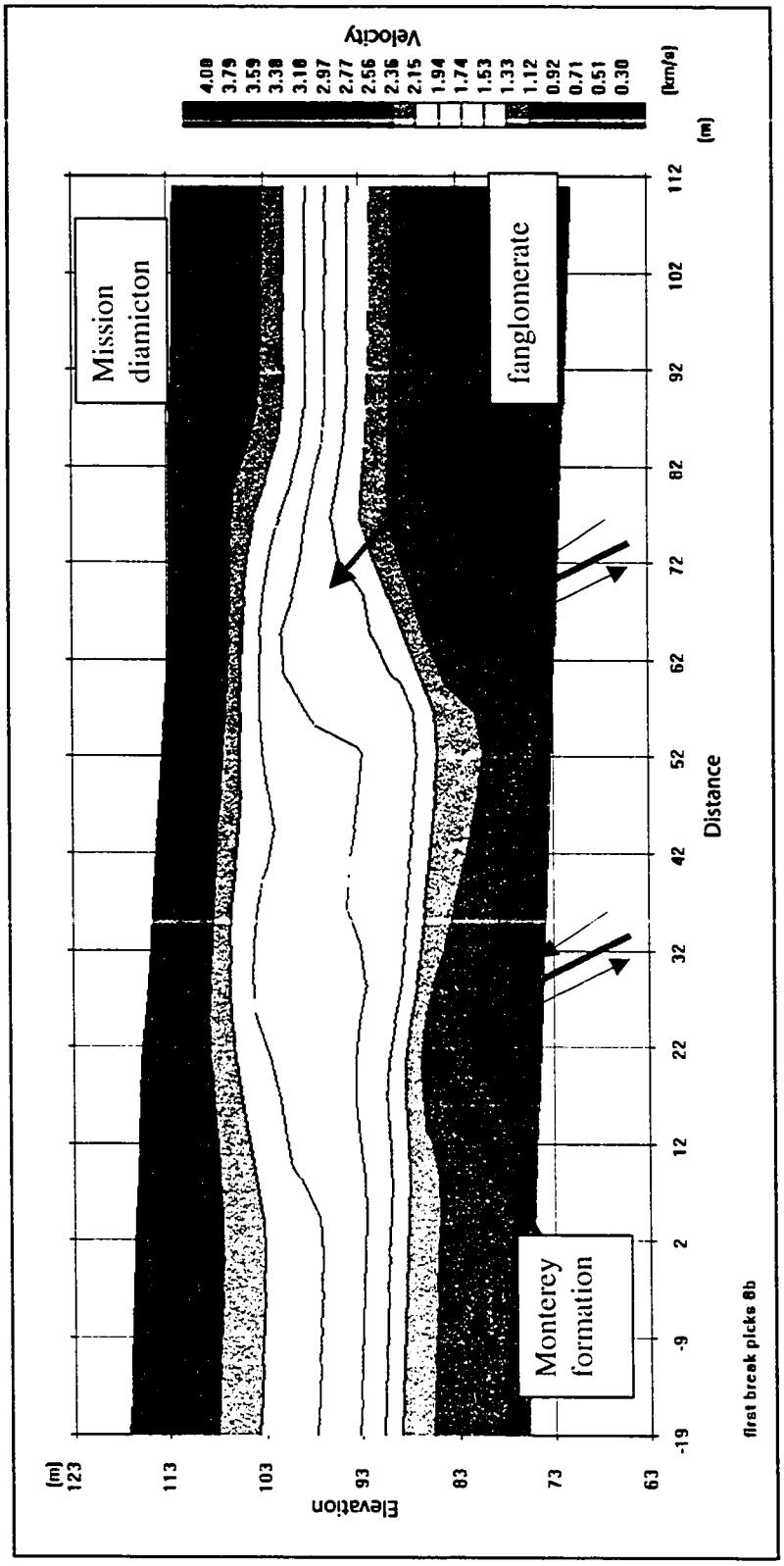

Figure A12. Tomographic analysis velocity model for survey 1008. Survey trends approximately N036E from right to left.

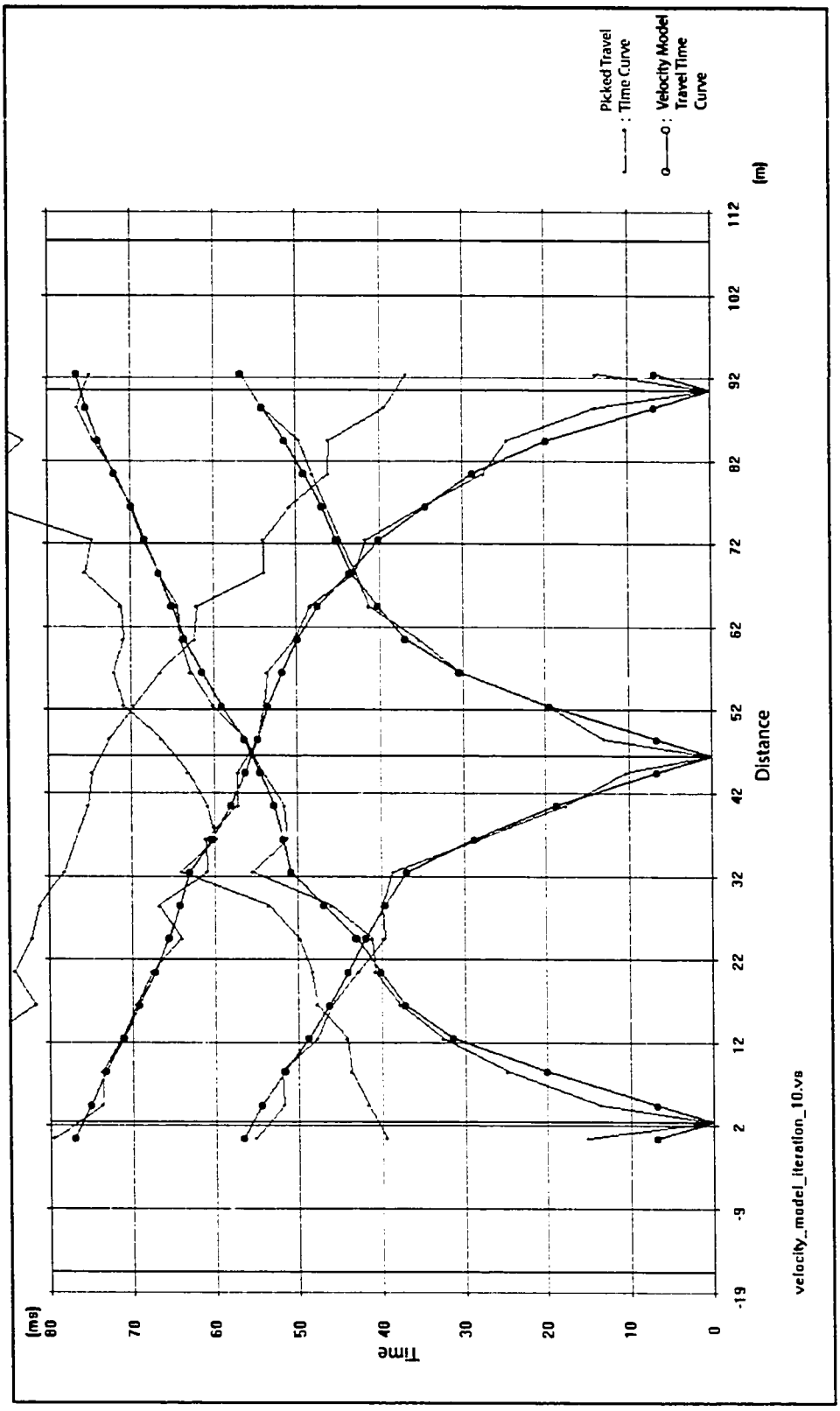

Figure A13. Tomographic analysis travel time curves for survey 1009.

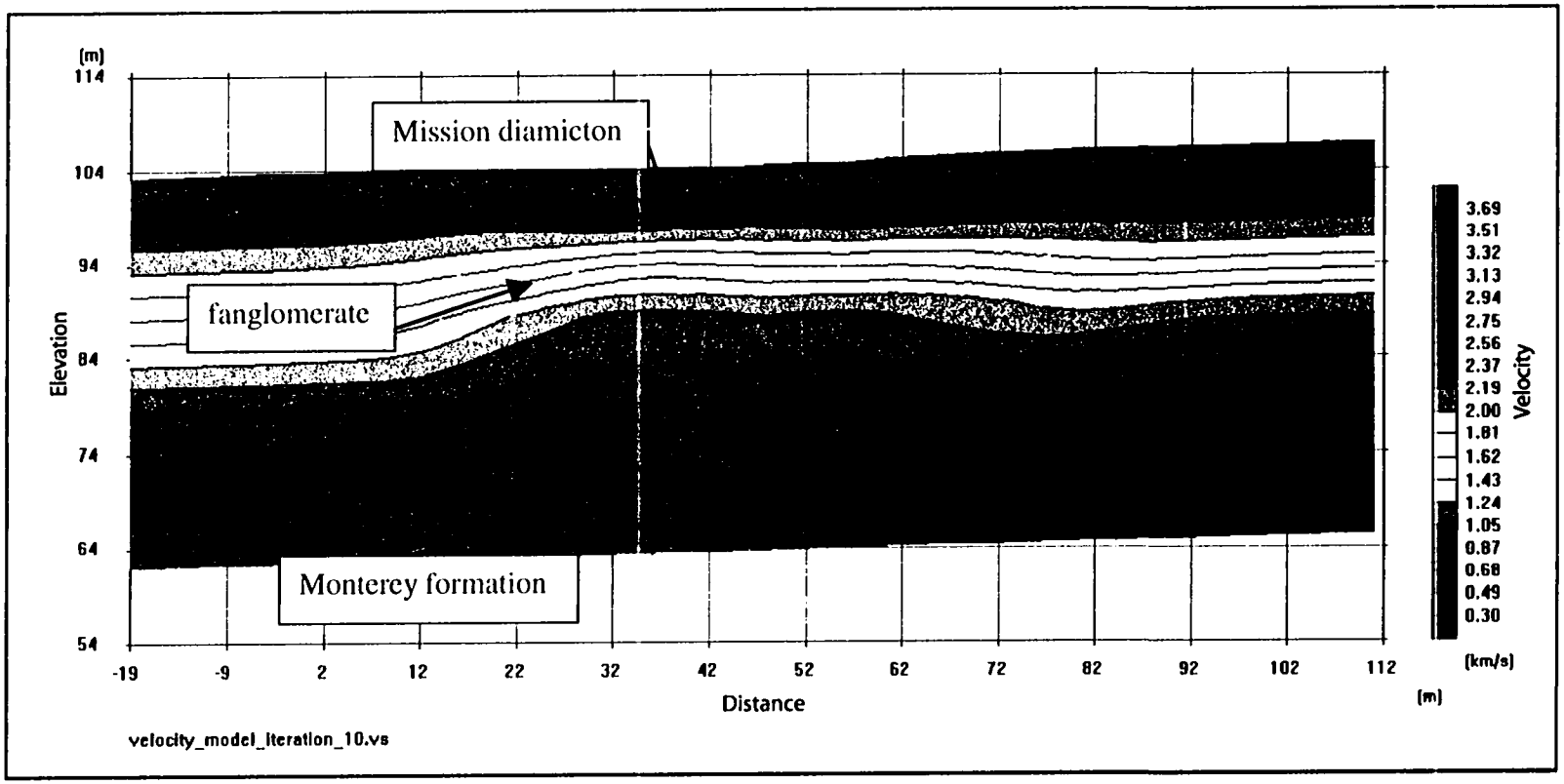

Figure A14. Tomographic analysis velocity model for survey 1009. Survey trends approximately N027E from left to right.

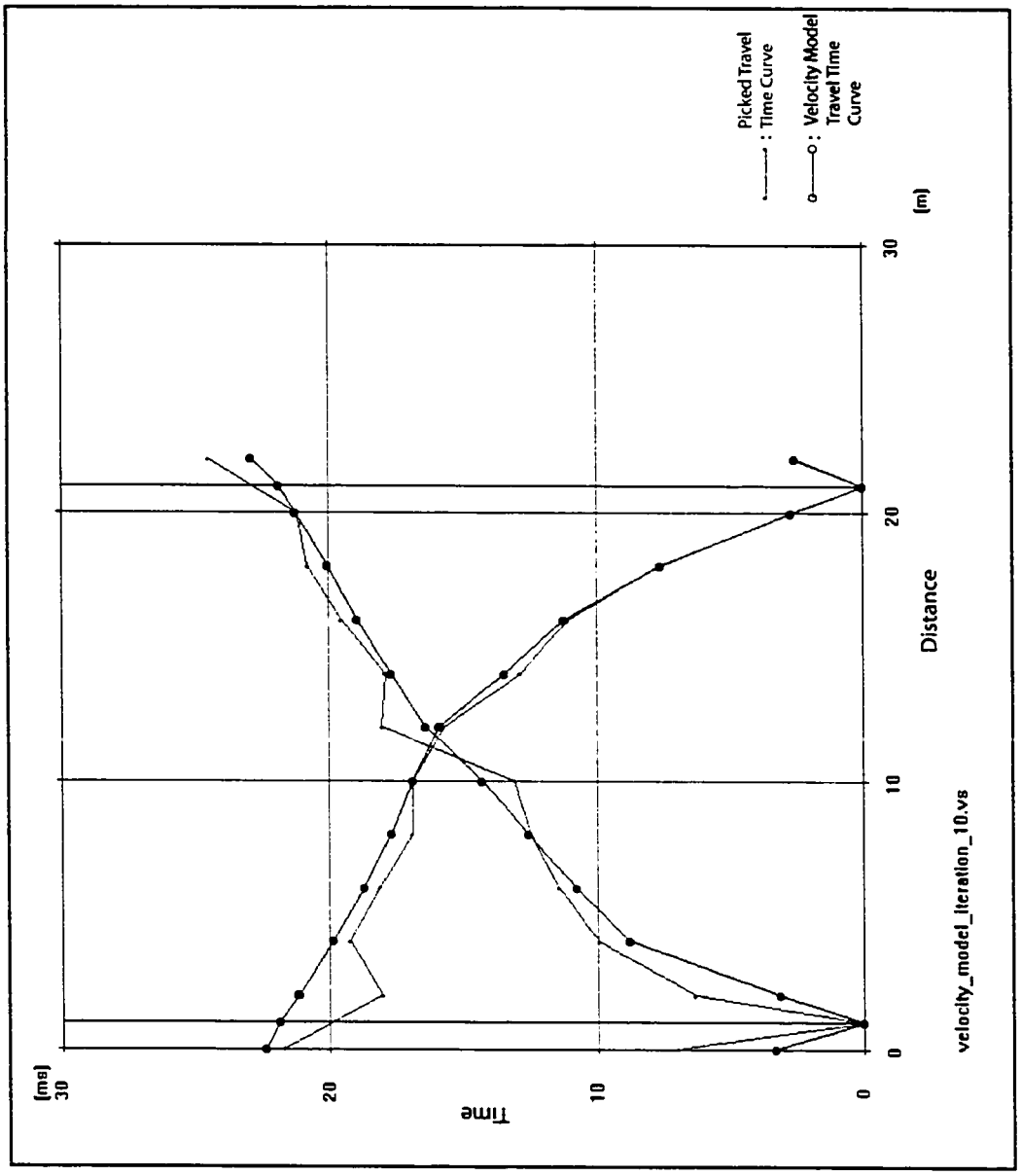

Figure A15. Tomographic analysis travel time curves for survey 1010.

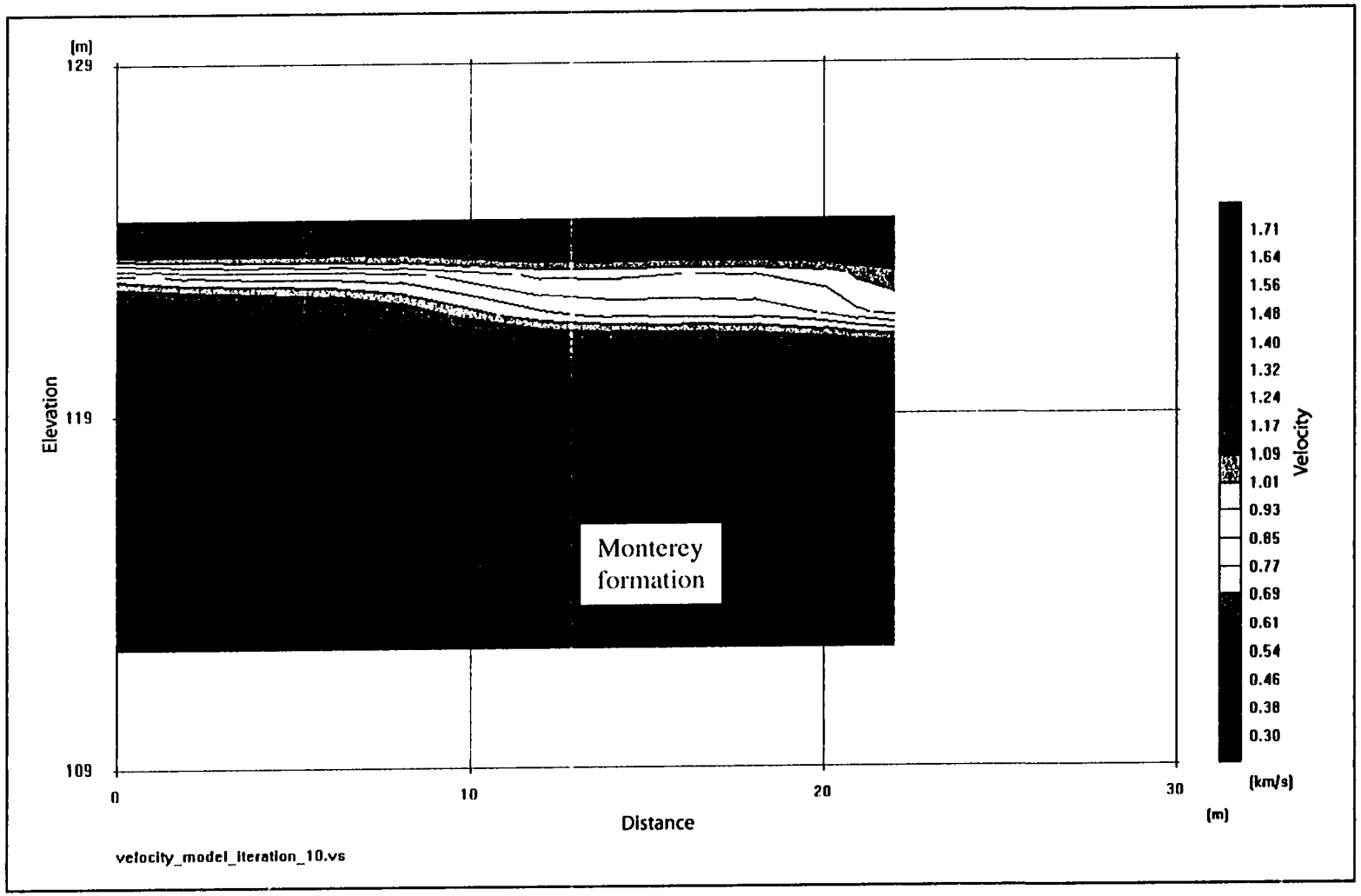

Figure A16. Tomographic analysis velocity model for survey 1010. Survey trends approximately N032E from right to left. Survey conducted directly on Monterey Formation outcrops.

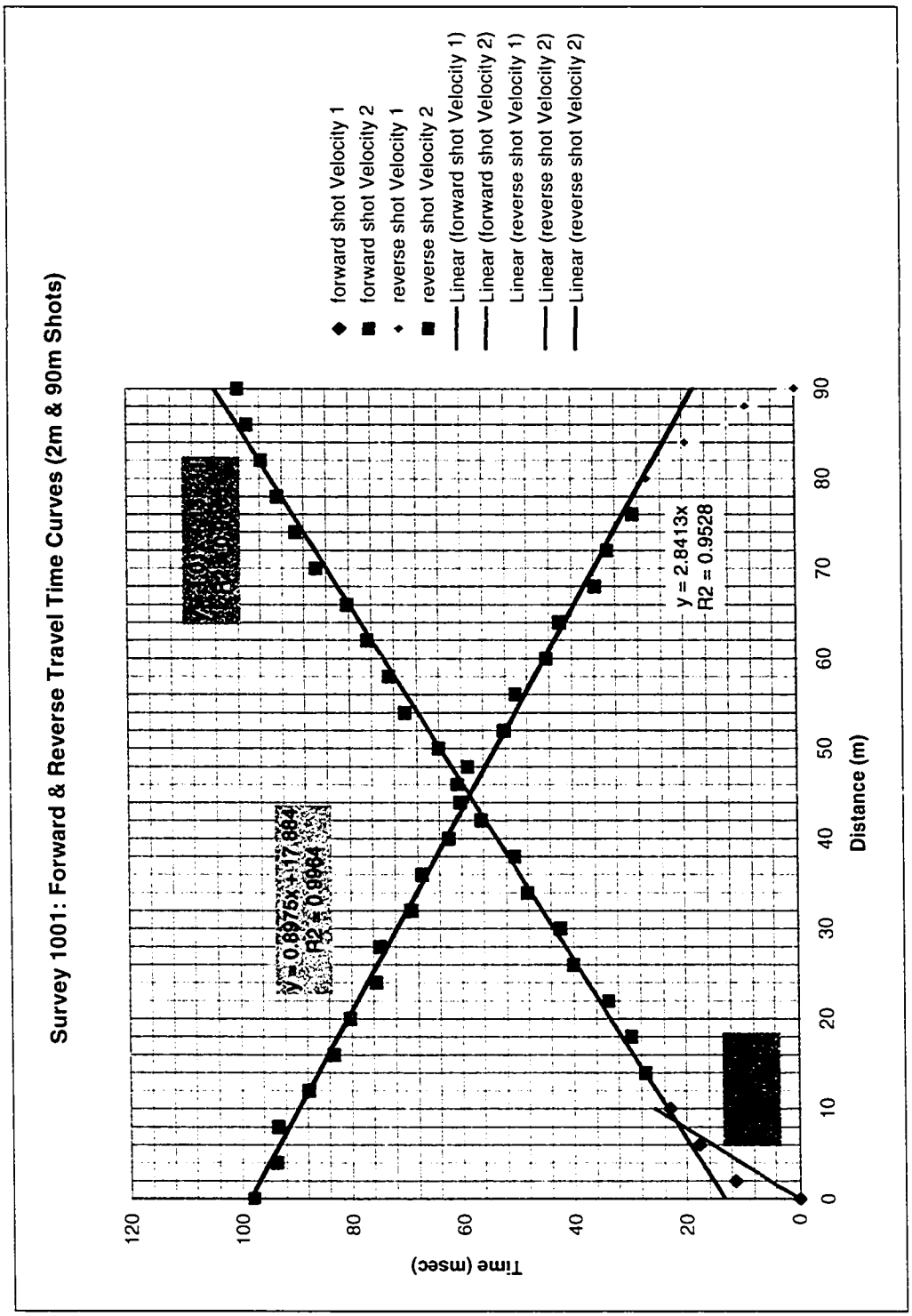

Figure A17. Survey 1001 two-way travel time analysis.

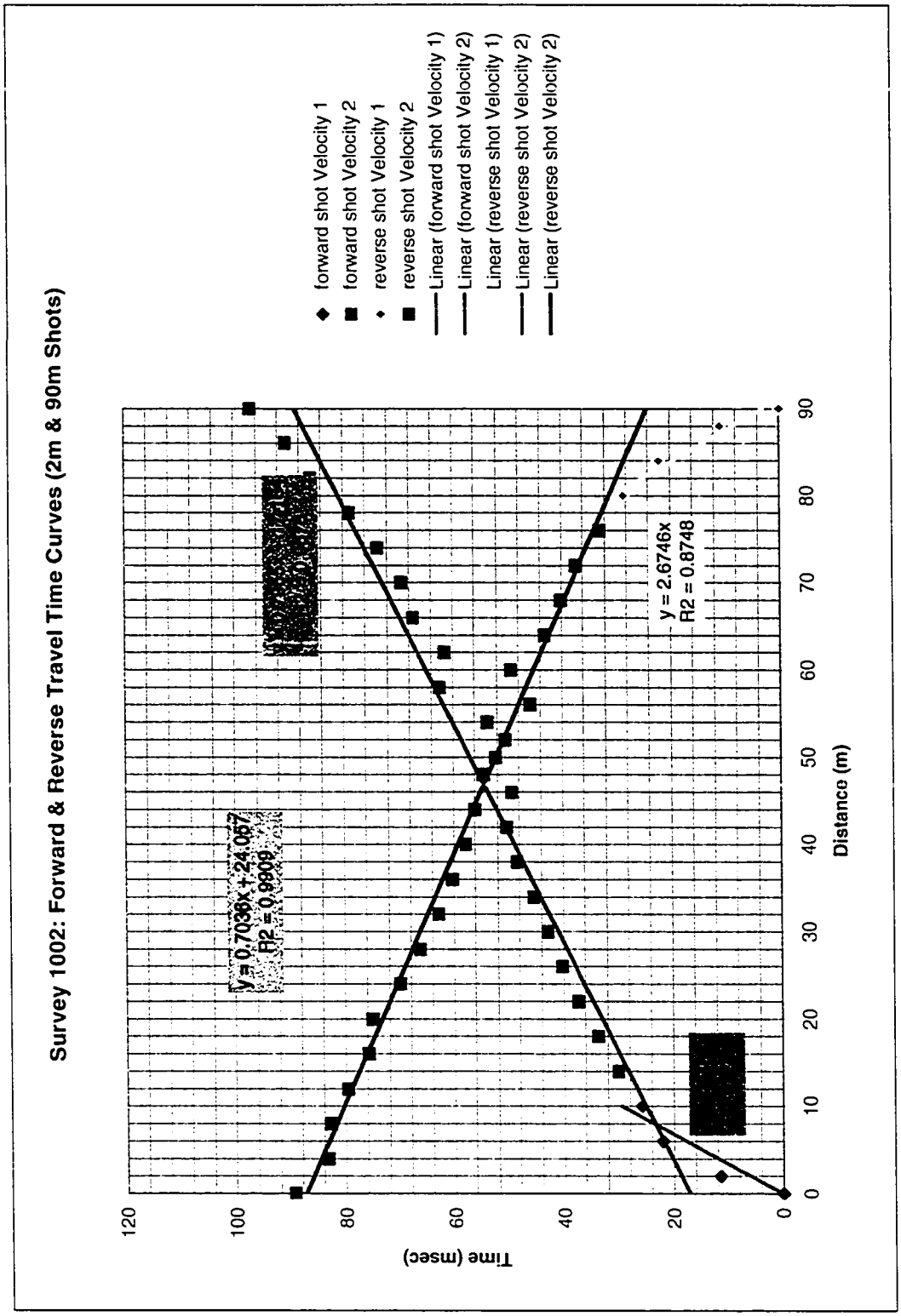

Figure A18. Survey 1002 two-way travel time analysis.

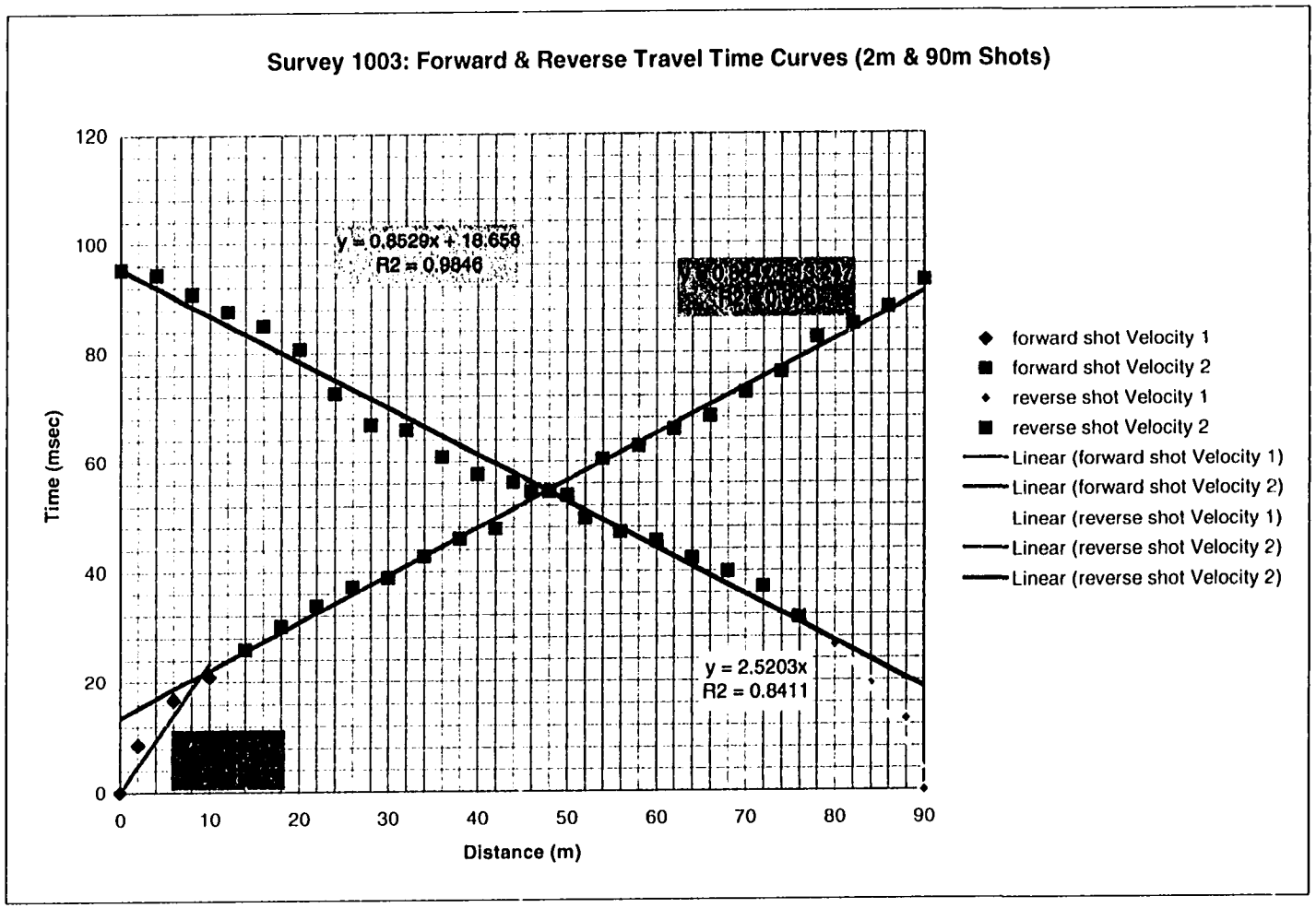

Figure A19. Survey 1003 two-way travel time analysis.

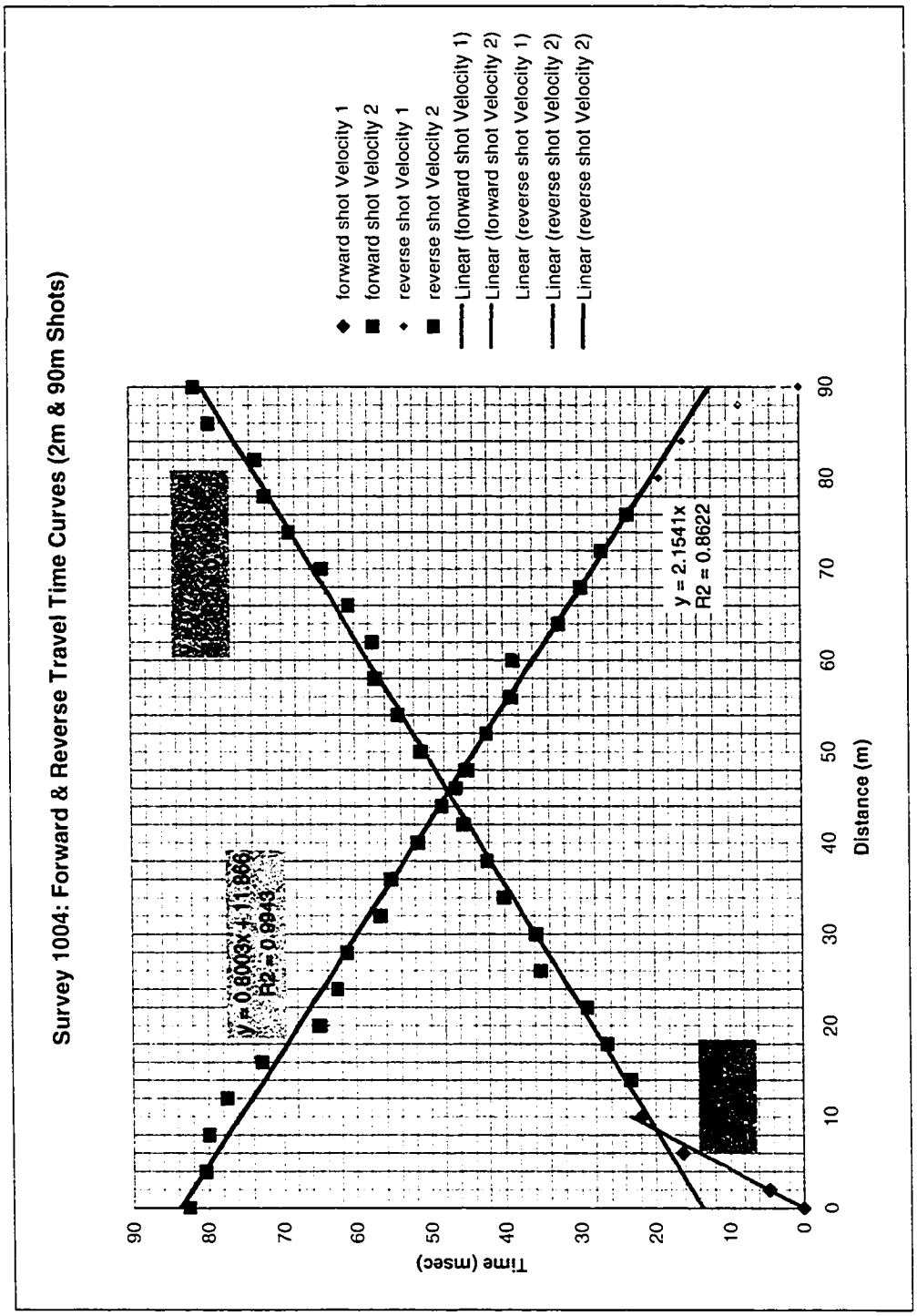

Figure A20. Survey 1004 two-way travel time analysis.

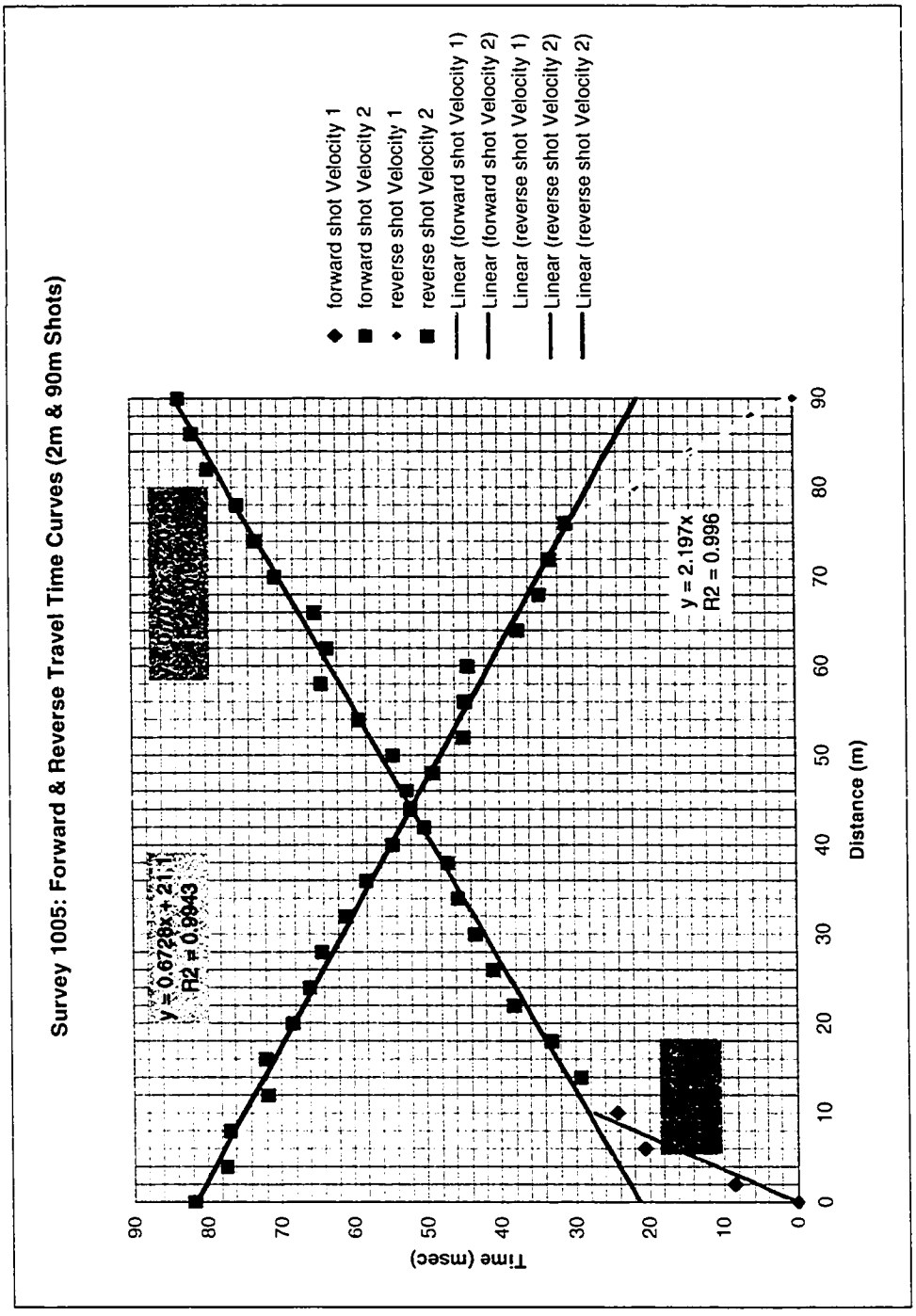

Figure A21. Survey 1005 two-way travel time analysis.

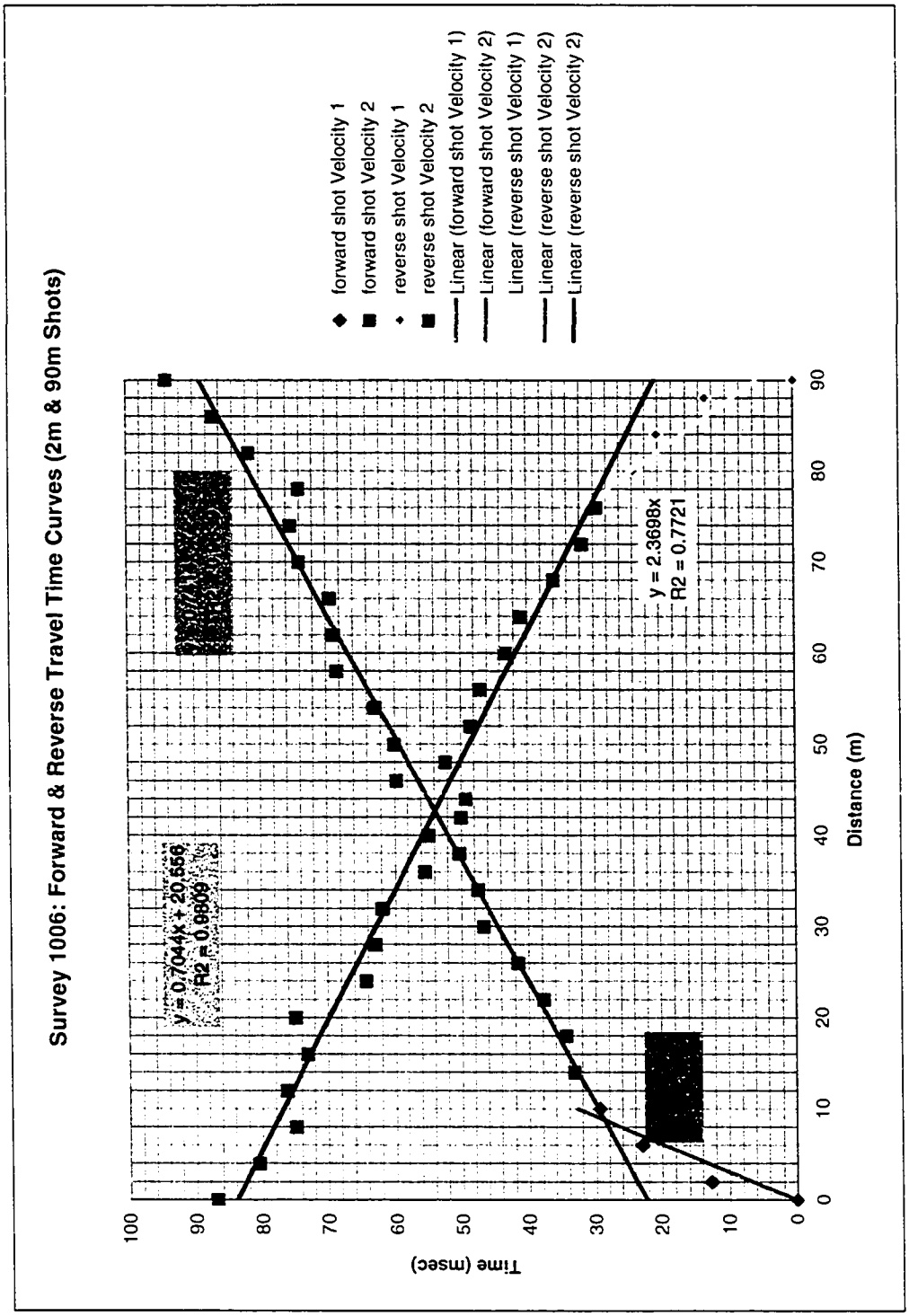

Figure A22. Survey 1006 two-way travel time analysis.

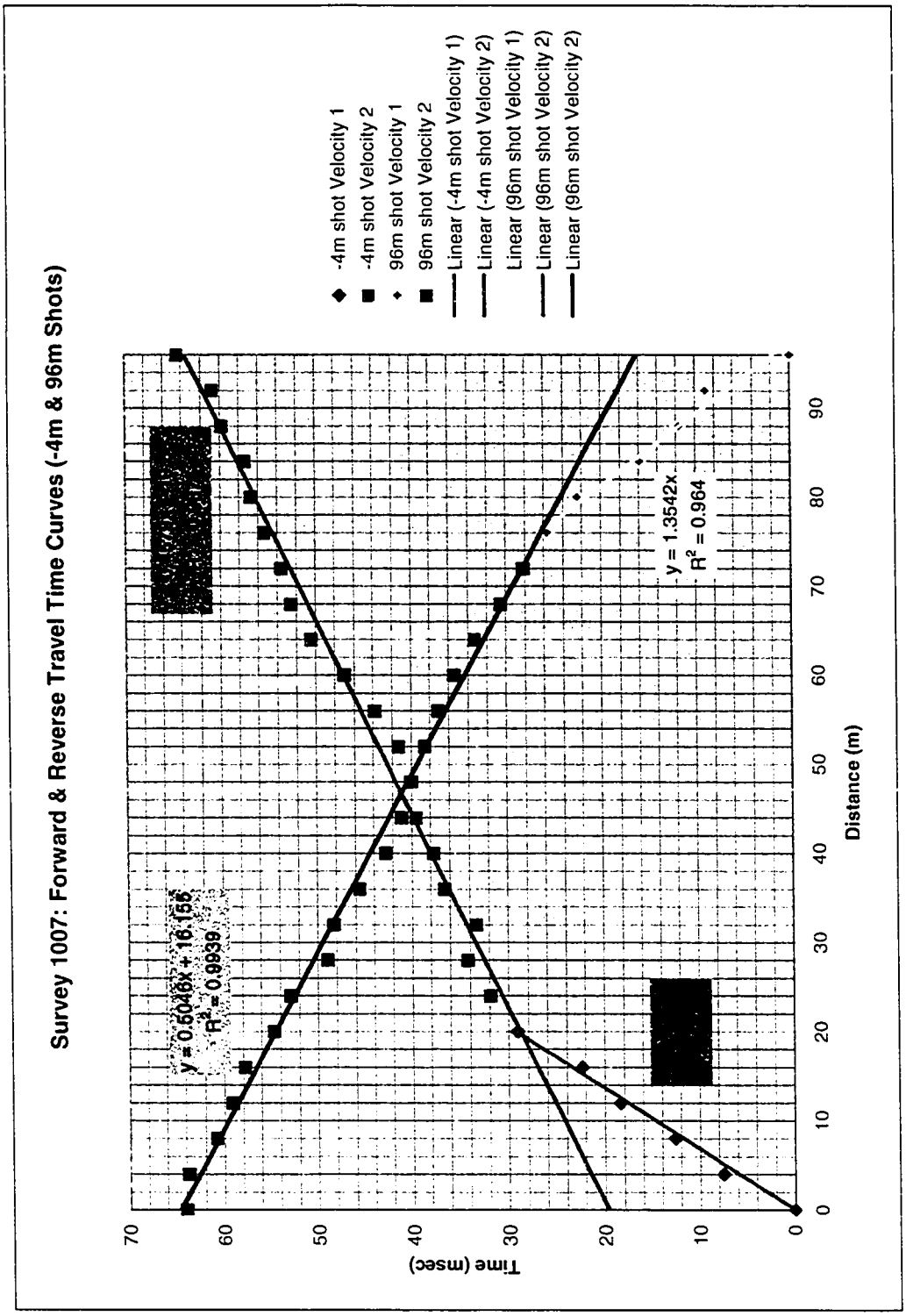

Figure A23. Survey 1007 two-way travel time analysis

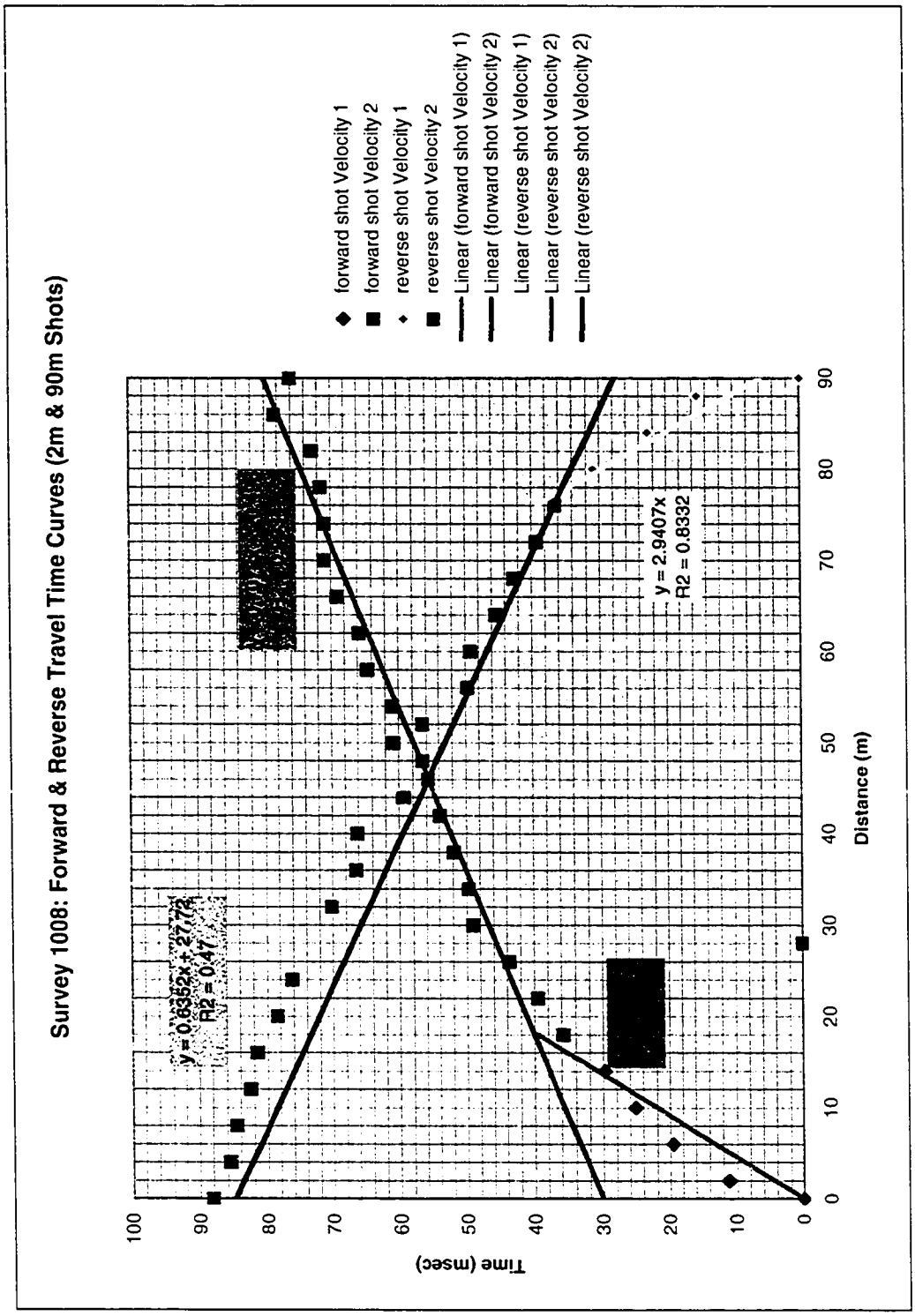

Figure A24. Survey 1008 two-way travel time analysis

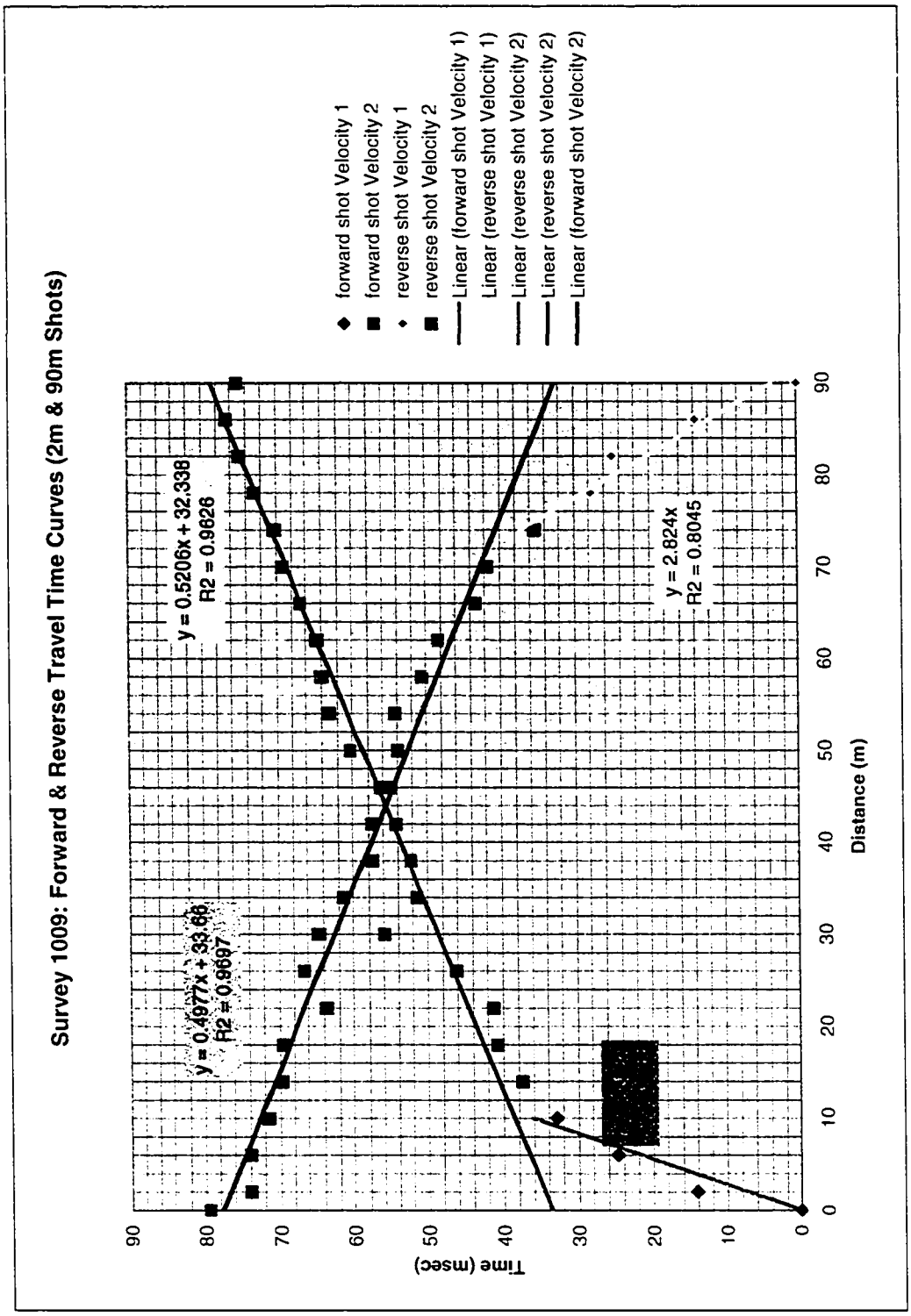

Figure A25. Survey 1009 two-way travel time analysis

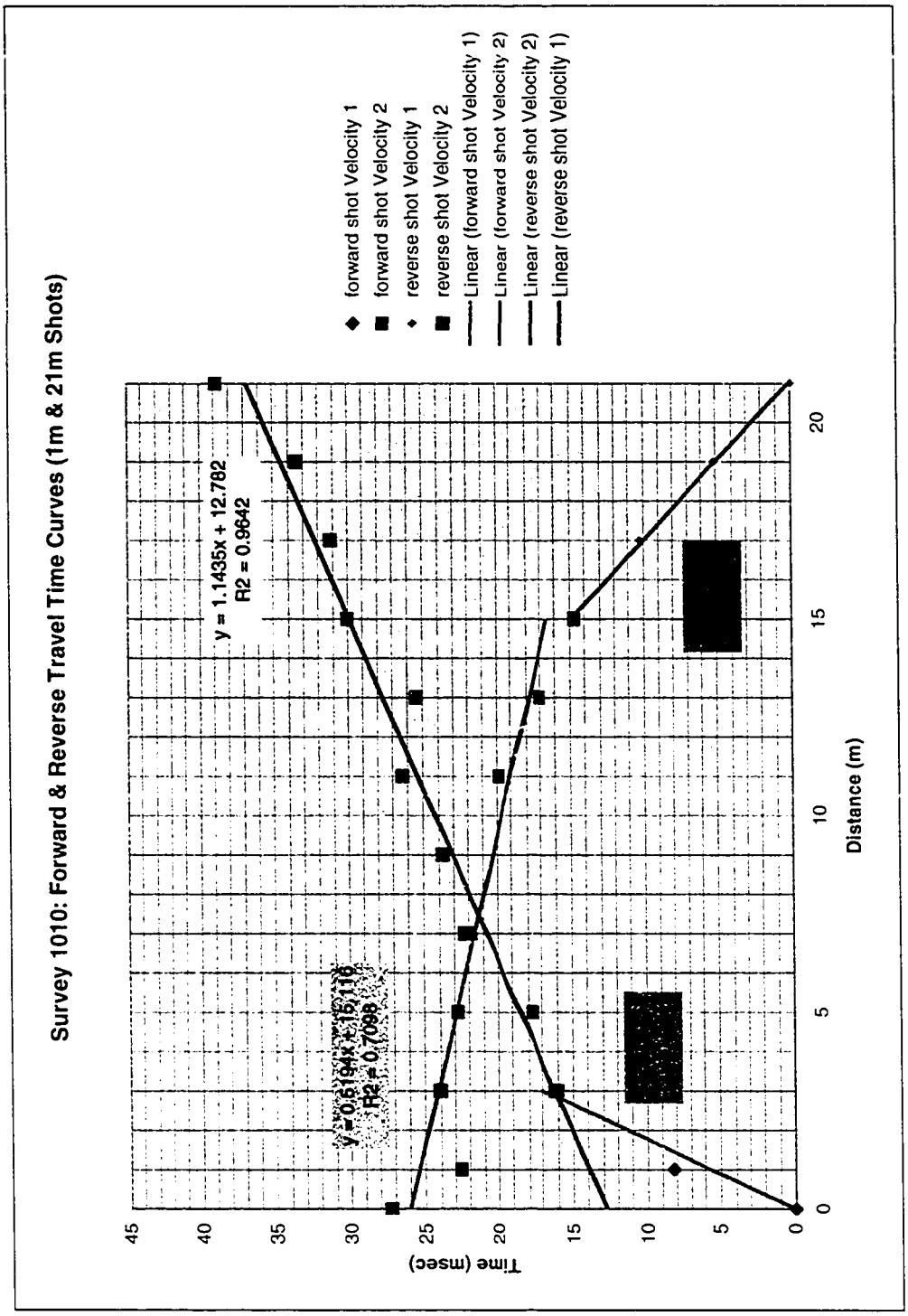

Figure A26. Survey 1010 two-way travel time analysis

APPENDIX B

RESISTIVITY DATA AND ANALYSIS

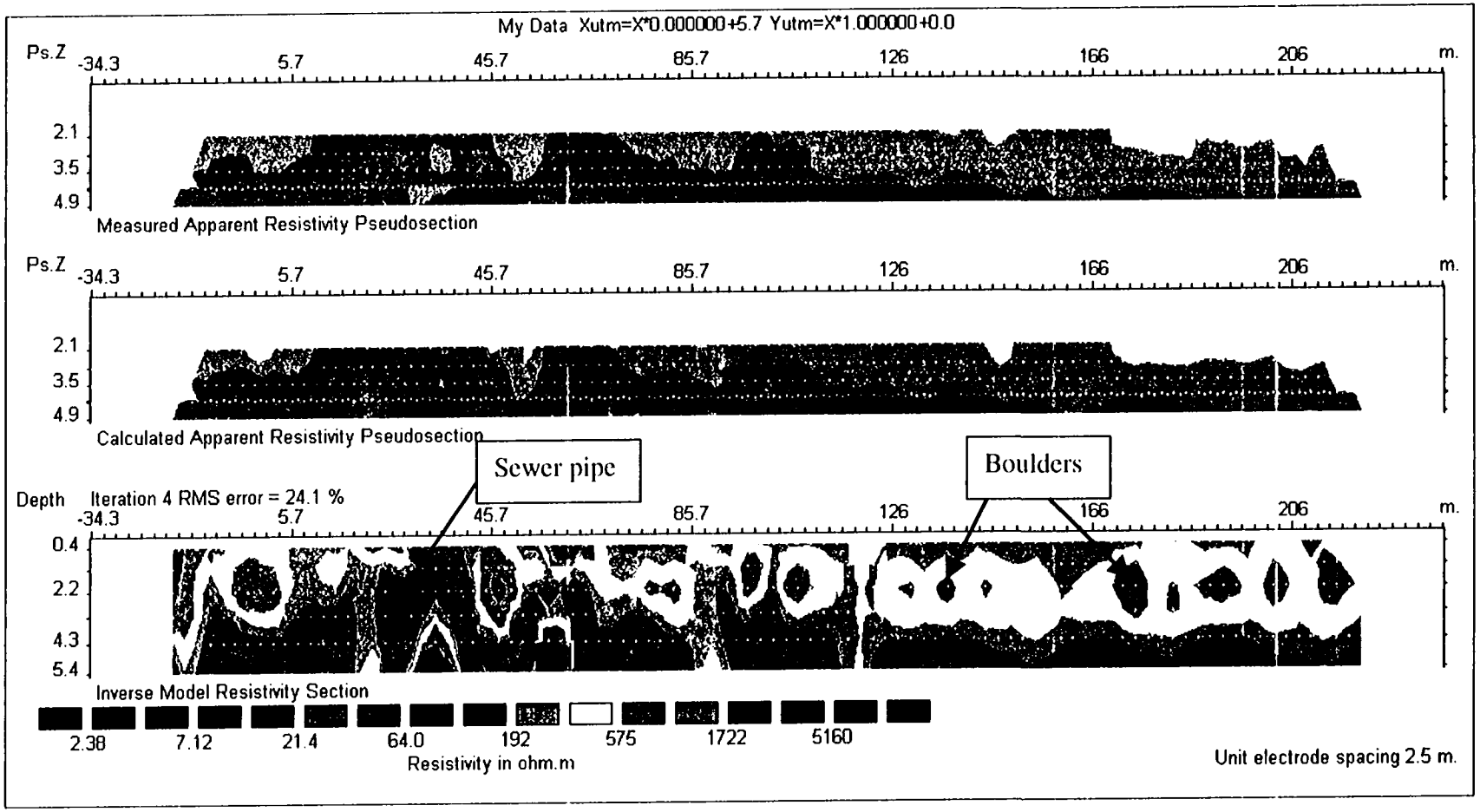

Figure B1. Resistivity Pseudosections and Model resistivity section. Resistivity survey approximately parallels seismic refraction surveys 1008 to 1007 from left to right.

APPENDIX C

BOREHOLE DATA

BOREHOLE DATA

The borehole information provided in Appendix C is from a report titled: *Summary of Monitoring Well Construction, Mission Canyon Wastewater Facilities Project*, prepared by Hoover and Associates (Hoover and Associates, 1984). The boring logs and table of monitoring well design and water levels provide subsurface information in the region of the study area. Although the report indicates the depth to water encountered in boreholes, there is no indication as to whether the water levels are first encountered water during drilling or static water levels measured after water level stabilization. However, the report indicates that the water-bearing zone is a "perched water zone" in the study area (Hoover and Associates, 1984). A complete copy of the report can be obtained from the Santa Barbara County Health Department or the City of Santa Barbara Public Works Department. The logs included in this document are copies of the original logs provided in the report by Hoover and Associates (1984).

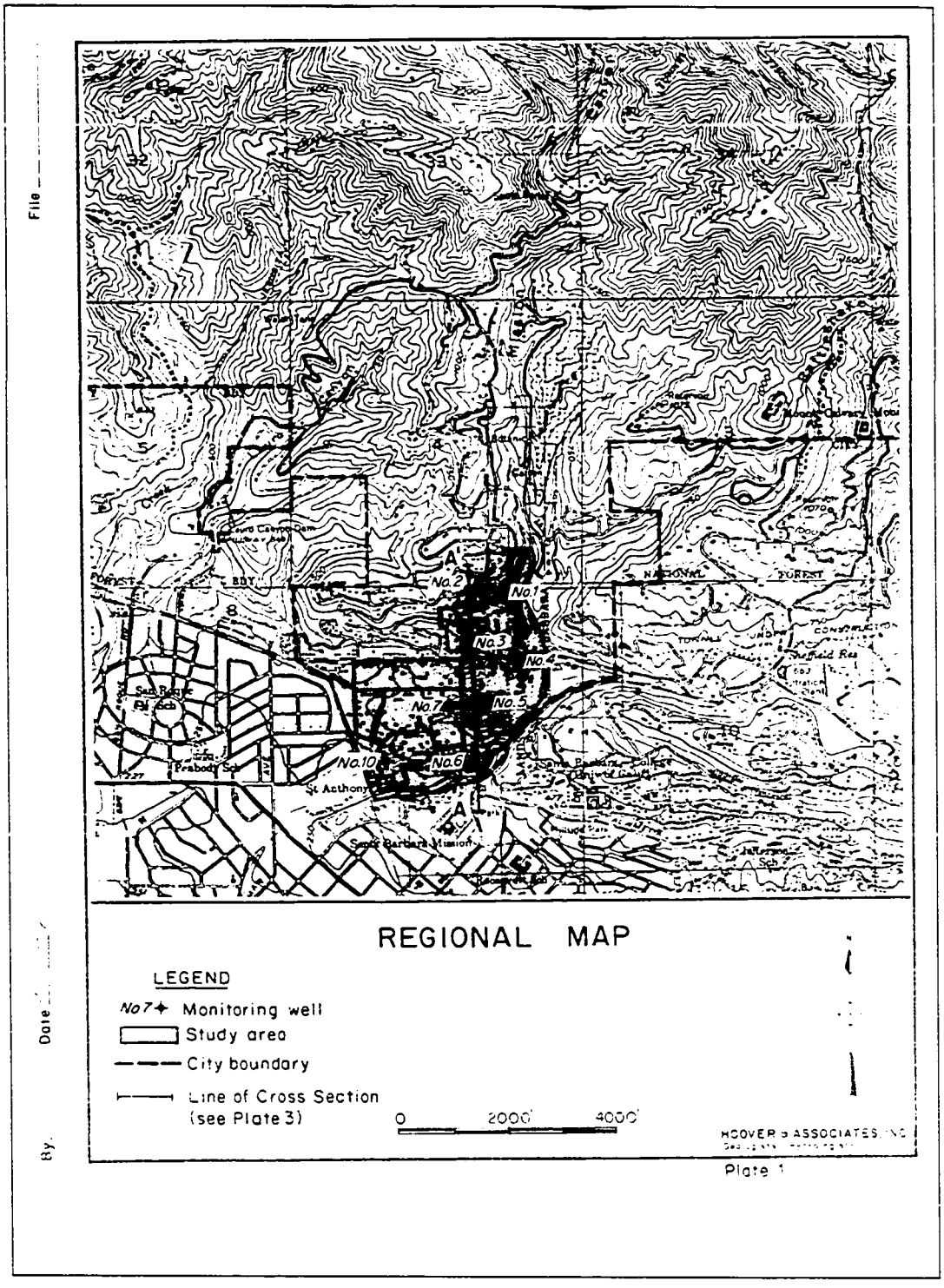

Figure C1. Borehole site index map.

File No. HC-911-1
March 30, 1984
Page Five

TABLE 1

Monitoring Well Design and Water Levels

Well No.	Location	Well Depth	Seal Depth	Design	Depth to Water
1	Upper Tornoe Road	50'	10'	0-20 Blank 20-50 Perf.	23' 4"
2	Dorking Road	70'	10'	0-30 Blank 30-70 Perf.	24' 9.5"
3	Tornoe Road and Foothill Road	30'	5'	0-10 Blank 10-30 Perf.	19' 6.5"
4	Firestation	60'	10'	0-30 Blank 30-60 Perf.	39' 0"
5	Near 720 Mission Canyon Road	30'	8'	0-20 Blank 20-30 Perf.	17' 1"
6	Rocky Nook Park	30'	10'	0-20 Blank 20-30 Perf.	15' 0"
7	Todos Santos Road	60'	10'	0-30 Blank 30-60 Perf.	27' 3"
10	Museum Property	26'	10'	0-16 Blank 16-26 Perf.	16' 6.5"

Figure C2. Borehole water level information.

BORING LOG

BORING NO. 1

LOCATION: End of Tornoe Road

Blows/ft.	Geol. Desig.	DEPTH IN FEET	DESCRIPTION
	Fill	0 - 9	Soft light and dark brown silty sand fill. with pebbles & cobbles
	Tr	9 - 50	Light brown silty clay. Damp at 13'. Checked for water @40' - 8" in hole after 5 min.
	Tr	TD 50'	Drilled to 50' with 6" auger. Cased 0 - 20 Blank 20 - 50 Perf. Reamed upper 5' with 8" auger Sealed to 10'

Figure C3. Borehole 1 log.

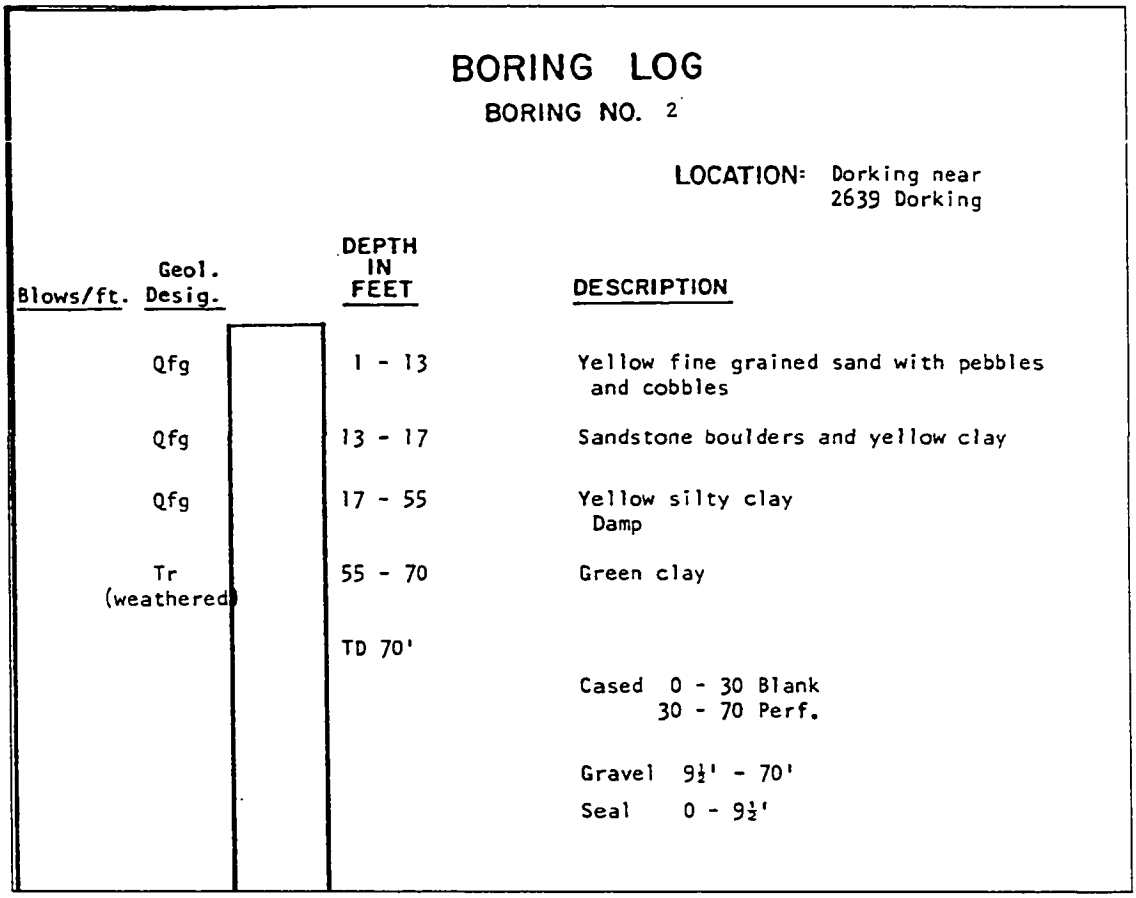

BORING LOG

BORING NO. 2

LOCATION: Dorking near 2639 Dorking

Blows/ft.	Geol. Desig.	DEPTH IN FEET	DESCRIPTION
	Qfg	1 - 13	Yellow fine grained sand with pebbles and cobbles
	Qfg	13 - 17	Sandstone boulders and yellow clay
	Qfg	17 - 55	Yellow silty clay Damp
	Tr (weathered)	55 - 70	Green clay
		TD 70'	
			Cased 0 - 30 Blank 30 - 70 Perf.
			Gravel 9½' - 70'
			Seal 0 - 9½'

Figure C4. Borehole 2 log.

BORING LOG

BORING NO. 3

LOCATION: Tornoe Road
near Foothill

Blows/ft.	Geol. Desig.	DEPTH IN FEET	DESCRIPTION
	Qfg	0 - 2	Reddish brown silty sand
	Qfg	2 - 6	Light brown sand with soft sandstone cobbles
	Qfg	6 - 7	Sandstone boulder
	Qfg	7 - 15	Light brown sand with cobbles and boulders
	Qfg	15 - 20	Wet silty sand
	Qfg	20 - 25	Dry silty sand with cobbles
	Qfg	25 - 30	Wet silty sand
	Qfg	30 - 35	Silty sand (dry) with cobbles
	Qfg	35 - 40	Wet silty sand.
			Cased with 2" 0 - 10 Blank 10 - 30 Perf. hole caved 30 - 40' Seal 0 - 5'

Figure C5. Borehole 3 log.

BORING LOG

BORING NO. 4

LOCATION: Fire Station
18' east of flag pole

Blows/ft.	Geol. Desig.	DEPTH IN FEET	DESCRIPTION
	Qfg	0 - 3	Dark brown clay silty sand
	Qfg	3 - 8	Light brown silty sand
	Qfg	8 - 10	Sandstone boulder
	Qfg	10 - 15	Brown sand and silt
	Qfg	15 - 18	Sandstone boulder
	Qfg	18 - 22	Yellow brown sand with boulders
	Qfg	22 - 25	Damp brown sand
	Qfg	25 - 34	Sandstone boulder
	Qfg	34 - 38	Brown silty sand (damp)
	Qfg	38 - 40	Sandstone boulder
	Qfg	40 - 42	Brown silty sand (damp)
	Qfg	42 - 45	Sandstone boulder
	Qfg	45 - 50	Damp brown sand and boulders
	Qfg	50 - 55	Soft brown sand
	Qfg	55 - 61	Damp brown sand with cobbles
		TD 61'	

0 - 30 Blank
30 - 60 Perf.
Cap on bottom

0 - 10 Concrete
10 - 30 Native firm sand
30 - 60 Lapis #3
7 7/8" hole

Figure C6. Borehole 4 log.

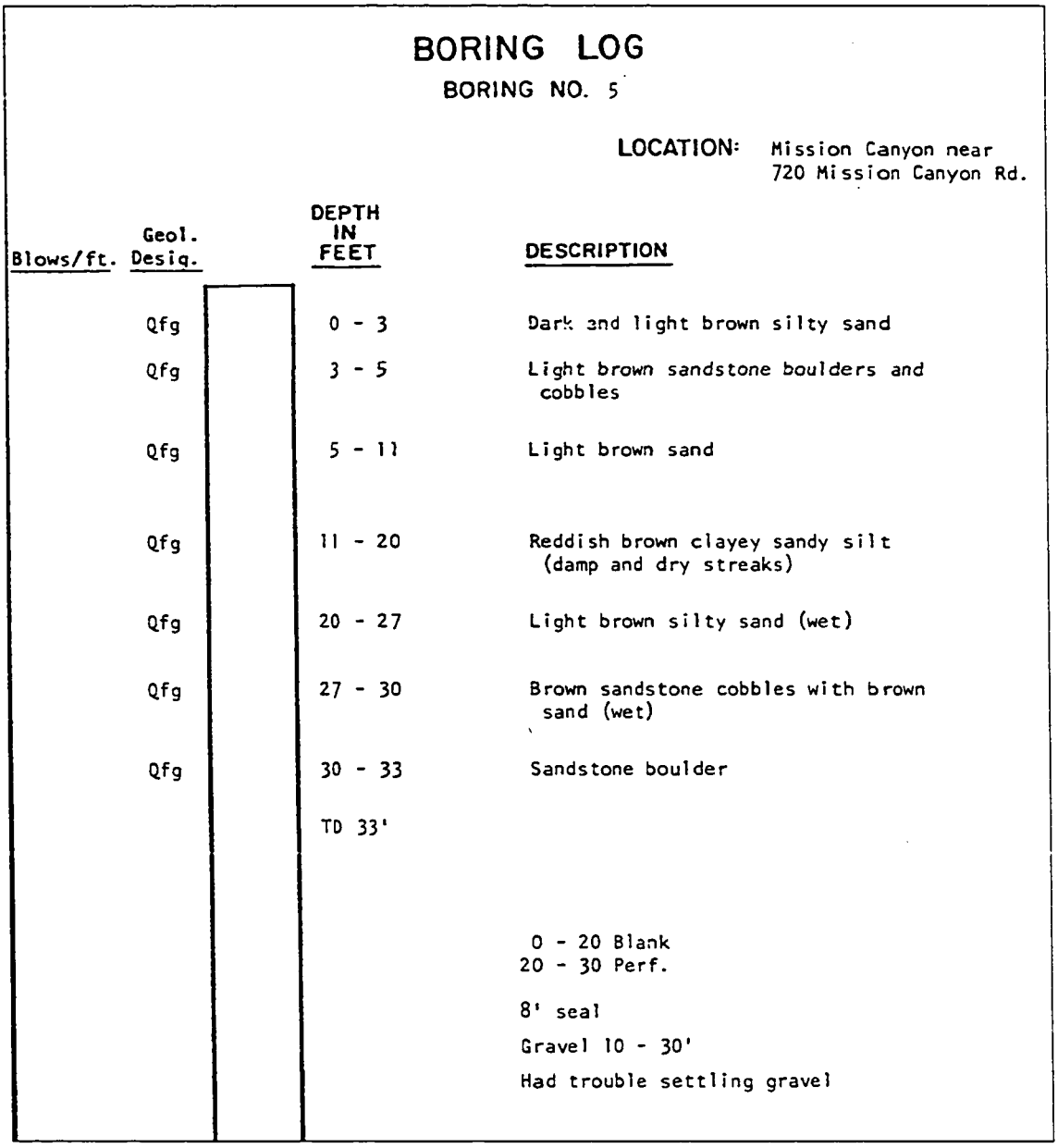

BORING LOG

BORING NO. 5

LOCATION: Mission Canyon near 720 Mission Canyon Rd.

Blows/ft.	Geol. Desig.	DEPTH IN FEET	DESCRIPTION
	Qfg	0 - 3	Dark and light brown silty sand
	Qfg	3 - 5	Light brown sandstone boulders and cobbles
	Qfg	5 - 11	Light brown sand
	Qfg	11 - 20	Reddish brown clayey sandy silt (damp and dry streaks)
	Qfg	20 - 27	Light brown silty sand (wet)
	Qfg	27 - 30	Brown sandstone cobbles with brown sand (wet)
	Qfg	30 - 33	Sandstone boulder
		TD 33'	

0 - 20 Blank
20 - 30 Perf.

8' seal

Gravel 10 - 30'

Had trouble settling gravel

Figure C7. Borehole 5 log.

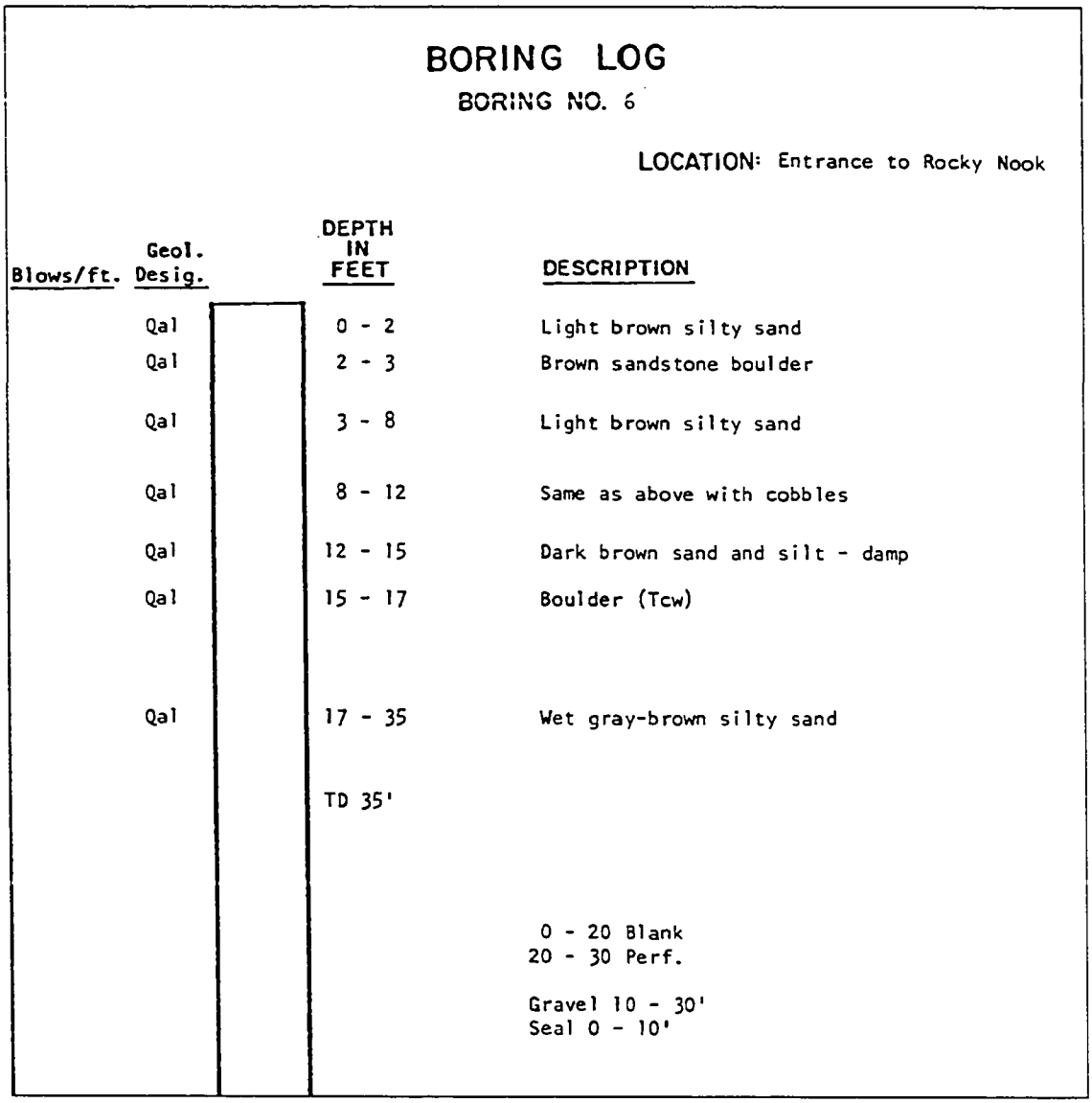

Figure C8. Borehole 6 log.

BORING LOG

BORING NO. 7

LOCATION: Todos Santos Drive

Blows/ft.	Geol. Desig.	DEPTH IN FEET	DESCRIPTION
	Qfg	0 - 2	Dark brown organic rich soil
	Qfg	2 - 4	Light brown silty sand
	Qfg	4 - 5.5	Boulder
	Qfg	5.5 - 8	Light brown silty clayey sand
	Qfg	8 - 9	Boulder
	Qfg	9 - 14	Light brown silty sand with small cobbles
	Qfg	14 - 16	Medium brown silty sand with pebbles
	Qfg	16 - 25	Light brown silty clayey sand
	Qfg	25 - 28	Medium brown clayey sand with pebbles
	Qfg	28 - 37	Boulders and clayey sand
	Qfg	37 - 48	Brown gray sand and clayey with boulders
	Qfg	48 - 64	Light brown sandy clay
		TD 64'	
			0 - 30 Blank 30 - 60 Perf.
			Seal 10'

Figure C9. Borehole 7 log.

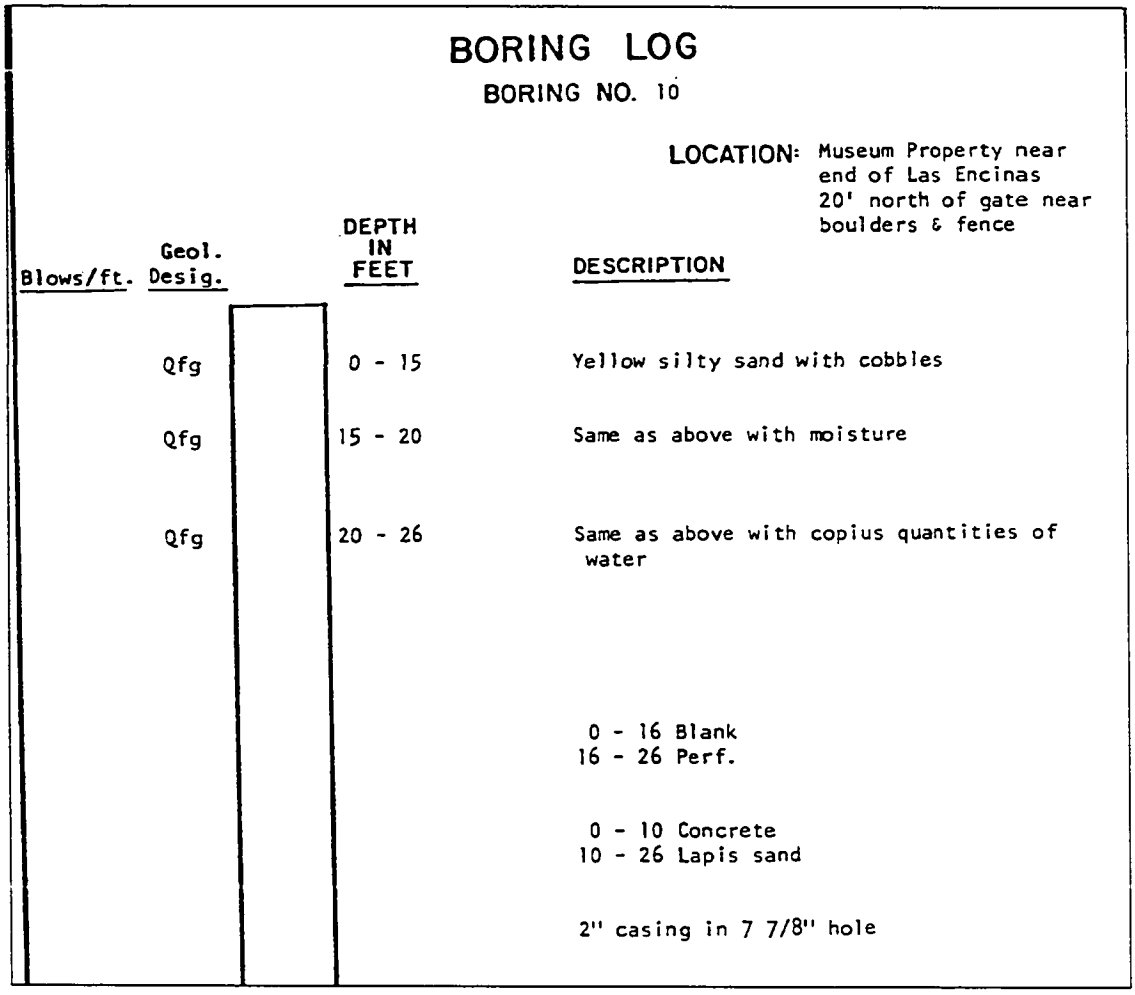

Figure C10. Borehole 10 log.

APPENDIX D

BULK VELOCITY CALCULATIONS

BULK VELCOCITY CALCULATIONS DISCUSSION

The bulk velocity calculations presented below show the maximum velocity contrast that is calculated for Mission diamicton sediments that transition from dry conditions, or the pore space is comprised of air, to saturated conditions, the pore space is completely filled with water. The calculated velocity contrast is compared to the observed velocity contrast between the first velocity layer, determined from direct seismic arrivals, as compared to the second velocity layer, determined from refracted seismic arrivals. These calculations indicate that the p-wave velocity boundary is not due to the detection of ground water as the velocity contrast observed during the seismic refraction surveys is greater than the maximum velocity contrast as determined by these calculations.

The following procedure is a step-by-step presentation of the method and assumptions used in the velocity calculations. Following the step-by-step procedure and equations used in the bulk velocity analysis, tables summarizing the bulk velocity analysis are presented below. The comparison of the observed velocity contrast between the first two velocity layers indicates that the velocity contrast for all of the seismic refraction surveys, accomplished to determine the thickness of the Mission diamicton sediments, is greater than what is anticipated for a seismic refractor that is due to ground water. Therefore, the seismic

refractor that is determined by the seismic refraction analysis is due to a change in geologic materials and not due to the presence of ground water.

BULK VELOCITY CALCULATION METHOD

The following method was described by Craig Lippus at Geometrics, Inc. for analyzing bulk p-wave velocities and analyzing seismic refraction data for determining the influence of ground water saturation in a geologic medium (Lippus, 2002 personal commun.).

Step 1:
P-wave velocity for a velocity layer is defined as:

Equation 1:
Bulk P-wave Velocity = (velocity of medium in pore space * pore volume) + (velocity of solids * volume of solids)

Step 2:

Solve for the velocity of solids using observed p-wave velocity observed in direct arrivals. This p-wave velocity is for unsaturated conditions, so medium and respective velocity used for pore space is air.

Equation 2:
Velocity of solids = [bulk velocity – (velocity of medium in pore space * pore volume)] / (volume of solids)

Step 3:

When velocity of the solids has been determined, resolve *equation 1* substituting the pore space medium with water and respective velocity.

Equation 1:
Bulk P-wave Velocity = (velocity of medium in pore space * pore volume) + (velocity of solids * volume of solids)

This bulk velocity calculation is the bulk p-wave velocity that is calculated for Mission diamicton sediments that are saturated for ground water.

Step 4:

Compare observed velocity contrast between velocity layers 1 and 2 for both observed and calculated conditions. If velocity contrasts for calculated and observed conditions do not match, then seismic refractor observed in seismic refraction analysis is not due to ground water saturation of sediments.

TABLE D: BULK VELOCITY CALCULATIONS SUMMARY

Survey 1001

Medium	Velocity	(meters/sec)	porosity (n)
Air	Va	335	0.5
Water	Vw	1340	0.5
Mission Diamicton	V1	370	0.5

pore space contains air (dry)	Velocity V1 to V2 contrast (m/s):	
V solids = 405 meters/sec	observed:	682
	calculated:	467.5
pore space contains water (saturated)		
V2 = 872.5 meters/sec		

Survey 1002

Medium	Velocity	(meters/sec)	porosity (n)
Air	Va	335	0.5
Water	Vw	1340	0.5
Mission Diamicton	V1	357	0.5

pore space contains air (dry)	Velocity V1 to V2 contrast (m/s):	
V solids = 379 meters/sec	observed:	982
	calculated:	480.5
pore space contains water (saturated)		
V2 = 859.5 meters/sec		

Survey 1003

Medium	Velocity	(meters/sec)	porosity (n)
Air	Va	335	0.5
Water	Vw	1340	0.5
Mission Diamicton	V1	413	0.5

pore space contains air (dry)	Velocity V1 to V2 contrast (m/s):	
V solids = 491 meters/sec	observed:	752
	calculated:	424.5
pore space contains water (saturated)		
V2 = 915.5 meters/sec		

Survey 1004

Medium	Velocity	(meters/sec)	porosity (n)
Air	Va	335	0.5
Water	Vw	1340	0.5
Mission Diamicton	V1	447	0.5

pore space contains air (dry)	Velocity V1 to V2 contrast (m/s):	
V solids = 559 meters/sec	observed:	854
	calculated:	390.5
pore space contains water (saturated)		
V2 = 949.5 meters/sec		

Survey 1005

Medium	Velocity	(meters/sec)	porosity (n)
Air	Va	335	0.5
Water	Vw	1340	0.5
Mission Diamicton	V1	410	0.5

pore space contains air (dry)	Velocity V1 to V2 contrast (m/s):	
V solids = 485 meters/sec	observed:	1040
	calculated:	427.5
pore space contains water (saturated)		
V2 = 912.5 meters/sec		

Survey 1006

Medium	Velocity	(meters/sec)	porosity (n)
Air	Va	335	0.5
Water	Vw	1340	0.5
Mission Diamicton	V1	364	0.5

pore space contains air (dry)	Velocity V1 to V2 contrast (m/s):	
V solids = 393 meters/sec	observed:	1320
	calculated:	473.5
pore space contains water (saturated)		
V2 = 866.5 meters/sec		

Survey 1007

Medium	Velocity	(meters/sec)	porosity (n)
Air	Va	335	0.5
Water	Vw	1340	0.5
Mission Diamicton	V1	711	0.5

pore space contains air (dry)	Velocity V1 to V2 contrast (m/s):	
V solids = 1087 meters/sec	observed:	1372
	calculated:	126.5
pore space contains water (saturated)		
V2 = 1213.5 meters/sec		

Survey 1008

Medium	Velocity	(meters/sec)	porosity (n)
Air	Va	335	0.5
Water	Vw	1340	0.5
Mission Diamicton	V1	353	0.5

pore space contains air (dry)	Velocity V1 to V2 contrast (m/s):	
V solids = 371 meters/sec	observed:	1141
	calculated:	484.5
pore space contains water (saturated)		
V2 = 855.5 meters/sec		

Survey 1009

Medium	Velocity	(meters/sec)	porosity (n)
Air	Va	335	0.5
Water	Vw	1340	0.5
Mission Diamicton	V1	316	0.5

pore space contains air (dry)	Velocity V1 to V2 contrast (m/s):	
V solids = 297 meters/sec	observed:	1649
	calculated:	521.5
pore space contains water (saturated)		
V2 = 818.5 meters/sec		

APPENDIX E

RADIOCARBON SAMPLES AND DATING

Radiocarbon sample preparation: Charcoal

Note: All materials used in this procedure are sterilized by washing in deionized water and dried in an oven at a temperature no greater than 90 degrees Celsius. All water used in this procedure must be and is DEIONIZED WATER.

1. Place portion of field sample in bucket.
2. Add water to sample and gently agitate.
3. Pour floating product (silt, clay, and charcoal) into a nest of sieves. (list sieves for my procedure)
4. Repeat steps 2 and 3 until no more floating product is present in the sample. This procedure should be completed fairly quickly and water should not be allowed to sit with the bulk sample too long. This prevents the targeted charcoal from being saturated making it no longer float and therefore making this procedure useless.
5. Using water, collect sample and place into beakers. Keep sample portions separated on sieves in separate beakers as well as remaining sample in bucket into separate beaker. LABEL BEAKERS FOR RECORDS.
6. Dry samples at a temperature no greater than 90 degrees Celsius.
7. After samples are dry, place sample from beaker with largest screen size onto dish for examination under binocular microscope. This sample should contain the largest charcoal fragments from your overall sample being analyzed.
8. Pick charcoal fragments out and place on aluminum foil.
9. Use smaller screen size sample if necessary to collect required amount of charcoal for radiocarbon dating.
10. Seal selected charcoal in aluminum foil and place in polyethylene bag with label.
11. Send prepared samples to USGS Reston, Virginia offices for radiocarbon dating.

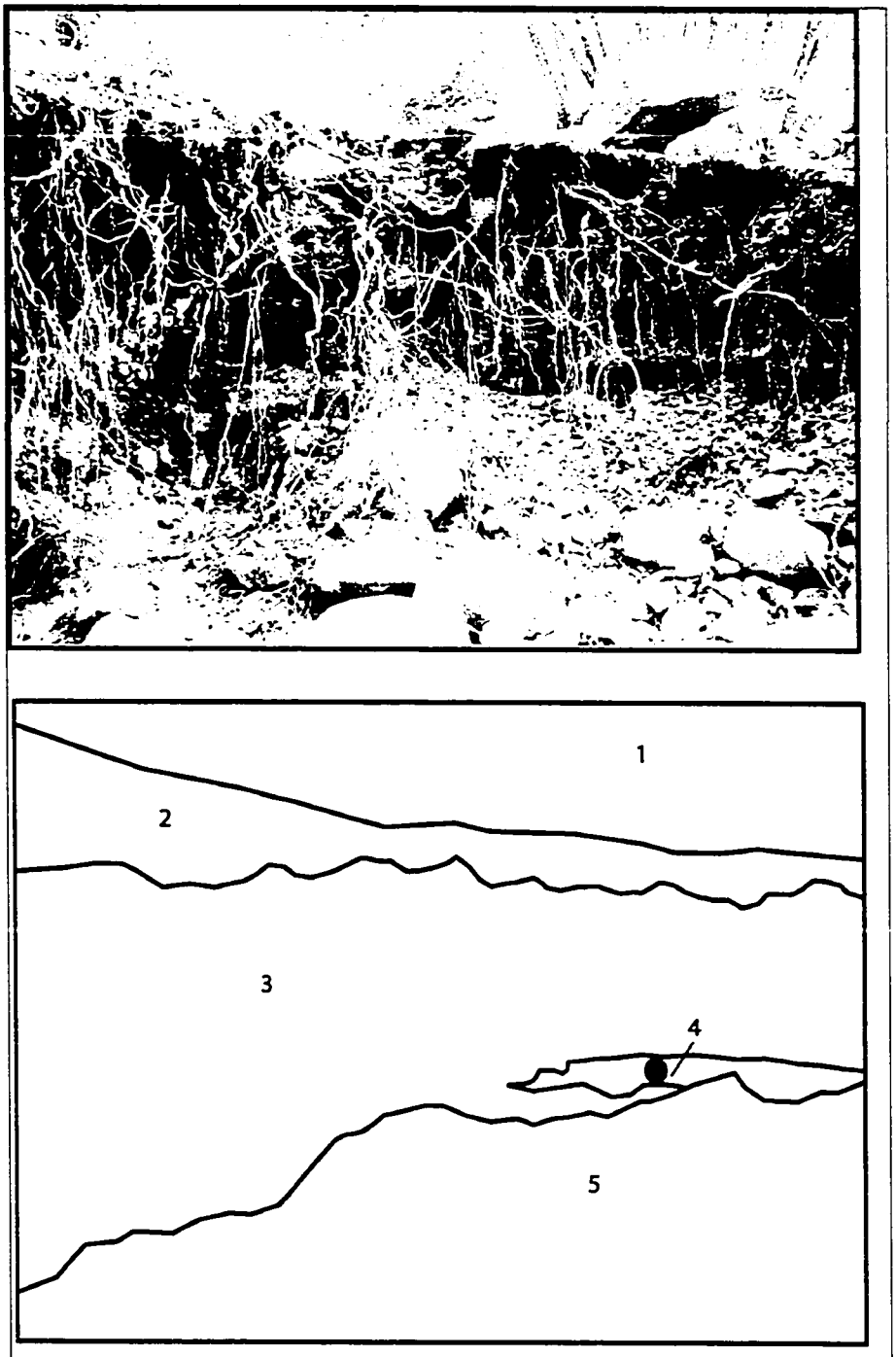

FIGURE E1. Photograph and geologic unit description of C14 sample number 02-01-03-1 location. Descriptions of unit numbers are: 1) aerial exposure, 2) landslide debris soil, 3) landslide debris, 4) sandy clay horizon with macroscopic charcoal, and 5) modern terrace debris and stream deposits. Red circle indicates location of bulk sample extraction. Rock hammer in blue ellipse is for scale.

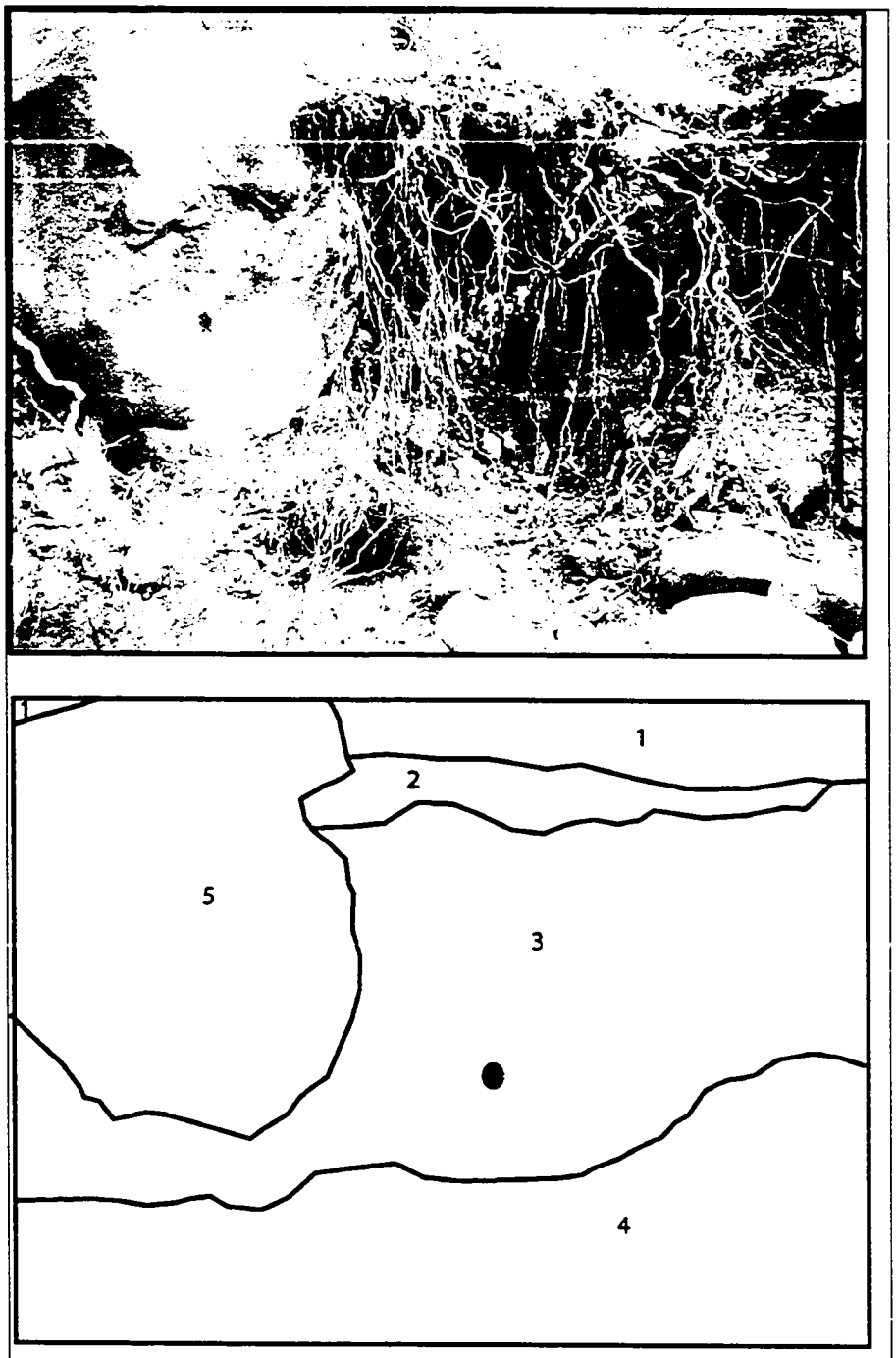

FIGURE E2. Photograph and geologic unit description of C14 sample number 01-20-03-B1 location. Descriptions of unit numbers are: 1) aerial exposure, 2) Mission diamicton soil, 3) Mission diamicton, 4) modern terrace debris and stream deposits, 5) boulder in the Mission diamicton. Red circle indicates location of bulk sample extraction. Blue bar is approximately 1 meter for scale.

APPENDIX F

GROUND PENETRATING RADAR DATA AND ANALYSIS

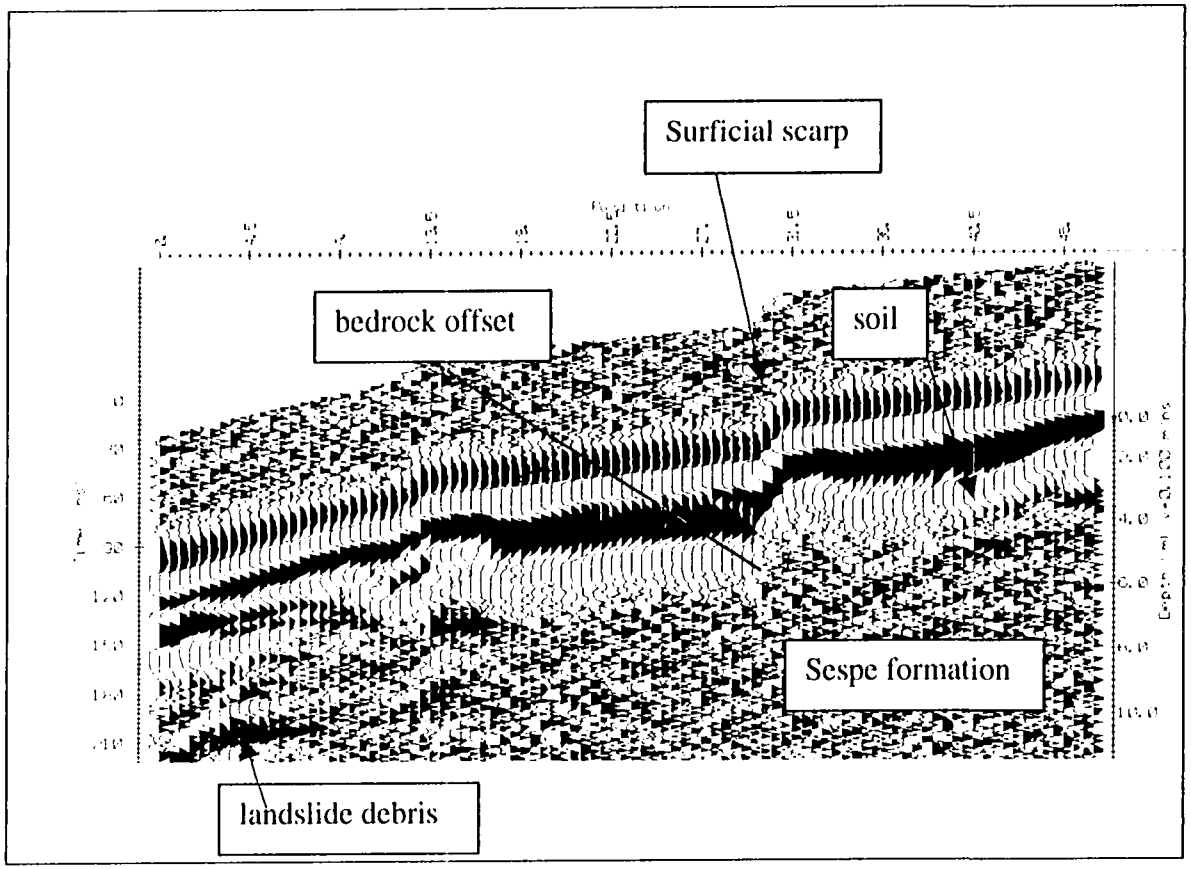

Figure F1. GPR survey 03-03-A. Horizontal and vertical scale in meters. Scarps located at approximately 12 and 29 meters along survey transect, repectively. Scarp at 29 meters is depicted in Figure 22. Survey transect from left to right trends S14E.

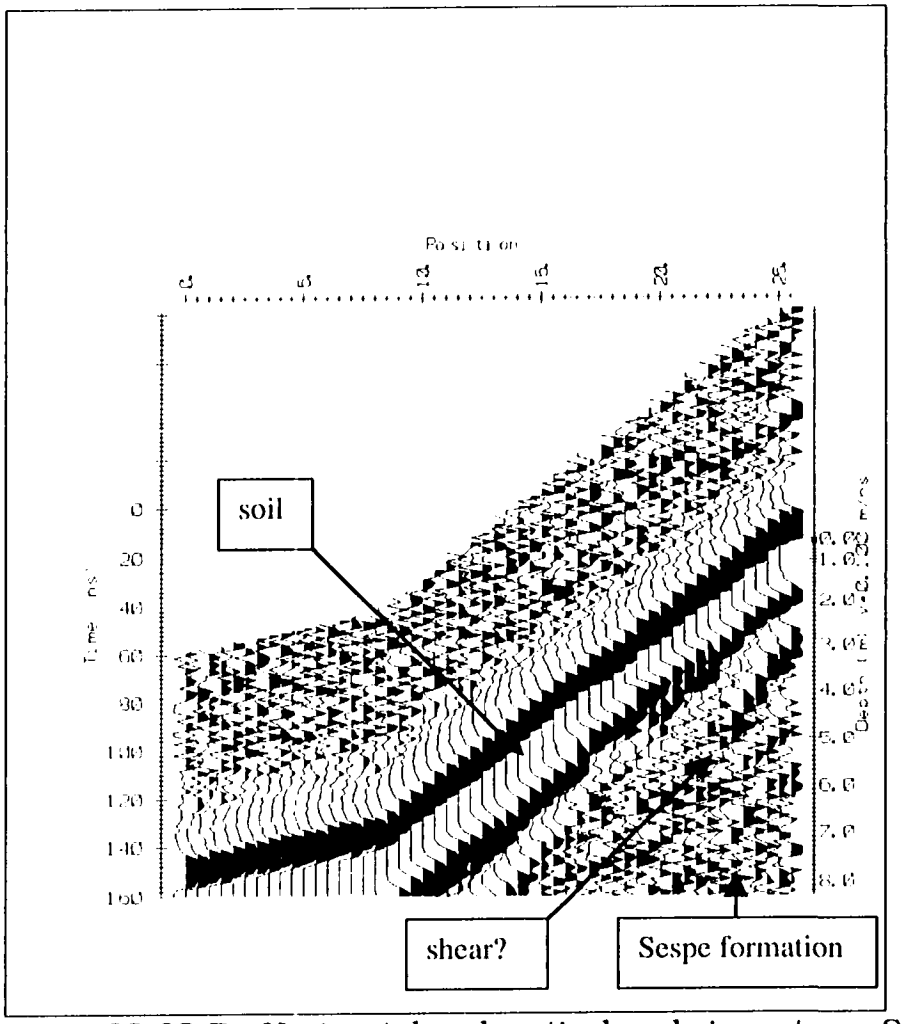

Figure F2. GPR survey 03-03-B. Horizontal and vertical scale in meters. Survey transect from left to right trends S34W.

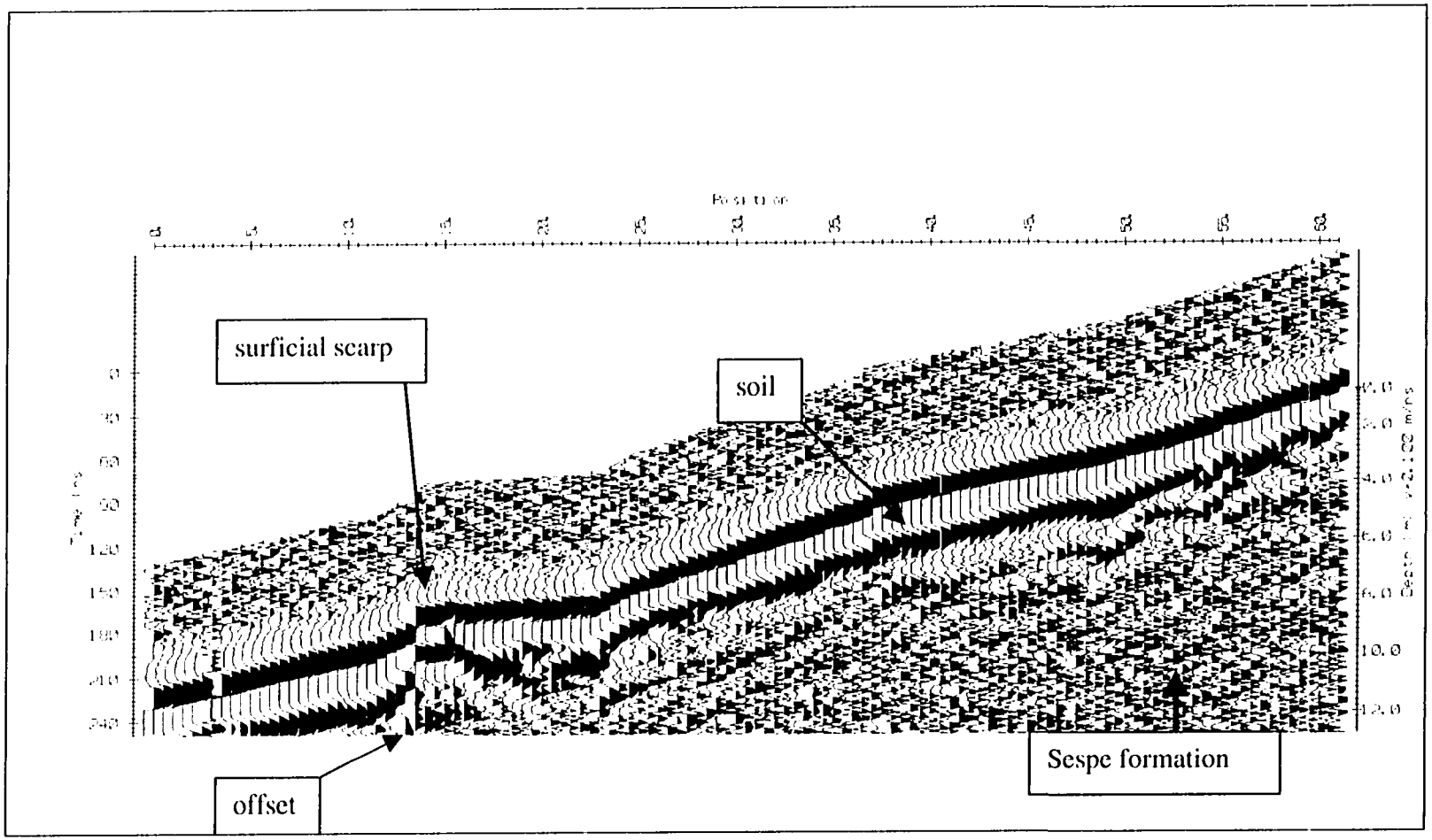

Figure F3. GPR survey 03-03-C. Horizontal and vertical scale in meters. Scarp located at approximately 13.5 meters along survey transect. Survey transect from left to right trends S26W.

APPENDIX G

SLOPE STABILITY DATA AND ANALYSIS

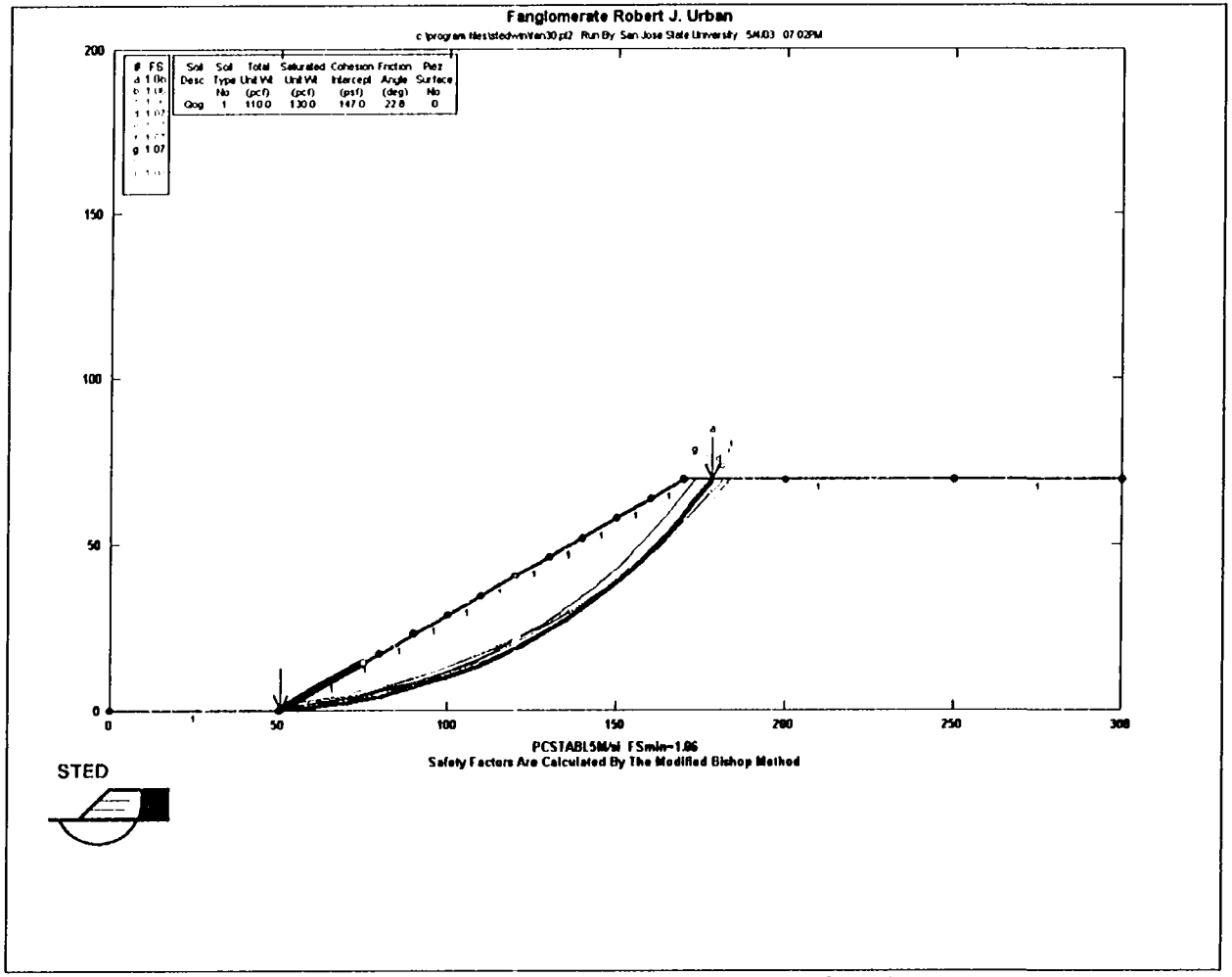

Figure G1. Fanglomerate Factor of Safety is greater than 1 for slopes angled less than 30 degrees.

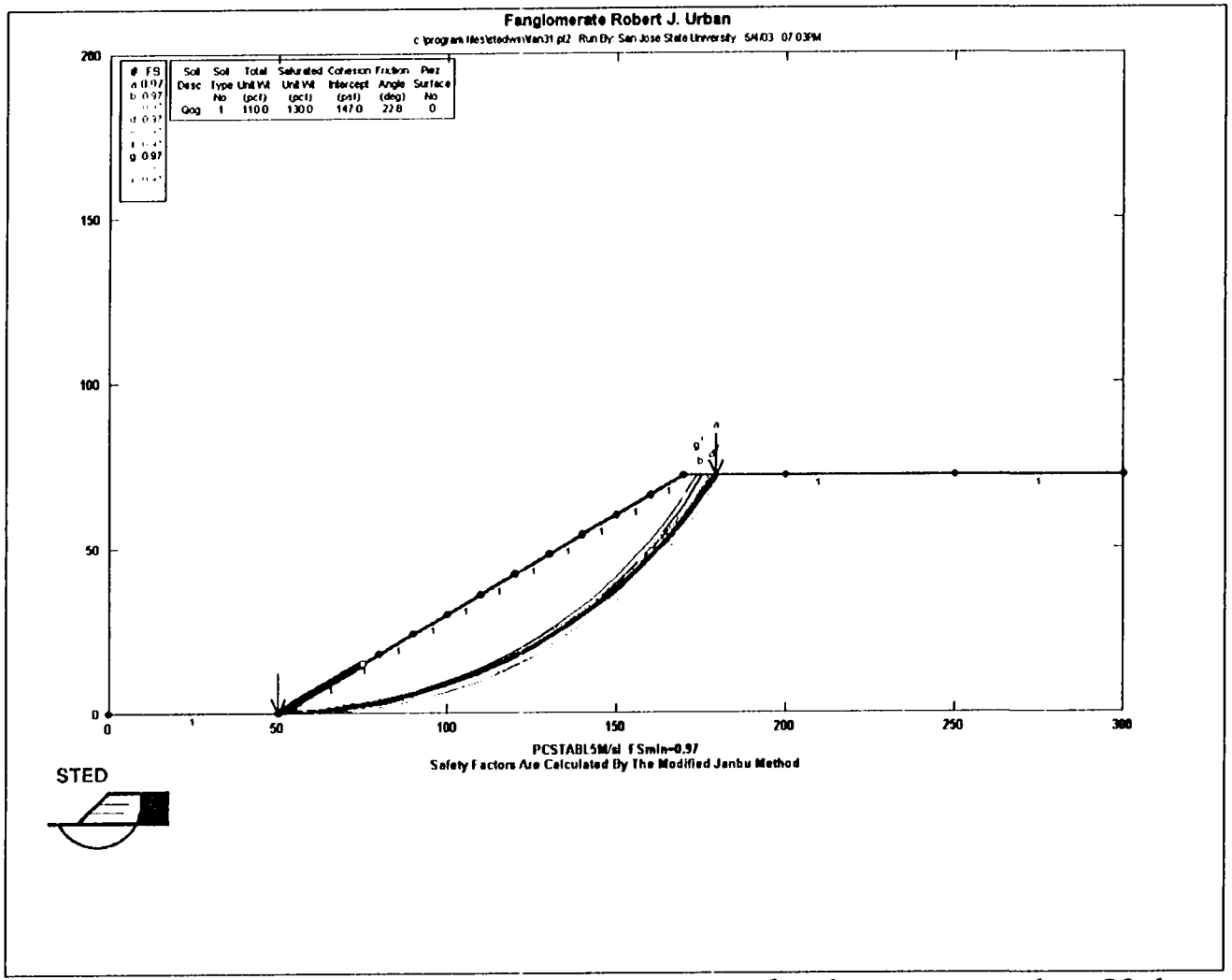

Figure G2. Fanglomerate Factor of Safety is less than 1 for slopes steeper than 30 degrees.

Output file for Fanglomerate steeper than 30 degrees

```
                    ** PCSTABL5M **
                          by
                    Purdue University
               --Slope Stability Analysis--
            Simplified Janbu, Simplified Bishop
               or Spencer`s Method of Slices
Run Date:                   5/4/03
Time of Run:                07:02PM
Run By:                     San Jose State University
Input Data Filename:        C:fan30.in
Output Filename:            C:fan30.OUT
Unit:                       ENGLISH
Plotted Output Filename:    C:fan30.PLT
PROBLEM DESCRIPTION   Fanglomerate
                      Robert J. Urban
BOUNDARY COORDINATES
   15 Top   Boundaries
   15 Total Boundaries
Boundary     X-Left     Y-Left    X-Right    Y-Right    Soil Type
   No.        (ft)       (ft)       (ft)       (ft)    Below Bnd
    1          .00        .00      50.00        .00        1
    2        50.00        .00      60.00       5.77        1
    3        60.00       5.77      70.00      11.54        1
    4        70.00      11.54      80.00      17.31        1
    5        80.00      17.31      90.00      23.08        1
    6        90.00      23.08     100.00      28.85        1
    7       100.00      28.85     110.00      34.62        1
    8       110.00      34.62     120.00      40.39        1
    9       120.00      40.39     130.00      46.16        1
   10       130.00      46.16     140.00      51.93        1
   11       140.00      51.93     150.00      57.70        1
   12       150.00      57.70     160.00      63.47        1
   13       160.00      63.47     170.00      69.24        1
   14       170.00      69.24     250.00      69.24        1
   15       250.00      69.24     300.00      69.24        1
ISOTROPIC SOIL PARAMETERS
  1 Type(s) of Soil
 Soil  Total  Saturated  Cohesion Friction   Pore   Pressure   Piez.
 Type Unit Wt. Unit Wt. Intercept   Angle  Pressure Constant Surface
  No.  (pcf)    (pcf)     (psf)     (deg)   Param.    (psf)    No.
   1   110.0    130.0     147.0     22.8     .00        .0      0
 A Critical Failure Surface Searching Method, Using A Random
 Technique For Generating Circular Surfaces, Has Been Specified.
1000 Trial Surfaces Have Been Generated.
  10 Surfaces Initiate From Each Of100 Points Equally Spaced
 Along The Ground Surface Between  X =  50.00 ft.
                                and  X =  75.00 ft.
 Each Surface Terminates Between   X = 150.00 ft.
                                and   X = 200.00 ft.
 Unless Further Limitations Were Imposed, The Minimum Elevation
 At Which A Surface Extends Is  Y =   .00 ft.
 10.00 ft. Line Segments Define Each Trial Failure Surface.
 Following Are Displayed The Ten Most Critical Of The Trial
       Failure Surfaces Examined.  They Are Ordered - Most Critical
       First.
       * * Safety Factors Are Calculated By The Modified Bishop Method * *
       Failure Surface Specified By 17 Coordinate Points
         Point      X-Surf      Y-Surf
```

No.	(ft)	(ft)
1	50.76	.44
2	60.74	1.07
3	70.66	2.32
4	80.49	4.17
5	90.18	6.62
6	99.71	9.66
7	109.03	13.27
8	118.12	17.46
9	126.93	22.19
10	135.43	27.45
11	143.59	33.22
12	151.39	39.49
13	158.79	46.21
14	165.76	53.38
15	172.28	60.97
16	178.32	68.94
17	178.52	69.24

Circle Center At X = 45.4 ; Y = 163.4 and Radius, 163.1

*** 1.063 ***

Individual data on the 28 slices

Slice No.	Width (ft)	Weight (lbs)	Water Force Top (lbs)	Water Force Bot (lbs)	Tie Force Norm (lbs)	Tie Force Tan (lbs)	Earthquake Force Hor (lbs)	Earthquake Force Ver (lbs)	Surcharge Load (lbs)
1	9.2	2411.9	.0	.0	.0	.0	.0	.0	.0
2	.7	400.5	.0	.0	.0	.0	.0	.0	.0
3	9.3	7350.7	.0	.0	.0	.0	.0	.0	.0
4	.7	686.5	.0	.0	.0	.0	.0	.0	.0
5	9.3	11731.7	.0	.0	.0	.0	.0	.0	.0
6	.5	714.5	.0	.0	.0	.0	.0	.0	.0
7	9.5	15660.3	.0	.0	.0	.0	.0	.0	.0
8	.2	332.3	.0	.0	.0	.0	.0	.0	.0
9	9.5	18650.5	.0	.0	.0	.0	.0	.0	.0
10	.3	608.6	.0	.0	.0	.0	.0	.0	.0
11	9.0	19805.8	.0	.0	.0	.0	.0	.0	.0
12	1.0	2218.6	.0	.0	.0	.0	.0	.0	.0
13	8.1	19081.2	.0	.0	.0	.0	.0	.0	.0
14	1.9	4535.5	.0	.0	.0	.0	.0	.0	.0
15	6.9	16807.3	.0	.0	.0	.0	.0	.0	.0
16	3.1	7484.6	.0	.0	.0	.0	.0	.0	.0
17	5.4	13114.3	.0	.0	.0	.0	.0	.0	.0
18	4.6	10832.2	.0	.0	.0	.0	.0	.0	.0
19	3.6	8310.2	.0	.0	.0	.0	.0	.0	.0
20	6.4	14131.5	.0	.0	.0	.0	.0	.0	.0
21	1.4	2933.4	.0	.0	.0	.0	.0	.0	.0
22	7.4	14473.6	.0	.0	.0	.0	.0	.0	.0
23	1.2	2170.5	.0	.0	.0	.0	.0	.0	.0
24	5.8	9318.8	.0	.0	.0	.0	.0	.0	.0
25	4.2	5675.2	.0	.0	.0	.0	.0	.0	.0
26	2.3	2404.9	.0	.0	.0	.0	.0	.0	.0
27	6.0	2850.0	.0	.0	.0	.0	.0	.0	.0
28	.2	3.4	.0	.0	.0	.0	.0	.0	.0

Failure Surface Specified By 17 Coordinate Points

Point No.	X-Surf (ft)	Y-Surf (ft)
1	50.00	.00
2	59.92	1.23
3	69.77	2.96
4	79.52	5.19
5	89.15	7.90
6	98.62	11.10
7	107.92	14.78

8	117.02	18.92
9	125.91	23.51
10	134.54	28.55
11	142.92	34.02
12	151.00	39.90
13	158.78	46.19
14	166.23	52.86
15	173.33	59.90
16	180.07	67.29
17	181.68	69.24

Circle Center At X = 30.6 ; Y = 196.8 and Radius, 197.7

*** 1.063 ***

Failure Surface Specified By 16 Coordinate Points

Point No.	X-Surf (ft)	Y-Surf (ft)
1	50.76	.44
2	60.74	1.02
3	70.67	2.22
4	80.50	4.04
5	90.20	6.48
6	99.73	9.52
7	109.04	13.15
8	118.12	17.36
9	126.91	22.12
10	135.38	27.43
11	143.51	33.26
12	151.25	39.59
13	158.58	46.39
14	165.47	53.64
15	171.90	61.30
16	177.75	69.24

Circle Center At X = 46.5 ; Y = 159.8 and Radius, 159.5

*** 1.063 ***

Failure Surface Specified By 16 Coordinate Points

Point No.	X-Surf (ft)	Y-Surf (ft)
1	54.29	2.48
2	64.26	3.26
3	74.17	4.64
4	83.97	6.60
5	93.65	9.14
6	103.15	12.25
7	112.45	15.92
8	121.52	20.13
9	130.32	24.87
10	138.83	30.13
11	147.01	35.89
12	154.83	42.12
13	162.27	48.80
14	169.29	55.92
15	175.89	63.44
16	180.39	69.24

Circle Center At X = 46.2 ; Y = 170.3 and Radius, 168.0

*** 1.069 ***

Failure Surface Specified By 16 Coordinate Points

Point No.	X-Surf (ft)	Y-Surf (ft)
1	50.00	.00
2	59.88	1.53
3	69.68	3.55
4	79.36	6.05
5	88.91	9.03
6	98.29	12.48

7	107.50	16.39
8	116.49	20.75
9	125.27	25.55
10	133.79	30.78
11	142.04	36.43
12	150.00	42.48
13	157.65	48.92
14	164.98	55.73
15	171.95	62.90
16	177.54	69.24

Circle Center At X = 24.2 ; Y = 199.6 and Radius, 201.3

*** 1.070 ***

Failure Surface Specified By 17 Coordinate Points

Point No.	X-Surf (ft)	Y-Surf (ft)
1	51.01	.58
2	60.89	2.13
3	70.69	4.12
4	80.39	6.55
5	89.97	9.43
6	99.40	12.74
7	108.68	16.47
8	117.78	20.62
9	126.68	25.18
10	135.36	30.14
11	143.81	35.49
12	152.01	41.22
13	159.93	47.31
14	167.58	53.76
15	174.92	60.55
16	181.94	67.67
17	183.35	69.24

Circle Center At X = 22.0 ; Y = 218.5 and Radius, 219.8

*** 1.071 ***

Failure Surface Specified By 16 Coordinate Points

Point No.	X-Surf (ft)	Y-Surf (ft)
1	52.27	1.31
2	62.23	2.22
3	72.11	3.75
4	81.88	5.90
5	91.49	8.67
6	100.91	12.03
7	110.09	15.98
8	119.01	20.50
9	127.63	25.58
10	135.91	31.19
11	143.82	37.30
12	151.33	43.91
13	158.41	50.97
14	165.02	58.47
15	171.16	66.37
16	173.11	69.24

Circle Center At X = 43.0 ; Y = 159.3 and Radius, 158.3

*** 1.074 ***

Failure Surface Specified By 17 Coordinate Points

Point No.	X-Surf (ft)	Y-Surf (ft)
1	54.29	2.48
2	64.27	3.13
3	74.20	4.36
4	84.03	6.16
5	93.75	8.51

6	103.32	11.42
7	112.70	14.88
8	121.87	18.87
9	130.80	23.38
10	139.45	28.39
11	147.80	33.89
12	155.82	39.86
13	163.49	46.29
14	170.77	53.14
15	177.65	60.40
16	184.10	68.04
17	185.00	69.24

Circle Center At X = 47.9 ; Y = 176.5 and Radius, 174.1

*** 1.075 ***

Failure Surface Specified By 16 Coordinate Points

Point No.	X-Surf (ft)	Y-Surf (ft)
1	54.04	2.33
2	63.95	3.68
3	73.78	5.51
4	83.51	7.81
5	93.12	10.59
6	102.58	13.83
7	111.87	17.52
8	120.97	21.67
9	129.86	26.25
10	138.52	31.25
11	146.92	36.68
12	155.05	42.50
13	162.88	48.71
14	170.41	55.30
15	177.60	62.25
16	184.18	69.24

Circle Center At X = 31.3 ; Y = 206.6 and Radius, 205.5

*** 1.076 ***

Failure Surface Specified By 16 Coordinate Points

Point No.	X-Surf (ft)	Y-Surf (ft)
1	52.78	1.60
2	62.78	1.82
3	72.73	2.75
4	82.59	4.41
5	92.31	6.77
6	101.83	9.83
7	111.10	13.58
8	120.08	17.98
9	128.71	23.03
10	136.96	28.69
11	144.77	34.93
12	152.12	41.71
13	158.95	49.02
14	165.23	56.80
15	170.94	65.01
16	173.44	69.24

Circle Center At X = 54.9 ; Y = 139.2 and Radius, 137.6

*** 1.077 ***

Output file for Fanglomerate steeper than 31 degrees

```
                    ** PCSTABL5M **
                          by
                    Purdue University
               --Slope Stability Analysis--
            Simplified Janbu, Simplified Bishop
               or Spencer`s Method of Slices
Run Date:                   7/27/03
Time of Run:                05:39PM
Run By:                     San Jose State University
Input Data Filename:        C:fan31.in
Output Filename:            C:fan31.OUT
Unit:                       ENGLISH
Plotted Output Filename:    C:fan31.PLT
PROBLEM DESCRIPTION   Fanglomerate
                      Robert J. Urban
BOUNDARY COORDINATES
   15 Top   Boundaries
   15 Total Boundaries
Boundary     X-Left     Y-Left     X-Right    Y-Right    Soil Type
   No.        (ft)       (ft)       (ft)       (ft)     Below Bnd
    1          .00        .00       50.00        .00        1
    2         50.00        .00       60.00       6.00        1
    3         60.00       6.00       70.00      12.02        1
    4         70.00      12.02       80.00      18.03        1
    5         80.00      18.03       90.00      24.03        1
    6         90.00      24.03      100.00      30.04        1
    7        100.00      30.04      110.00      36.05        1
    8        110.00      36.05      120.00      42.06        1
    9        120.00      42.06      130.00      48.07        1
   10        130.00      48.07      140.00      54.08        1
   11        140.00      54.08      150.00      60.09        1
   12        150.00      60.09      160.00      66.09        1
   13        160.00      66.09      170.00      72.10        1
   14        170.00      72.10      250.00      72.10        1
   15        250.00      72.10      300.00      72.10        1
ISOTROPIC SOIL PARAMETERS
  1 Type(s) of Soil
 Soil  Total  Saturated  Cohesion Friction   Pore   Pressure   Piez.
 Type Unit Wt. Unit Wt. Intercept   Angle  Pressure Constant Surface
  No.  (pcf)    (pcf)     (psf)     (deg)   Param.    (psf)    No.
   1   110.0    130.0     147.0     22.8     .00        .0      0
 A Critical Failure Surface Searching Method, Using A Random
 Technique For Generating Circular Surfaces, Has Been Specified.
1000 Trial Surfaces Have Been Generated.
  10 Surfaces Initiate From Each Of100 Points Equally Spaced
 Along The Ground Surface Between  X =  50.00 ft.
                             and  X =  75.00 ft.
 Each Surface Terminates Between   X = 150.00 ft.
                            and    X = 200.00 ft.
 Unless Further Limitations Were Imposed, The Minimum Elevation
 At Which A Surface Extends Is  Y =   .00 ft.
 10.00 ft. Line Segments Define Each Trial Failure Surface.
 Following Are Displayed The Ten Most Critical Of The Trial
       Failure Surfaces Examined.  They Are Ordered - Most Critical
       First.
       * * Safety Factors Are Calculated By The Modified Janbu Method * *
       Failure Surface Specified By 17 Coordinate Points
         Point      X-Surf      Y-Surf
          No.        (ft)        (ft)
           1        50.25         .15
```

2	60.25	.46
3	70.20	1.43
4	80.07	3.05
5	89.81	5.32
6	99.38	8.22
7	108.74	11.74
8	117.85	15.87
9	126.67	20.58
10	135.15	25.87
11	143.28	31.70
12	151.00	38.05
13	158.29	44.90
14	165.11	52.21
15	171.44	59.95
16	177.25	68.09
17	179.72	72.10

*** .967 ***

Individual data on the 28 slices

Slice No.	Width (ft)	Weight (lbs)	Water Force Top (lbs)	Water Force Bot (lbs)	Tie Force Norm (lbs)	Tie Force Tan (lbs)	Earthquake Force Hor (lbs)	Earthquake Force Ver (lbs)	Surcharge Load (lbs)
1	9.7	2971.7	.0	.0	.0	.0	.0	.0	.0
2	.2	153.2	.0	.0	.0	.0	.0	.0	.0
3	9.8	8738.1	.0	.0	.0	.0	.0	.0	.0
4	.2	235.8	.0	.0	.0	.0	.0	.0	.0
5	9.8	13849.1	.0	.0	.0	.0	.0	.0	.0
6	.1	114.0	.0	.0	.0	.0	.0	.0	.0
7	9.7	18009.6	.0	.0	.0	.0	.0	.0	.0
8	.2	390.6	.0	.0	.0	.0	.0	.0	.0
9	9.4	20691.1	.0	.0	.0	.0	.0	.0	.0
10	.6	1467.9	.0	.0	.0	.0	.0	.0	.0
11	8.7	21700.7	.0	.0	.0	.0	.0	.0	.0
12	1.3	3279.0	.0	.0	.0	.0	.0	.0	.0
13	7.8	20995.3	.0	.0	.0	.0	.0	.0	.0
14	2.2	5912.5	.0	.0	.0	.0	.0	.0	.0
15	6.7	18521.9	.0	.0	.0	.0	.0	.0	.0
16	3.3	9335.1	.0	.0	.0	.0	.0	.0	.0
17	5.2	14373.5	.0	.0	.0	.0	.0	.0	.0
18	4.8	13335.6	.0	.0	.0	.0	.0	.0	.0
19	3.3	8845.4	.0	.0	.0	.0	.0	.0	.0
20	6.7	17456.0	.0	.0	.0	.0	.0	.0	.0
21	1.0	2500.7	.0	.0	.0	.0	.0	.0	.0
22	7.3	17157.2	.0	.0	.0	.0	.0	.0	.0
23	1.7	3720.6	.0	.0	.0	.0	.0	.0	.0
24	5.1	10207.6	.0	.0	.0	.0	.0	.0	.0
25	4.9	8297.1	.0	.0	.0	.0	.0	.0	.0
26	1.4	2064.3	.0	.0	.0	.0	.0	.0	.0
27	5.8	5158.5	.0	.0	.0	.0	.0	.0	.0
28	2.5	545.7	.0	.0	.0	.0	.0	.0	.0

Failure Surface Specified By 17 Coordinate Points

Point No.	X-Surf (ft)	Y-Surf (ft)
1	51.26	.76
2	61.26	.81
3	71.23	1.59
4	81.12	3.11
5	90.86	5.35
6	100.42	8.30
7	109.73	11.95
8	118.74	16.28
9	127.42	21.26
10	135.70	26.86

11	143.55	33.06
12	150.91	39.82
13	157.77	47.10
14	164.06	54.87
15	169.77	63.08
16	174.85	71.69
17	175.06	72.10

*** .967 ***

Failure Surface Specified By 17 Coordinate Points

Point No.	X-Surf (ft)	Y-Surf (ft)
1	50.76	.45
2	60.75	.96
3	70.68	2.11
4	80.52	3.91
5	90.21	6.35
6	99.73	9.42
7	109.03	13.10
8	118.06	17.38
9	126.80	22.25
10	135.20	27.68
11	143.23	33.64
12	150.85	40.12
13	158.03	47.08
14	164.74	54.49
15	170.95	62.33
16	176.63	70.55
17	177.56	72.10

*** .968 ***

Failure Surface Specified By 17 Coordinate Points

Point No.	X-Surf (ft)	Y-Surf (ft)
1	50.76	.45
2	60.74	1.02
3	70.67	2.21
4	80.50	4.04
5	90.20	6.50
6	99.71	9.57
7	109.01	13.24
8	118.06	17.50
9	126.82	22.33
10	135.25	27.71
11	143.32	33.62
12	150.99	40.03
13	158.24	46.92
14	165.03	54.26
15	171.34	62.02
16	177.14	70.16
17	178.34	72.10

*** .969 ***

Failure Surface Specified By 17 Coordinate Points

Point No.	X-Surf (ft)	Y-Surf (ft)
1	52.02	1.21
2	62.02	.91
3	72.01	1.35
4	81.94	2.54
5	91.75	4.46
6	101.39	7.11
7	110.81	10.47
8	119.95	14.53
9	128.76	19.25
10	137.20	24.62

11	145.21	30.60
12	152.76	37.16
13	159.79	44.27
14	166.28	51.88
15	172.18	59.96
16	177.46	68.45
17	179.37	72.10
***	.970	***

Failure Surface Specified By 17 Coordinate Points

Point No.	X-Surf (ft)	Y-Surf (ft)
1	51.01	.61
2	61.00	.26
3	71.00	.65
4	80.93	1.77
5	90.76	3.62
6	100.43	6.19
7	109.87	9.47
8	119.06	13.42
9	127.92	18.05
10	136.43	23.31
11	144.52	29.19
12	152.16	35.64
13	159.30	42.64
14	165.91	50.14
15	171.95	58.11
16	177.39	66.50
17	180.46	72.10
***	.970	***

Failure Surface Specified By 16 Coordinate Points

Point No.	X-Surf (ft)	Y-Surf (ft)
1	51.01	.61
2	61.00	.96
3	70.95	2.02
4	80.79	3.78
5	90.49	6.23
6	99.98	9.36
7	109.24	13.16
8	118.20	17.60
9	126.82	22.66
10	135.07	28.32
11	142.89	34.55
12	150.25	41.31
13	157.12	48.58
14	163.46	56.32
15	169.23	64.48
16	173.85	72.10
***	.970	***

Failure Surface Specified By 17 Coordinate Points

Point No.	X-Surf (ft)	Y-Surf (ft)
1	52.27	1.36
2	62.26	.79
3	72.25	1.03
4	82.20	2.09
5	92.02	3.96
6	101.66	6.64
7	111.04	10.09
8	120.11	14.31
9	128.80	19.25
10	137.06	24.90
11	144.82	31.20

12	152.04	38.11
13	158.68	45.60
14	164.67	53.60
15	169.99	62.07
16	174.59	70.95
17	175.07	72.10

*** .970 ***

Failure Surface Specified By 16 Coordinate Points

Point No.	X-Surf (ft)	Y-Surf (ft)
1	54.04	2.42
2	64.04	2.34
3	74.02	3.02
4	83.91	4.47
5	93.67	6.67
6	103.22	9.61
7	112.52	13.28
8	121.52	17.66
9	130.15	22.71
10	138.36	28.41
11	146.11	34.73
12	153.36	41.62
13	160.05	49.05
14	166.15	56.98
15	171.63	65.34
16	175.34	72.10

*** .971 ***

Failure Surface Specified By 16 Coordinate Points

Point No.	X-Surf (ft)	Y-Surf (ft)
1	52.27	1.36
2	62.26	.81
3	72.25	1.10
4	82.19	2.23
5	92.00	4.18
6	101.61	6.95
7	110.95	10.51
8	119.96	14.85
9	128.58	19.92
10	136.74	25.70
11	144.39	32.14
12	151.48	39.19
13	157.95	46.82
14	163.75	54.96
15	168.86	63.56
16	173.00	72.10

*** .972 ***

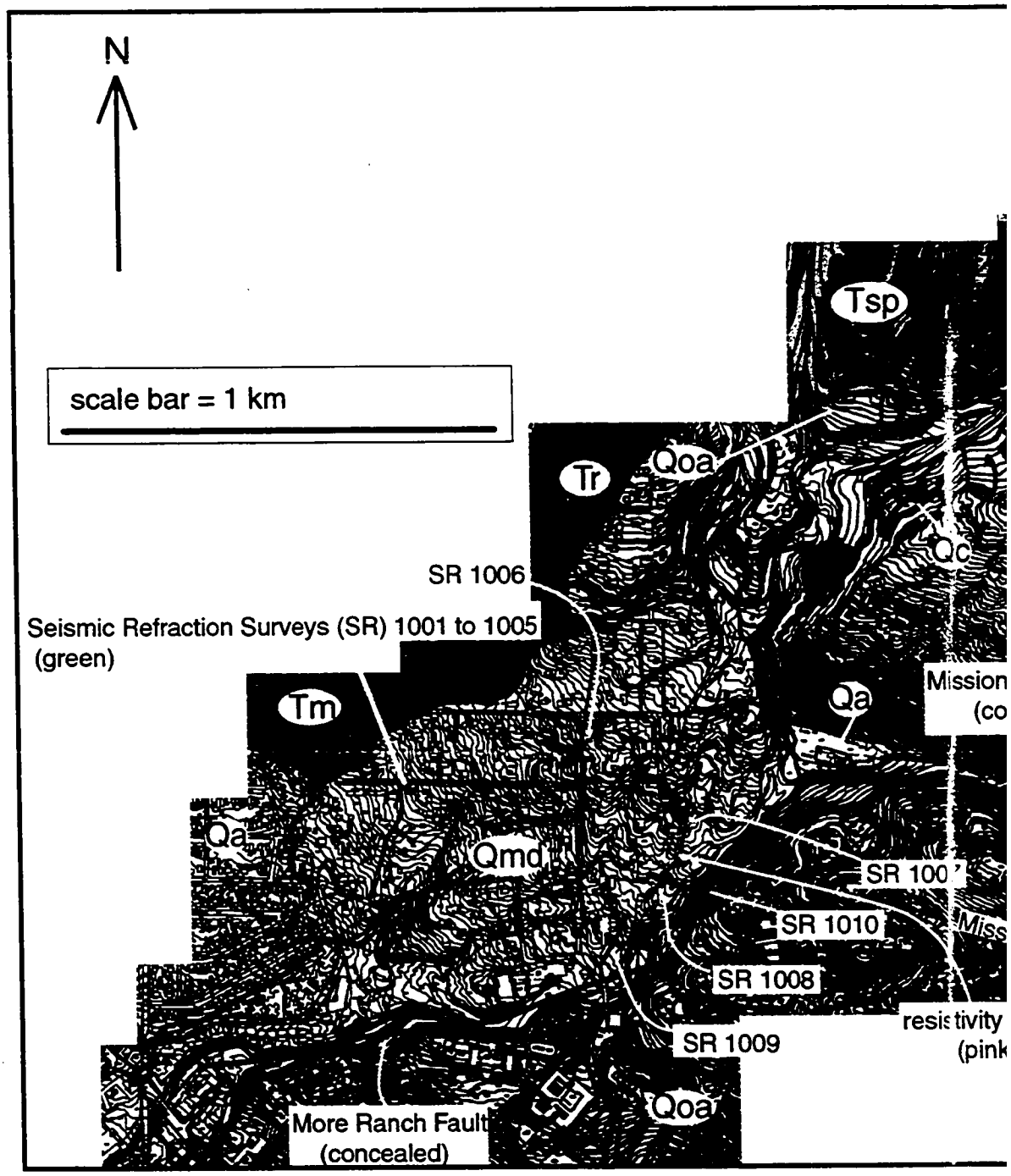

Figure 3. Geologic map of the Mission diamicton and associated features, Santa Ba abbreviated (SR). Resistivity survey indicated with pink line parallel to refraction surveys indicates anticline axis and direction of plunge. Minor green arrows indicate dip directio

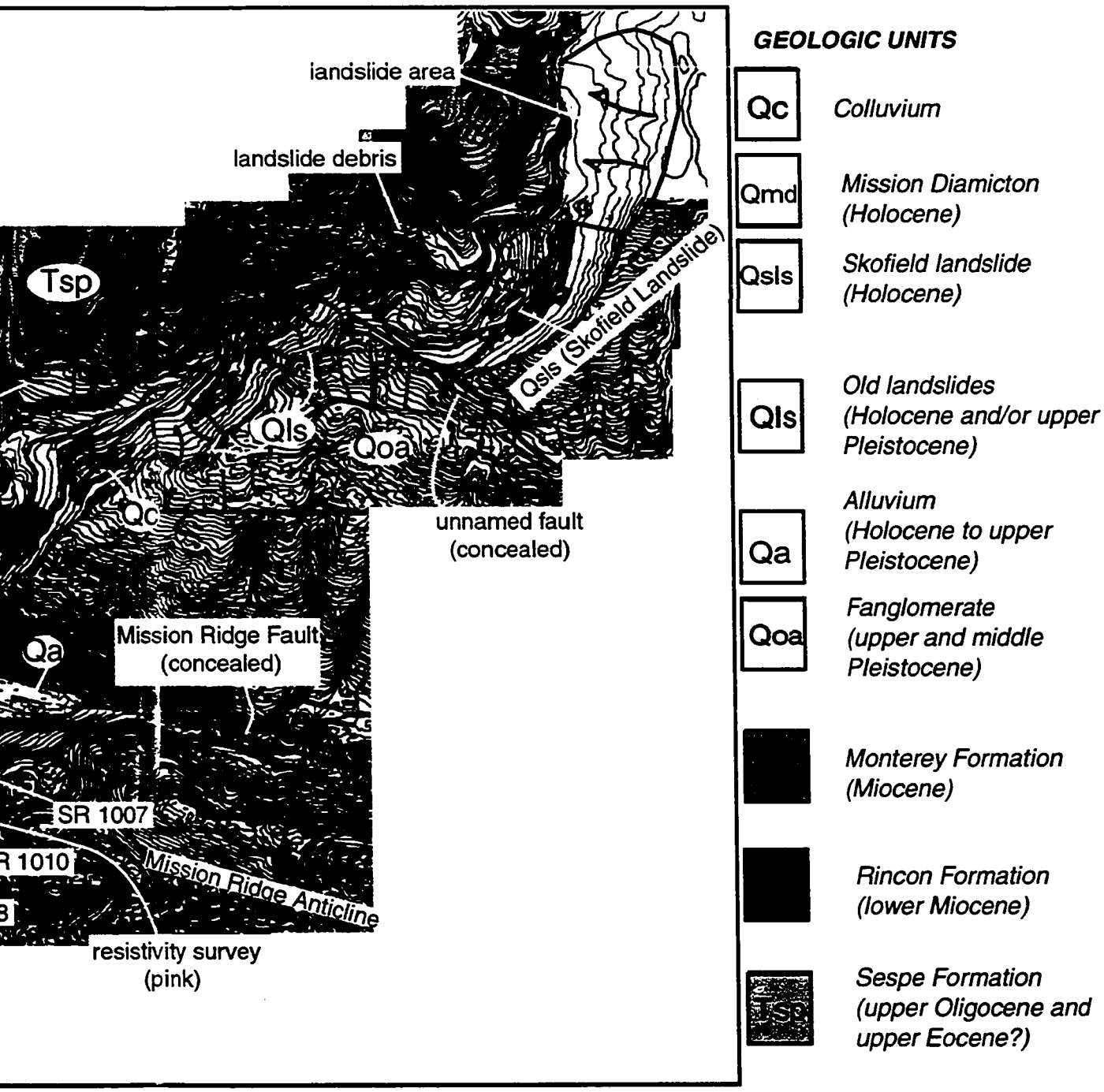

atures, Santa Barbara, California. Seismic refraction surveys indicated with bright green lines and fraction surveys 1006 and 1007. Red lines indicate locations of concealed faults. Major green arrow cate dip direction of anticline limbs.